Tracking the evolution of late Mesozoic arc-related magmatic systems in Hong Kong using in-situ U-Pb dating and trace element analyses in zircons

Revised manuscript 1

Denise L.K. Tang[a,b], Colin J.N. Wilson[a*], Roderick J. Sewell[b], Diane Seward[a], Lung S. Chan[c], Trevor R. Ireland[d], Joseph L. Wooden[e]

[a] School of Geography, Environment and Earth Sciences, Victoria University of Wellington, P.O. Box 600,Wellington 6140, New Zealand

[b] Hong Kong Geological Survey, Civil Engineering and Development Department, HKSAR Government, 101 Princess Margaret Road, Kowloon, Hong Kong

[c] Department of Earth Sciences, The University of Hong Kong, Pokfulam Road, Hong Kong

[d] Research of School of Earth Sciences, Australian National University, Canberra, ACT 0200, Australia

[e] SUMAC, Department of Geological and Environmental Sciences, Stanford University, Stanford, CA 94350, USA

* Corresponding author. Email address: colin.wilson@vuw.ac.nz

ABSTRACT

The links between large-scale silicic volcanism and plutonism offer insights into the dynamics of crustal magmatic systems and growth of continental crust. In Hong Kong, voluminous silicic ignimbrites and linked plutons record a ~26-Myr period of magmatism from ~164 to 138 Ma. We present data from these linked volcanic-plutonic assemblages at the Lantau and High Island caldera complexes, with an emphasis on the ~143-138 Ma activity from the latter. To track the evolution of these magmatic systems, U-Pb dating and trace element analyses using secondary-ion mass spectrometry (SIMS) were carried out on zircons from 21 samples from both volcanic and plutonic samples. The SIMS age datasets divide into two groups across volcanic and plutonic origins: (1) seven samples with unimodal age spectra (five of which have the same mean value as the published Isotope Dilution Thermal Ionization Mass Spectrometry (ID-TIMS) age from the same sample); and (2) fourteen samples yielding multiple age components. Age patterns from both groups suggest that the previously separated ~143 Ma Repulse Bay (RBVG) and ~141-140 Ma Kau Sai Chau volcanic groups (KSCVG) instead represent activities over a single ~5 Myr period. Direct linkages previously proposed between some volcanic and plutonic units for this period (e.g. High Island Tuff, Kowloon Granite) are no longer supported, and magmatism represented by exposed plutons continued until 137.8±0.8 Ma (Mount Butler Granite). Under CL imagery, a wide range of zircon textures identified in both volcanic and plutonic samples is indicative of complex processes, some of which are identified through trace element data coupled with textural characteristics. Overall, intra-grain (cores versus rims; sector-zonation) and intra-sample variations in trace element abundances and ratios are larger than those between samples. Zircon chemistries in both volcanic and plutonic samples fall into two groups during the ~5 Myr history of the High Island caldera magmatic system. One group (RBVG and "cold" granites) includes inherited grains back to 164 Ma and wider ranges in Hf, Y, total trivalent elements, Th and U concentrations and Th/U, Yb/Gd and U/Yb ratios than the other (KSCVG and "hot" granites). Two possible evolutionary models of the High Island caldera magmatic system are: (1) the system randomly tapped a single crustal domain that fluctuated in temperature as a result of varying interactions of hotter melts, or (2), the volcanic and plutonic records reflect the interplay of two crustal domains with contrasting "low-" and "high-temperature" characteristics. In Hong Kong, some plutonic bodies were comagmatic with large-scale volcanism, while others were emplaced at shallow crustal levels independently of volcanism, matching the current two end-member views of the volcanic-plutonic relationship.

Keywords: Volcanism, plutonism, granite, rhyolite, Hong Kong, Mesozoic, caldera, zircon

INTRODUCTION

Large silicic magmatic systems predominantly generate two contrasting products: voluminous ignimbrite sheets and granitic batholiths that accumulate at shallow crustal levels (e.g. Smith 1979; Lipman 1984, 2007; Shaw 1985). Although there have been considerable advances in our understanding of how such systems operate, there remain contrasting views on the relationships between silicic volcanic and plutonic rocks (e.g. Lundstrom and Glazner 2016).

From the volcanic perspective, a popular model infers that magma chambers are volumetrically and temporally dominated by crystal mush that is rheologically locked (Mahood 1990; Brophy 1991; Bachmann and Bergantz 2004; Hildreth 2004; Hildreth and Wilson 2007; Bachmann and Huber, 2016). Two end-member volcanic products are envisaged to be generated by such systems (Bachmann and Bergantz 2008). The first is crystal-rich intermediate (broadly dacitic) ignimbrites, considered to represent erupted crystal mushes that have been thermally recharged and mobilised by mafic magma inputs (e.g. Bachmann et al. 2002; Huber et al. 2011, 2012). The second is crystal-poor rhyolites, extracted from the mush system and accumulated for a short time period (decades to millennia) at shallow levels prior to eruption (Bachmann and Bergantz 2004; Hildreth and Wilson 2007; Allan et al. 2017). This model implies that there are sub-volcanic granitic plutons that represent either the crystallised mush itself, or the residue left after melt extraction (Bachmann and Bergantz 2004; Hildreth 2004; Hildreth and Wilson 2007; Barker et al., 2015). Based on the degrees of crystal fractionation required to yield rhyolitic melts (or the volumes of mafic intrusions required to cause crustal melting) and the thermal fluxes in young systems like Yellowstone (USA), or the central Taupo Volcanic Zone (TVZ) in New Zealand, it is evident that large volumes of intrusive materials (in proportions from 3:1 to 10:1) are associated with erupted rhyolite (e.g. Smith 1979; Cameron et al. 1980; Hildreth 1981; Lipman and Bachmann 2015). Consequently, there should be a close temporal and compositional link between large ignimbrite eruptions and plutonic bodies, and thus granitic plutons have generally been considered by some as ‘frozen’ magma chambers (e.g. Sides et al. 1981; Lipman 1984; Macdonald and Smith 1988).

The plutonic records of large silicic magmatic systems are, however, usually inferred to represent longer timescales. Geochronological arguments suggest that large granitic batholiths grow incrementally over time periods of >10^6–10^7 years (e.g. Coleman et al. 2004; Glazner et al. 2004; Matzel et al. 2006; Gaschnig et al. 2010, 2017; Davis et al. 2012; Frazer et al. 2015). Such protracted, stepwise incremental growth of granitic plutons is taken to imply that only small quantities of magma exist at any particular time during the construction of granitic batholiths and, therefore, these plutons were not linked to any large magma chamber that fed voluminous ignimbrite eruptions. This inference also implies that silicic magmatic chambers that erupt thousands of cubic kilometers of magma are geologically rare and short-lived (Glazner et al. 2004; Miller 2008).

These contrasting views imply orders of magnitude timescale differences in the generation of voluminous eruptible magma and emplacement of large sub-volcanic plutons. Lipman (2007) proposed that the eruption of large silicic ignimbrites and emplacement of plutons reflect the variable waxing and waning stages of a magmatic system with a total lifespan of 10^7 years. Investigation of such systems is generally limited by the uncommon preservation of both the volcanic and sub-volcanic roots of a magmatic system (e.g. Lipman and McIntosh 2008; Quick et al. 2009; Barth et al. 2012; Zimmerer and McIntosh 2012) and seems to be favoured mostly in syn-magmatic extension tectonic settings (e.g. Schermer and Busby 1994). Questions remain about (1) how silicic magmatic systems build spatially and temporally, and (2) how the volcanic and sub-volcanic plutonic rocks relate to each other. Here we address these questions using a case study from the detailed volcano-plutonic record available in Hong Kong.

The surface geology of Hong Kong is dominated by late Mesozoic, large caldera-related silicic ignimbrites and granitic plutons, now exposed together (Sewell et al. 2000, and references therein; Sewell et al. 2012a). Their relationships are constrained through field observations (Campbell and Sewell 1997; Sewell et al. 2000; 2012a; Tang 2016), Isotope Dilution Thermal Ionization Mass Spectrometry (ID-TIMS) U-Pb zircon ages (Davis et al. 1997; Campbell et al. 2007; Sewell et al. 2012b), whole-rock geochemical data (Sewell et al. 1992; Darbyshire and Sewell 1997; Sewell and Campbell 1997, 2001) and geophysical surveys (Fletcher et al. 1997). The scale of the Hong Kong systems permits comparisons with their broadly coeval counterparts in the western USA, particularly in the Sierra Nevada Batholith. To address the volcanic-plutonic relationships, we focus on ignimbrites and granitic plutons from two caldera complexes in southeast Hong Kong and Lantau Island and examine their >~26 Myr history of magmatic evolution. We use Secondary-Ion Mass Spectrometry (SIMS) techniques to undertake in-situ U-Pb dating and trace element analyses on zircons from the ignimbrites and sub-volcanic plutons. The age data are used to explore whether the more-precise ID-TIMS data yield accurate ages, or represent average values concealing patterns of inheritance. Such inherited zircons might be xenocrysts, incorporated from older, unrelated host rocks, or antecrysts, derived from crystal mush or plutons of earlier magmatic episodes (see Charlier et al. 2005). The trace element data are used to assess genetic connections of the paired volcanic-plutonic assemblages, and to unravel crystallisation/fractionation paths within the volcanic and plutonic units.

GEOLOGICAL BACKGROUND

Geology of Hong Kong

Hong Kong is located on the southern margin of the 1,300 x 400 km Southeast China Magmatic Belt. Its surface geology is dominated by volcanic and plutonic rocks reflecting large-scale late Mesozoic silicic magmatism associated with the Yanshanian Orogeny (Zhou et al. 2006; Li and Li 2007). Four volcanic groups, their source calderas and plutonic equivalents have been identified (Fig. 1; Table 1; Campbell and Sewell 1997). They comprise dacitic to rhyolitic ignimbrites and lavas with intercalated volcaniclastic sediments, plus intrusions of granodiorite, granite, quartz monzonite and minor dikes of various compositions (Sewell et al. 2000, 2012a, b). They record events over a nominal ~ 24 Myr period (164-140 Ma), clustered into four episodes (Campbell and Sewell 1997; Sewell et al. 2012a, b). Here, we focus on the caldera complexes centred on Lantau Island and the High Island area (Fig. 1) to investigate the evolution of their magmatic systems. The volcanic rocks, associated calderas and intrusive units of these two complexes are documented by Langford et al. (1995), So (1999) and Campbell et al. (2007) for Lantau, and Sewell et al. (2012a) and Tang (2016) for High Island.

Lantau caldera complex. Lantau caldera complex (Fig. 1) contains an abridged record of all four volcanic episodes (Campbell et al. 2007). The ~164 Ma Shing Mun rhyolitic ignimbrite unconformably overlies Early Jurassic sediments and is overlain by the ~148-146 Ma Lantau Volcanic Group (LVG: Langford et al. 1995; Campbell and Sewell 1997). On Lantau Peak, small outcrops of volcanic rocks from the ~143 Ma and ~141-140 Ma episodes occur (Langford et al. 1995; So 1999; Sewell et al. 2000; Campbell et al. 2007).

Outcrops of the ~160 Ma Lamma Suite granites in northern and northeastern Lantau Island have been largely dismembered by emplacement of ~146 Ma felsic to intermediate dikes (East Lantau Dyke Swarm) and faulting (Langford et al. 1995). The dike swarm forms a 6-km wide, ENE-trending zone of multiple intrusions accompanying a period of rapid crustal extension (Langford et al. 1995; Li et al. 2000). The Chi Ma Wan Granite (~143 Ma) is exposed on the southern fringe of the Lantau caldera complex, while the ~140 Ma Tong Fuk Quartz Monzonite consists of multiple bodies interpreted as ring fault intrusions (Langford et al. 1995; Campbell and Sewell 1997; Sewell et al. 2000; Campbell et al. 2007).

High Island caldera complex. Voluminous dacitic to rhyolitic ignimbrites and lavas of the two younger volcanic episodes (~143 Ma and ~141-140 Ma) spatially overlap and, with associated granitic plutons, are exposed within the nested High Island caldera complex (Fig. 1). The ~143 Ma Repulse Bay Volcanic Group (RBVG) comprises two main sub-groups (Table 1): (1) dacitic to rhyolitic crystal-rich ignimbrites of the Long Harbour and Mount Davis formations, and (2) trachytic to high-silica rhyolitic, crystal-poor, locally-welded ignimbrites of the Ap Lei Chau and Che Kwu Shan formations. The ~141-140 Ma Kau Sai Chau Volcanic Group (KSCVG) began with the Pan Long Wan Formation trachydacite lava, then the Clear Water Bay rhyolite lava and densely welded ignimbrites, and culminated in the caldera-forming High Island Tuff (Strange et al. 1990; Sewell et al. 2012a).

Two plutonic suites, Cheung Chau (~143 Ma) and Lion Rock (~140 Ma), were linked to the RBVG and KSCVG, respectively, as paired volcanic-plutonic assemblages by Campbell and Sewell (1997) and Sewell et al. (2000, 2012a). The Shui Chuen O Granite, exposed in the southern New Territories, is the only Cheung Chau Suite pluton that forms part of the High Island caldera complex (Sewell et al. 2000; 2012a). Several plutons of the Lion Rock Suite, including the Kowloon, Mount Butler and Sok Kwu Wan granites and D'Aguilar Quartz Monzonite, are thought to represent the sub-volcanic roots of the High Island caldera (Sewell et al. 2012a).

Samples and methods

Sample preparation

Zircons from 21 representative samples (12 volcanic, 9 granitic) from units in the Lantau and High Island caldera complexes have been analysed (Fig. 1; Table 1; Electronic Appendix 1 for details). For 17 samples, zircon separates remaining from previous ID-TIMS studies were obtained from the Hong Kong Geological Survey archive. In addition, extra material was obtained from the same localities of two previously dated samples (HK11052 and HK12070) and two new samples (HK13343 and HK13407). Zircons were separated from rock samples by crushing, sieving, and then standard heavy-liquid and magnetic separation methods. Zircon grains were mounted in epoxy resin and polished to expose the approximate mid-section of the grains. Cathodoluminescence (CL) images of the polished mounts were taken on a JEOL JSM6610 LV Scanning Electron Microscope at Victoria University of Wellington (VUW). The CL images were used to guide age and trace element analyses in specific growth zones of representative grains.

In-situ U-Pb age determinations

In-situ U-Pb age determinations were carried out using the Sensitive High Resolution Ion Microprobe – Reverse Geometry (SHRIMP-RG) instruments at the joint USGS-Stanford University facility (SUMAC) and at the Research School of Earth Sciences, Australian National University (ANU). In this study, we have aimed towards an improved precision level approaching that of the previous ID-TIMS ages by carrying out numerous analyses that were targeted at specific growth zones, such as cores, intermediate zones or rims of grains. By calculating the weighted means from these spatially targeted groups of analyses, a better precision than that achievable for individual age determinations was obtained, linked to intra-grain characteristics and tested against the published ID-TIMS age data on multiple grain aliquots (Davis et al. 1997; Campbell et al. 2007; Sewell et al. 2012b).

Mounts were cleaned thoroughly in detergent, ethanol and 1 M HCl, rinsed in distilled water, and gold coated. Analytical spots were carefully located to avoid inclusions visible in CL imagery or reflected light. Prior to data acquisition, the primary beam was rastered for 2 minutes over an area of 35 x 45 µm to remove the gold coat and any surface contamination. Secondary ions were then sputtered from zircons with a 3-6 nA primary O_2^- beam focused to a ~25 x 35 µm spot. The mass spectrometer was cycled through peaks corresponding to $^{90}Zr_2{}^{16}O$ (2 s), ^{204}Pb (2 s), background (10 s), ^{206}Pb (30 s), ^{207}Pb (10 s), ^{208}Pb (2 s), ^{238}U (7 s), $^{232}Th^{16}O$ (2 s) and $^{238}U^{16}O$ (2 s). Six scans were run through the mass sequence for each analytical spot. The concentration standard was MAD (Madagascar green: Barth and Wooden 2010; 4196 ppm U) at SUMAC and SL13 (238 ppm U) at ANU. The U-Pb age standards used were R33 (420 Ma: ID-TIMS age from Zeh et al. 2015) or Temora 2 (417 Ma: Black et al. 2004). The concentration standard was measured once for each session, and the U-Pb age standard was measured three times at the beginning of each round of analyses then subsequently once for every four unknowns. Data reduction was carried out using SQUID 2 (version 1.5.1: Ludwig 2009) and data plotted using Isoplot version 3.7.6 (Ludwig 2008). All uncertainties are reported here at 1σ, while for grouped data sets, uncertainties are given at 95% confidence interval, as generated in Isoplot. The full age dataset is presented in Electronic Appendix 2. Common Pb was monitored by the measured ^{204}Pb and $^{207}Pb/^{206}Pb$ values. A correction for common Pb was applied using the recorded $^{207}Pb/^{206}Pb$ values and an average crustal common Pb isotopic composition for the sample age (Stacey and Kramers 1975). Analyses of grains with <20% common Pb were considered acceptable. No correction has been made for initial ^{230}Th disequilibrium because of its trivial influence (<100 kyr) on the individual ages.

Zircon trace element analytical techniques

Trace element analyses on zircons were undertaken by SIMS techniques on the SHRIMP-RG instrument at SUMAC. After U-Pb dating, the mounts were re-polished to remove the earlier analytical spots. A primary beam current of 2.4 nA, spot size of 20 μm and mass resolution of 10,000 were used. The concentration standard was MAD (Barth and Wooden 2010). Data reduction was carried out using SQUID 2 (version 1.51, Ludwig 2009) and data plots were generated using Isoplot (version 3.75, Ludwig 2008). MAD was measured repeatedly during each session to determine the overall reproducibility of the trace element data. To track contamination we used: Li, Ca, Al, Na, K, La for feldspar or glass; Ca, P, F for apatite; Fe for Fe-Ti oxides, and Ca, Fe, La for allanite. Analyses that yielded strong enrichment in these elements were considered contaminated, and the data reported below exclude any considered to be significantly affected. The full dataset is presented in Electronic Appendix 3. The external reproducibility of zircon trace element data (Mazdab and Wooden 2006) varies with counting statistics and heterogeneities in the MAD standard. The majority of measured elements are reproduced to within ~2-5 % 2 s.d., whereas the low-concentration elements (usually Li, Be, F, Ca, La and Eu) show poorer reproducibility (Electronic Appendix 3). For each sample, 60 to 120 analyses were carried out. Analytical spots were located to cover the range of textural variations seen in the zircon populations from individual samples, including core-rim, tip-side, and sector-zoned pairs from the same growth zone and, if feasible, placed in the same growth zones as the age spots.

RESULTS

Zircon zoning patterns from CL imagery

For each sample >150 grains were classified based on their zoning patterns, including the presence or absence of cores, the relative CL intensity (brightness) of the cores versus rims, and the presence or absence of oscillatory and/or sector zoning in the rim areas (Fig. 2). All samples, both volcanic and plutonic, yield zircons with a widely diverse range of textures and zoning patterns in CL imagery (Fig. 2; Table 2). Four zoning features were quantified to describe the crystal textures.

1): *Definable discrete cores* were observed in 34-85% of zircon grains in all samples. Three main types were classified: Types A and B cores are rounded; Type C cores are euhedral (Fig. 2). Type A cores generally have dark CL emission but lack internal zoning while Type B cores exhibit complex textures, sometimes with multiple truncated internal zones. Type C euhedral cores are mostly structureless or show simple growth zones, and have intermediate CL emission. It is common that the zircon population from individual volcanic and plutonic samples comprises a combination of different types of cores (Table 2). Furthermore, these cores are overgrown by rims of varying CL intensities which may be darker, brighter or show oscillatory zoning, implying a diversity of later crystallization histories.

2): *Plain, euhedral grains* with no zoning pattern are present in all samples (volcanic and plutonic) in abundances from 2-20%, with one sample (HK12070) having ~30% of such grains (Table 2).

3): *Oscillatory zoning* occurs in most samples (volcanic and plutonic) in ~40%, and in some cases up to ~90%, of crystals (Table 2).

4): *Sector zoning* in the outer growth zones is generally more common (Table 2) in zircons from volcanic than plutonic samples (sector zoning in zircon cores is not counted). Volcanic samples contain 9-36% of grains with sector zoning, except for the High Island Tuff (HK12001: 2%). For plutonic units, the zircon populations contain 2-24% of grains with sector zoning, with the exceptions of the Shui Chuen O Granite (47%) and D'Aguilar Quartz Monzonite (38%).

Zircon U-Pb age data

In total 883 age determinations were carried out on the 21 samples (Table 3: Electronic Appendix 2). For individual samples, the weighted mean ages of all data, or the rim analyses separately when multiple age components are present, are compared against published ID-TIMS age data. Probability distribution curves and histograms of the SIMS age data for the volcanic and plutonic units within the Lantau and High Island caldera complexes are presented in Figs. 3 to 8.

Lantau caldera complex: volcanic units. Volcanic units from the Lantau caldera complex all contain multiple age components (Fig. 3, Table 4). The Shing Mun ignimbrite (HK12025) and undifferentiated Kau Sai Chau tuff (HK12070) yield weighted mean rim ages of 164.7±0.8 Ma and 140.7±0.7 Ma, respectively, the same (within error) as the respective ID-TIMS ages (Table 3). Zircon rims in the Lantau tuff (HK11052) yield a weighted mean of 144.5±0.7 Ma, which is ~2 Myr younger than its ID-TIMS age estimate (Table 3).

Lantau caldera complex: plutonic units. The East Lantau porphyry and Tong Fuk Quartz Monzonite both yield single age components (Fig. 4, Table 3). Data from the East Lantau porphyry (HK11831) yield a weighted mean of 144.6±0.8 Ma, almost ~2 Myr younger than its ID-TIMS age (Table 3). Note, however, that the core analyses of this unit yield multiple peaks in the relative probability curve (Fig. 4B). The weighted mean rim age of the Tong Fuk Quartz Monzonite (HK8758) is 140.6±1.5 Ma, identical within error to its ID-TIMS value (Table 3). Multiple age components are identified in the Lantau Granite and Chi Ma Wan Granite (Fig. 4, Table 4). The weighted mean rim age of Lantau Granite (HK11822) is 161.4±1.4 Ma, which is identical within error to the ID-TIMS value (Table 3). In contrast, analyses from zircon rims of the Chi Ma Wan Granite (HK8353) yield a weighted mean of 140.0±1.0 Ma, at least 2-3 Myr younger than its ID-TIMS age (Table 3).

High Island caldera complex: volcanic units. All units analysed from the RBVG contain multiple age components (Fig. 5, Table 3). The Mount Davis ignimbrite (HK13275) yields mean rim age of 142.3±1.2 Ma, overlapping within error its ID-TIMS age (Table 3). Three other samples give younger weighted mean rim ages than the reported ID-TIMS ages (Table 3). These are the Long Harbour ignimbrite (HK11835: 141.4±1.0 Ma), Ap Lei Chau ignimbrite (HK11840: 141.0±0.7 Ma) and Che Kwu Shan ignimbrite (HK11836: 141.6±1.0 Ma). Age components younger than ~140 Ma are identified from all the RBVG units (except the Che Kwu Shan ignimbrite), but are associated with very high U concentrations.

The KSCVG units, excepting the Pan Long Wan trachydacite, yield unimodal, normally distributed age spectra (Fig. 6). The Pan Long Wan trachydacite (HK13277) contains multiple age components and yields a weighted mean rim age of 141.0±1.3 Ma, identical within error to its ID-TIMS age (Table 3). The weighted mean ages (all analyses) of the Clear Water Bay ignimbrite (HK11834) and lava (HK12073) are closely comparable: 139.1±0.8 Ma and 139.0±0.6 Ma, respectively. These mean ages overlap within error, but are slightly younger than, the reported ID-TIMS ages (Table 3). However, if the weighted mean ages of cores and rims from these two samples are considered separately, the cores are younger (see the section 'Effects of U contents on zircon U-Pb ages', below). For the High Island Tuff (HK12001), the weighted mean of all analyses is 140.9±0.4 Ma, identical to the ID-TIMS age (Table 3), and the rim and core analyses separately are also identical (Fig. 6). The post-High Island rhyolite lava (HK13343, not previously dated) yields a weighted mean of 139.6±0.4 Ma.

High Island caldera complex: plutonic units. Three of the units contain single age populations (Table 3; Fig. 7). The Sok Kwu Wan Granite (HK12023) yields a weighted mean of 139.8±0.9 Ma, with the rims (identical within error to the ID-TIMS age: Table 3) defining a slightly older peak than the cores (Fig. 7). The weighted mean of the D'Aguilar Quartz Monzonite (HK12022) is 140.5±1.0 Ma, identical within error to its ID-TIMS age (Table 3). The

Shui Chuen O Granite (HK12072) zircons yield a weighted mean of 142.1±0.6 Ma, ~2 Myr younger than the ID-TIMS age.

In contrast, multiple age components occur in the Kowloon and Mount Butler granites (Table 3). The Kowloon Granite (HK11042) yields a weighted mean of 140.0±0.8 Ma, similar to the ID-TIMS age (Fig. 8; Table 3). Three age components are identified (Table 3), suggesting the zircons were crystallised in, or recycled from, several magmatic phases. The Mount Butler Granite (HK13407, not previously dated), yields a weighted mean of 138.0±0.6 Ma, while if only rim analyses are considered, the weighted mean is 137.8±0.8 Ma.

Trace element data

A total of 1,681 acceptable zircon trace element analyses (i.e. those without significant contamination) was obtained (Table 4). The samples studied represent a wide compositional spectrum, from trachydacite to high-K high-silica rhyolite, and from quartz monzonite to highly-evolved granites. Data are summarised in Table 4, and the full dataset and summary plots are in Electronic Appendices 3 and 4. In general, the volcanic and plutonic zircons yield very similar or identical trace element concentration ranges and patterns (Fig. 9).

Hafnium. Hf concentrations in zircon are a tracer of melt evolution, with higher values linked to increasing degrees of melt differentiation and cooling (e.g. Claiborne et al. 2006; 2010; Barth and Wooden 2010; Reid et al. 2011; Chamberlain et al. 2014). Most zircons from the older volcanic units within the Lantau caldera complex and the RBVG units contain Hf from ~7,000-14,000 ppm, but some CL-darker cores reach ~16,000 ppm. For these volcanic units, the ranges of Hf concentrations in cores are generally larger than in the rims. The lowest Hf concentrations occur in the Che Kwu Shan tuff (HK11836: ~5,500 ppm) and Pan Long Wan trachydacite (HK13277: ~6,500 ppm). The KSCVG units yield zircons with Hf of ~6,000-13,000 ppm (both cores and rims: Table 4). The plutonic units contain zircons with Hf typically ~6,000-19,000 ppm, with some extreme enrichment in zircon rims of the Kowloon and Mount Butler granites (HK11042, HK13407: >21,000 ppm). In contrast, the quartz monzonites and So Kwu Wan Granite (HK8758, HK12022, HK12023) have zircons with ~6,000-12,000 ppm Hf for both cores and rims, comparable to the volcanic samples.

Uranium and Thorium. For all samples, concentrations of U and Th (Fig. 9) show intra- and inter-grain variations over two to three orders of magnitude, from tens to several thousands of ppm (Table 4). Zircon rims from the Pan Long Wan trachydacite (HK13277) record the lowest values: 50% of the analyses contain less than ~50 ppm U and ~30 ppm Th. Rare zircon cores and rims from the Che Kwu Shan ignimbrite (HK11836) also show similarly low abundances in U and Th down to ~10 ppm. Enrichment of U and Th is common in zircon cores from the volcanic units, for example up to ~8,000 ppm U and ~7,000 ppm Th in the undifferentiated Lantau ignimbrite (HK11052). For the plutonic units, the highly-evolved Kowloon (HK11042) and Mount Butler (HK13407) granites contain some rims with >~12,000 ppm U, although accompanying Th concentrations are lower.

Trivalent trace elements. For all samples, the total Sc + Y + REE^{3+} (hereafter 'total 3+ elements') concentrations co-vary with U (Fig. 9). In general, zircons from the volcanic units contain from several hundred up to ~10,000 ppm total 3+ elements, although some analyses from CL-dark cores yield ~10,000-16,000 ppm. The RBVG and Pan Long Wan zircons exhibit a wide range of total 3+ element concentrations that spread across the minima and maxima of the other units. Among all the samples, zircons from the KSCVG units (except the Pan Long Wan trachydacite) contain the highest values. If only rim analyses are considered, the ranges and absolute concentrations of total 3+ elements in all volcanic samples are comparable. The plutonic zircons generally have similarly wide ranges of total 3+ element concentrations to the volcanic samples. Zircon cores from the plutonic units generally contain higher concentrations than the rims, with the extremes of the Kowloon and Mount Butler granites having rim values up to ~20,000 ppm. In contrast, total 3+ element abundances as low as ~100 ppm occur in some zircon cores from the Chi Ma Wan Granite (HK8353, Lantau caldera complex).

Scandium. Sc concentrations range from 10-270 ppm for the volcanic samples, although core analyses commonly yield wider ranges than rims. Considering only rim analyses, older volcanic units have generally lower Sc than the younger units. Plutonic units, except for the Tong Fuk and D'Aguilar quartz monzonites, generally yield lower Sc concentrations (10-200 ppm) than the volcanic rocks, but similarly show lower values in the older granite samples. The two quartz monzonites (HK8758 and HK12022) contain the highest Sc, up to ~290 ppm. In all cases, Sc concentrations generally show a negative trend with respect to Hf (Fig. 9).

Yttrium. Y in zircons from all samples ranges from ~ 200 to several thousand ppm. Significant intra- and inter-grain variations in Y abundance occur in all samples. In general, zircon cores contain higher Y than the rims, with the exceptions of the Shing Mun ignimbrite (HK12025), Lantau Granite (HK11822) and Mount Butler Granite (HK13407). The highest Y values occur in rims from the Mount Butler Granite (to ~14,000 ppm).

Titanium. Ti in zircons from the volcanic units ranges from ~1-40 ppm. The highest values (>25 ppm), associated with bright CL emissions, occur in cores from the undifferentiated Kau Sai Chau tuff (HK12070), and rims in the Chek Kwu Shan ignimbrite (HK11836) and Pan Long Wan trachydacite lava (HK13277). For the plutonic units, Ti concentrations typically range between 1 and 25 ppm, with only one value (of 36 analyses) from the Chi Ma Wan Granite (HK8353) reaching 37 ppm. The maximum Ti concentration is ~40 ppm in the Pan Long Wan trachydacite (HK13277) and the minimum is ~1 ppm in the post-High Island rhyolite lava (HK13343) and Mount Butler Granite (HK13407).

Europium anomaly and Cerium/Samarium ratio. The typical Eu/Eu* values (calculated as Eu/Eu* = [Eu] / ((([Sm]^0.5) x ([Gd]^0.5)) of the volcanic units range from 0.01 to 1. More pronounced anomalies (Eu/Eu* <0.01) occur in some cores, notably from the Pan Long Wan trachydacite (HK13277, 43 of 48), undifferentiated Kau Sai Chau tuff (HK12070, 1 of 28), Chek Kwu Shan ignimbrite (HK11840, 9 of 31), Ap Lei Chau ignimbrite (HK11836, 7 of 37) and Long Harbour ignimbrite (HK11835, 1 of 52). The High Island Tuff (HK12001) and post-High Island rhyolite lava (HK13343) are the only volcanic units that contain zircons (both cores and rims) with Eu/Eu* >1.0 (up to 1.9). Zircons from the plutonic units generally have smaller ranges in Eu/Eu* than the volcanic zircons, typically from 0.01 to <0.6 but with some outliers (Table 4). Some zircons from the Chi Ma Wan (HK8353, 7 of 36 core analyses) and Mount Butler (HK13407, 4 of 49 rim analyses) granites have deeper Eu anomalies (Eu/Eu* <0.01), whereas others from the Shui Chuen O Granite (HK12072), So Kwu Wan Granite (HK12023), and D'Aguilar Quartz Monzonite (HK12022) yield positive Eu anomalies. All units show a common trend with Eu/Eu* decreasing with increasing Hf concentration (Fig. 9).

To investigate Ce behaviour (cf. Trail et al. 2012) we use the Ce/Sm ratio rather than calculating a Ce anomaly directly due to the generally very low concentrations of La and its extreme susceptibility to contamination by inclusions (cf. Cooper et al. 2014). Ranges of Ce/Sm in volcanic zircons are typically ~1-30 (Table 4) with extreme outliers (Ce/Sm ~160, 260) in the Ap Lei Chau tuff (HK11840). There appears to be a slight decreasing trend in Ce/Sm ratios from older to younger volcanic units. The plutonic zircons yield a slightly smaller range in Ce/Sm ratios (~1-20: Table 4).

Elemental ratios: Th/U, Yb/Gd, U/Yb. Trace element ratios of zircons from all volcanic and plutonic units are comparable, although some volcanic units have notably higher Yb/Gd (>80) and Th/U (~2) ratios (e.g. the Shing Mun and undifferentiated Kau Sai Chau ignimbrites: HK12025, HK12070, respectively). Th/U ratios (Table 4) mostly range from 0.1 to 2, but extremely low values (<0.1) occur in rims in the Kowloon (HK11042) and Mount Butler (HK13407) granites, accompanying enrichment in U. For all volcanic and plutonic samples Yb/Gd ratios gradually converge on ~10-15 at Th/U ratios > ~0.8 (Fig. 9), as seen also in younger silicic systems (e.g. Bishop Tuff, Chamberlain et al. 2014; Ongatiti and Kidnappers units, Cooper et al. 2014). U/Yb ratios show a positive relationship with Hf concentration (Fig. 9). The two Jurassic units and the early RBVG units have a wide inter-grain variation of U/Yb ratio, between around 0.4 and 3.0. A decline in U/Yb values to <1.5, is found in the later RBVG units and Pan Long Wan trachydacite. Zircons from the remaining KSCVG samples have a slightly higher U/Yb ratio (~0.1 to 2.5), but the correlation with Hf concentration is less well-defined.

Molar (total 3^+)/P ratio. Values of the molar ($Y+REE^{3+}$)/P ratio around 1.0 led to the proposed 'xenotime' substitution mechanism for trivalent trace elements in zircons, coupled with P incorporation for charge balancing (Speer 1980). Departure of the ($Y+REE^{3+}$)/P ratio from unity has, however, now been widely recognised (e.g. Finch et al. 2001; Hoskin and Schaltegger 2003; Chamberlain et al. 2014; Cooper et al. 2014). Here, the molar ($Sc+Y+REE^{3+}$)/P ratios in most samples range between 1 and 6 (Table 4), with some grains, especially from plutonic samples, having values up to ~9 (e.g. Mount Butler Granite, HK13407). When plotted against Yb, U, Hf, or Ti concentrations or U/Yb ratios, in many cases two arrays are apparent which reflect sector zoning (cf. Chamberlain et al., 2014). Values of the (Sc+Y+REE^{3+})/P ratio become more scattered with higher U and Hf concentrations and U/Yb ratios.

DISCUSSION

Limitations on the SIMS age data sets

The previous geochronological framework of volcanic-plutonic assemblages in Hong Kong was established using single- or multi-crystal ID-TIMS techniques with high analytical precision (normally <0.2% 2 s.d.; Davis et al. 1997; Campbell et al. 2007; Sewell et al. 2012b). Here, we employ statistical treatments on a larger quantity of spatially-constrained SIMS U-Pb age deteminations to improve the precision towards that of the ID-TIMS ages (e.g. Crowley et al. 2007; Chamberlain et al. 2014). Modern analogues show that the replenishment times of volcanic systems following eruptions, as measured from zircon age spectra, are usually less than 10^3 to 10^5 years (e.g. Taupo Volcanic Zone: Charlier et al. 2005; Wilson and Charlier 2009; Charlier and Wilson 2010; Storm et al. 2012; Barker et al. 2014; Cooper et al. 2014; Rubin et al. 2016). In addition, field data and crystal specific studies demonstrate that magmatic processes in modern caldera systems operate on time-scales of months to >10^5 years (e.g. Barker et al. 2015, 2016; Allan et al. 2017 for Taupo volcano). These timeframes imply that for the Mesozoic systems in Hong Kong, even with the ± 0.2-0.3 Myr resolution of ID-TIMS ages, detailed linkages of individual volcanic and plutonic units and the dynamic processes within magmatic system cannot be discerned. Within the limits of precision, the geochronological data presented here nonetheless provide insights into the longer-term evolution of silicic systems over timescales of 10^6 to 10^7 years and can address the lifespan and the demise of volcanism in an arc system.

Comparisons between the new SIMS age data and published ID-TIMS ages

The data presented here reveal the presence of two groups: samples that yield normally-distributed unimodal age spectra, and those that show multiple age components, with the implication that there are inherited components (Table 3).

Samples showing unimodal age datasets. An important observation is that five of the unimodal age data sets yield weighted mean ages that are the same within error to their published ID-TIMS ages (Table 3). This concurrence of ages provides confidence that the ages of the relevant units are accurately defined. Such results also imply that where the two methodologies yield contrasting results, these reflect analytical issues (e.g. Pb loss) or genuine differences in the age spectra.

Three interpretations are possible. First, these samples essentially lack any inherited grains recycled from pre-existing crustal materials, possibly because the silicic magmas were fractionated directly from hot, mafic sources. This interpretation implies that all the zircons analysed were newly crystallised, and that new crust was formed by these magmatic events. Second, generation of the magmas involved partial melting of existing crust, but all recycled zircons, if present, were completely re-dissolved. Such complete resorption could be caused by zircon-undersaturation, either through increased magma temperatures and/or by influx of less evolved melts (Watson and Harrison 1983; Reid et al. 2011; Boehnke et al. 2013). Third, inherited grains are present but the age variations between different zircon domains defined by CL tones are too small to be resolved by SIMS (and obscured by ID-TIMS) techniques. For comparison, mean age differences between zircon cores and CL-light rims in the Bishop Tuff are $<10^4$ years (Chamberlain et al. 2014). In those Hong Kong samples with a single age component, some (e.g. HK12022) yield zircon with discrete resorbed cores (i.e. Types A and B: Fig. 2) visible in CL images, but the age of these cores are analytically indistinguishable from the rims.

Samples with multiple age-components. From both the new SIMS and the previous ID-TIMS age data, inherited grains are apparent in 14 of the 21 samples studied here (Table 3). Note that five samples (volcanic HK11052, HK13275, HK12070, HK13277; plutonic HK11042) yielded multiple age components (inheritance) that was not identified in the ID-TIMS studies. Inheritance ages from these 14 samples are either late Mesozoic, or much older (Palaeozoic to Archean). For the late Mesozoic grains, age modes from Sambridge and Compston (1994) mixture modelling methods (as utilised in Isoplot) are broadly coincident with the major local magmatic episodes identified by Davis et al. (1997) and Sewell et al. (2012b). These zircons (or parts thereof) thus are interpreted to represent crystals that grew in earlier magmatic pulses and were later recycled (cf. Bacon and Lowenstern 2005; Charlier et al. 2005).

Some zircon cores, from both volcanic and plutonic units, yielded Palaeozoic to Archean ages (Table 3), the oldest being ~ 2.8 Ga (HK12025: Shing Mun ignimbrite). These grains are xenocrysts, incorporated from the host basement rocks. They do not represent any of the Yanshanian episodes. The Kowloon and Mount Butler granites also yield Neo-Proterozoic and Palaeo-Proterozoic grains, respectively, showing the presence of basement rocks of these ages beneath this part of Hong Kong, as proposed by Fletcher et al. (1997) and Darbyshire and Sewell (1997).

For volcanic units that yield multiple age components, the weighted means of rim analyses provide the best estimate of eruption age, but these are often younger than their respective ID-TIMS ages. The clearest cases are the RBVG units, which have weighted mean SIMS rim ages between 0.5 Myr and ~2 Myr younger. The Pan Long Wan trachydacite lava (HK13277) also has multiple age components, but the rim age (141.0±1.3 Ma) is indistinguishable from the ID-TIMS age (Sewell et al. 2012b). The SIMS age data thus suggest that the RBVG units represent a sequence of eruptions covering ~143-141 Ma, which were closely followed by the Pan Long Wan trachydacite that overlies the RVBG. There are two obvious explanations for the differences between SIMS and ID-TIMS age estimates. First, in the ID-TIMS studies zircon grains were pre-treated by either air abrasion (Krogh 1982) or chemical abrasion (Mattinson 2005) before they were dissolved for analysis (Davis et al. 1997; Campbell et al. 2007; Sewell et al. 2012b). Both methods, however, unavoidably remove some geochronological information present in the crystals. Second, the ID-TIMS techniques required dissolution of single grains or a group of grains for age determination (Davis et al. 1997; Campbell et al. 2007; Sewell et al. 2012b). In the Hong Kong rocks, however, the presence of older zircon cores (antecrysts and/or xenocrysts) is common, based on observations from our CL images as well as from the SIMS age data. The reported ID-TIMS ages therefore represent averaged values for the grain or grains, obscuring any age variations present that had survived the pre-treatment process. Both the pre-treatment processes and the averaging effect of the ID-TIMS methods inhibit a sound estimate of crystallisation ages in cases where multiple age components are present.

Effects of high U contents on zircon U-Pb ages. Some samples (volcanic and plutonic) show younger peak ages for analyses for the cores than the rims (Figs. 3 to 8), usually from cores that are U-rich. There are two explanations for this: matrix effects in the analytical protocols (White and Ireland 2013), or Pb gains/losses associated with metamictization. Matrix effects in isolation cause an apparent increase in age of high-U zircon grains (White and Ireland 2013), but almost all dated grains in the Hong Kong samples yield U concentrations (Table 4) well below the values at which matrix effects were considered to be present by them. However, if the SIMS

U-Pb age data are plotted against U contents there are sometimes distinct trends (Figs. 3 to 8). In some grains with >1,000 ppm U the ages form a younging trend with increasing U concentration. We thus consider there to be a bias in U-Pb ages caused by Pb loss in some of higher-U analyses, which happen also to be in crystal cores. The Pb-losses are attributed to metamictization of the higher-U domains, coupled with Pb leaching during later hydrothermal events that are inferred from thermochronology (Tang et al. 2014) and seen in the alteration mineralogy (e.g. epidote and chlorite from the breakdown of primary ferromagnesian minerals) observed by us in the volcanic and plutonic rocks. The weighted mean ages of the rim analyses from the above samples are thus inferred to be more accurate estimates of the eruption or final solidification ages of the units. However, not all high-U grains appear to yield inconsistent, young ages and also some grains with only several hundred ppm U still yield <140 Ma ages. The latter occur particularly in the Kowloon and Mount Butler granites and are interpreted to represent magmatism occurring as late as ~138 Ma (Table 3).

Implications for the magmatic cycles in Hong Kong. With our SIMS age data, the earlier ID-TIMS geochronology of the Mesozoic magmatic episodes in Hong Kong (Davis et al. 1997; Campbell et al. 2007; Sewell et al. 2012b) can be reconsidered. First, we suggest that the RBVG, instead of being a single pulse of volcanism at ~143 Ma, reflects eruptions from ~143 to 141 Ma that were followed closely by the Pan Long Wan trachydacite lava and other KSCVG units. Two plutonic units, the Shui Chuen O and Chi Ma Wan granites (Cheung Chau Suite: Table 1), were originally considered as the plutonic equivalents of the RBVG (Sewell et al. 2000, 2012b). These two plutons yield SIMS ages that are younger than the ID-TIMS ages (Table 3), implying that a discrete ~143 Ma pulse of granitic intrusions (corresponding to RBVG eruptions) is absent and that the pairing of the RBVG with the Cheung Chau Suite intrusions is no longer valid.

Second, the final solidification age estimates of some plutonic rocks are also shifted. The Kowloon and Mount Butler granites are inferred here to have ages at 139.1±1.0 Ma and 137.8±0.8 Ma, respectively, >1 Myr younger than the eruption ages of the previously linked KSCVG units, inferred here to be ~141-140 Ma. These age differences imply that that the volcanic and plutonic components were not coeval, and not necessarily co-genetic even if the rocks spatially overlap (cf. Sewell et al. 2012a). In contrast the Sok Kwu Wan and Chi Man Wan granites and D'Aguilar and Tong Fuk quartz monzonites all yield age estimates at ~140 Ma (Table 3), closely matching the eruption ages of the KSCVG units, and implying a peak in the magmatic flux at that time. Third, the SIMS data for the Shui Chuen O Granite yield a unimodal pattern with an estimated final solidification age of 141.9±0.8 Ma, i.e. younger than the published ID-TIMS age (Table 3). However, the ID-TIMS studies identified the presence of multiple age components, separated by <1 Myr, in this pluton (Sewell et al. 2012b; Fig. 7A), a range that is not resolvable in SIMS analyses. Instead of being generated as a single intrusion at ~144 Ma, the pluton probably underwent multiple stages of thermal waxing and waning before a final crystallisation event at ~142 Ma.

Petrogenetic information from zircon textural and trace element information

A wide range of zircon growth patterns and textures in different units implies a corresponding diversity in the magmatic systems. Here we discuss the zircon trace element variations in different growth zones, especially core-versus-rim relationships.

CL-dark cores and bright rims. The Ap Lei Chau (HK11840) and Che Kwu Shan (HK11836) ignimbrites and Pan Long Wan (HK13277) trachydacite lava belong to this group (~60-70% of the zircons show this pattern: Table 3, Fig. 2). Of these, the Pan Long Wan lava exhibits the clearest variations (Fig. 10): cores have significantly higher Hf, U, Th, total 3+ trace elements and lower Ti than rims. Significant proportions of the cores from the Ap Lei Chau (31%) and Che Kwu Shan (27%) ignimbrites are CL-dark and rounded (Type A cores: Table 2) and have trace element signatures like those of the Pan Long Wan lava (HK13277; 48%: Fig. 10). Some dark cores from the two ignimbrites plot similarly to the Pan Long Wan lava in the Eu/Eu*, Ti and U/Yb versus Hf, and Y versus Nd plots (Fig. 10). In addition, some cores from all three units yield similar inheritance ages of ~143-162 Ma (Table 3). CL-bright rims in these three samples show similarly low Hf, U, Th and higher Ti abundances (as a proxy of melt temperature). The dark cores are inferred to have been entrained into hotter and less-evolved melts in which they were partly resorbed then overgrown. Similar features, although without resorption, occur prominently in late-erupted Bishop Tuff zircons (Chamberlain et al. 2014). In the Hong Kong examples, the assembly process must have been rapid, or otherwise the entrained grains would have wholly dissolved (cf. Charlier et al. 2005, 2010). Furthermore, similarities in trace element signatures and CL appearances suggest that the zircon cores of the three volcanic units came from a single plutonic source, which was reactivated and mobilised to yield the volcanic units.

Apart from these volcanic samples, the D'Aguilar and Tong Fuk quartz monzonites also yield zircon populations dominated (~60-80%: Table 2) by 'dark core-light rim' textures. Such zircon textures have rarely been reported from plutonic rocks (e.g. Poller et al. 2001; Corfu et al. 2003; Wang et al. 2012). Most of these cores (which are of similar age to the rims) were resorbed and rounded (i.e. Types A or B in Table 2) prior to being overgrown by CL-light rims, the occurrence of which implies that the plutons finally crystallised from higher-temperature and/or less-evolved melts.

CL-light cores and dark rims. The Lantau, Chi Ma Wan, Kowloon and Mount Butler granites have significant proportions (~40-80%) of grains with CL-dark rims and -light cores. Some volcanic samples also yield less abundant proportions of grains with similar textures (Table 2). The dark CL-growth zones are enriched in U, Th, Hf and total 3+ elements coupled with low Ti concentrations, collectively interpreted to reflect crystallisation from cooler, more-evolved melts and corresponding to the thermally waning stage of the relevant magmatic system. In particular, the Mount Butler Granite zircons record exceptional rimward enrichments of Hf and U reflecting extended fractionation before final solidification, consistent with the highly evolved geochemistry of the unit (Sewell and Campbell 1997, 2001).

Structureless cores. Zircon populations of the Clear Water Bay Formation and High Island Tuff include euhedral cores (Type C cores: ~20-30%: Table 2), some of which show vague, thin (generally <10 μm), CL-light, resorption boundaries. Unlike in the Pan Long Wan trachydacite, however, zircon cores (both types B and C) and rims from these two units have identical trace element characteristics and the SIMS core and rim ages are indistinguishable (Fig. 6). The thin resorption boundary around the cores is interpreted to represent a transient change in environment (e.g. minor changes in melt temperature and/or composition: e.g. Reid et al. 2011), rather than reflecting major recycling or resorption events because of the compositional similarity of the subsequent overgrowths. The SIMS age data also show that the High Island Tuff does not contain any inheritance signature.

Zircons with complex zoning textures. Some units yield a wide variety of zircon textures and complex resorption boundaries. In cores from the Lantau Granite and East Lantau porphyry, and Shing Mun, Lantau, Long Harbour and Mount Davis ignimbrites, there is a combination of various types of cores and CL intensities. The undifferentiated Kau Sai Chau ignimbrite zircons exhibit the widest range in CL intensity (Table 2), which is also reflected in notably large ranges in trace element concentrations when compared to other volcanic units (except the Pan Long Wan trachydacite: Table 4). The complexity of these zircon textures, with evidence of inherited cores (antecrystic or xenocrystic cores with multiple age components), reflects multiple episodes of zircon growth and resorption, sometimes with distinct trace element patterns. Zircons from the Kowloon Granite exhibit systematic trace element variations that can be linked with specific CL-dark growth zones, characteristically lacking oscillatory zoning. These intermediate growth zones are distinctive; higher in Hf, U, total 3+ elements and Yb/Gd ratios, lower in Ti concentrations and Th/U ratios and with a deeper Eu/Eu* anomaly (<0.1) (Fig. 11). These zircons are inferred to have experienced a more-evolved, cooler melt when compared with earlier or later stages, consistent with a magmatic system that was cooling towards full crystallisation before being rejuvenated as seen in the CL-lighter rims. Intermediate dark-CL growth zones with similar characteristics and inferred origins are common in the Long Harbour and Mount Davis ignimbrites (Type B zircon cores: 50% and 62% of all grains respectively: Table 2). Analysed examples of the associated cores yield ages of ~144-146 Ma and ~165 Ma (Table 3), implying that they were recycled from earlier magmatic episodes.

Role of sector zoning on trace element patterns. The effects of sector zoning on distributions of trace elements in zircons are important, especially when considering such parameters as Ti-in-zircon temperatures (e.g. Corfu et al. 2003; Reid et al. 2011; Chamberlain et al. 2014; Cooper et al. 2014). Several factors have been proposed to explain sector zoning (e.g. Paterson and Stephens 1992; Hanchar and Miller 1993; Watson and Liang 1995; Vavra et al. 1996). Here, sector zoning in the volcanic and plutonic zircons (Fig. 12) is most marked in plots of total 3+ elements and the molar total 3+/P ratio versus U, where two sub-parallel arrays are generally evident (cf. Chamberlain et al. 2014). Note that for some trace elements and their ratios, the variations across dark-light sectors are non-systematic, i.e. particular trace elements may show enrichment, depletion or no difference in dark versus light sectors in individual grains, as seen in the variable gradients (negative/positive) of tie-lines connecting data within individual grains (Fig. 12). Cooper et al. (2014) reported that the CL-lighter sectors from the Kidnappers ignimbrite (New Zealand) generally returned molar ratios of total 3+/P close to unity, independent of Yb or Hf concentrations, and as such approximated to the 'xenotime substitution' (Hoskin and Schaltegger 2003). Hong Kong samples, in contrast, yield total 3+/P molar ratios of 1-3 in the lighter sectors and show gentle positive trends with increasing Hf, U and Yb. The positive trends reflect either a different substitution mechanism or, more likely, a relative depletion of P with the enrichment of trivalent elements in the progressively more evolved melt (higher Hf or U). In such more evolved melts, charge balancing with the incorporation of trivalent trace elements thus has to be through mechanisms other than the 'xenotime substitution' (Hoskin and Schaltegger 2003).

Xenocrysts versus antecrysts: inheritance patterns in the age and trace element data

The presence of inherited zircons or parts thereof, identified from age data or contrasting trace element abundances, provides direct evidence for involvement (recycling) of crustal materials in the Hong Kong magmatic systems. The inherited grains can be xenocrysts, sourced from older, unrelated host rocks, or antecrysts, derived from crystal mush or from rejuvenated fully crystallized plutons of earlier magmatic episodes (Mahood 1990; Charlier et al. 2005). Based on CL imagery, 34-85% of grains contain noticeable cores (Table 2), and on that basis alone, there could be significant amounts of inheritance. Here, age and trace element data are used to see whether origins of these diverse cores could be distinguished.

For late Mesozoic inherited cores, whether they are considered as antecrystic or xenocrystic depends on the time gap between their growth and remobilisation, and the extent to which the two magmatic events are geochemically linked. The distinction may thus be challenging. For example, the 137.8±0.8 Ma Mount Butler Granite contains inherited zircon cores of Mesozoic (~160 Ma) and Palaeoproterozoic (~2.1 Ga) ages (Table 3). The Mesozoic inherited grains are here interpreted as antecrysts, i.e. remobilised from precursor crystal mush or plutons of earlier magmatic episodes (cf. Bacon and Lowenstern 2005; Charlier et al. 2005; Miller et al. 2007; Gaschnig et al. 2010), despite being ~20 Myr older than the host granite. A large age gap between the cores and host units was, however, used as a key criterion for discriminating xenocrysts and antecrysts in other studies, albeit on younger systems (e.g. Bacon and Lowenstern 2005; Charlier et al. 2005; Miller et al. 2007).

Our data thus suggest that survival of whole or partial zircons in successive magmatic episodes implies that the magmatic conditions of these inheritance-bearing units did not greatly exceed those for zircon saturation (cf. Miller et al. 2003; Charlier et al. 2010). In addition, the presence of inheritance implies that the crystallisation ages of zircons may differ from their eruption or final solidification ages as normally considered. The presence of multiple zircon age components in some of the granitic plutons in Hong Kong has thus led to complications in interpreting the age data from ID-TIMS versus SIMS techniques.

Some cores that are inferred to be xenocrystic from age data show distinctly different trace element characteristics (Fig. 13). Xenocrystic 1.1-2.8 Ga cores from the Shing Mun ignimbrite (Fig. 13A) in general show broader ranges and more variable trace element characteristics than the rims. These xenocrystic cores are commonly distinctive, characterised by dark CL emission with oscillatory zoning and complex multiple resorption boundaries (i.e. Type B cores), implying multiple recycling and growth stages. Some cores were surrounded by CL-lighter intermediate growth zones that plot within the main trace element trends and yield ages broadly similar to the weighted mean age of the unit (i.e. ~164 Ma, Table 3). The light-CL zones are therefore likely antecrystic. Similarly, the undifferentiated Kau Sai Chau ignimbrite (Lantau caldera) also yields xenocrystic grains with trace element characteristics that deviate from the main trends (Fig. 13B).

Variations in trace element patterns through time

Here, we use the trace element signatures of volcanic zircons to track the evolution of the Middle Jurassic to Early Cretaceous Yanshanian magmatic episodes in Hong Kong. Since zircon cores show wider compositional variations (Table 4), due in part to their inherited nature, only rim analyses are used. Variations in the ranges of Sc, Ti and Hf concentrations and Th/U, Yb/Gd and U/Yb ratios (e.g. Barth et al. 2013) are used to see if there are temporal changes in evolution of the crust and magmatic systems (Fig. 14). In general, zircon trace element data from all units exhibit similar, partly overlapping trends, but the two Jurassic units (Shing Mun and Lantau ignimbrites) have narrower ranges than the younger RBVG and KSCVG units (Table 4). Generally higher Hf concentrations occur in zircons from the two Jurassic units together with the RBVG units (Long Harbour and Mount Davis ignimbrites, Fig. 14). Sc shows a general increase from the oldest Shing Mun ignimbrite, through the Lantau tuff and the RBVG units.

A decrease in Sc with increasing Hf (i.e. melt evolution) has been used to imply the co-crystallisation of amphibole and biotite, and vice versa (e.g. Barker et al. 2014; Cooper et al. 2014). The relatively low and stable Sc concentrations in zircons from the Shing Mun and Lantau ignimbrites suggest either fractionation of Sc-bearing phases (particularly amphibole) or depletion of Sc in the source. In contrast, the gradual increase in Sc for the RBVG units and Pan Long Wan trachydacite implies a limited involvement of amphibole fractionation. However, zircons from the remaining KSCVG units show no obvious trend in Sc versus Hf, despite having the highest Sc abundances (~50-260 ppm: Table 4). Combined with an apparent increase in melt temperatures as monitored by Ti concentrations, dissolution of Sc-bearing phases may have contributed to the higher levels of Sc in zircons from these later units (cf. Barker et al. 2014).

Elemental ratios (e.g. Yb/Gd, Th/U, U/Yb) have been used as tracers of sources and magmatic evolution (e.g. Barth et al. 2013; Cooper et al. 2014; Grimes et al. 2015). Zircons from the Shing Mun ignimbrite and the RBVG are characterised by generally higher Yb/Gd and U/Yb, and lower Th/U ratios. In contrast, zircons from the younger Lantau ignimbrite and KSCVG units give a lower range of Yb/Gd and U/Yb ratios (Fig. 14), inferred to reflect HREE-depletion involved in their melt generation. The decrease in Yb/Gd ratios in these units may reflect either (1) host melts from sources where fractionation of higher pressure mineral assemblages including garnet and/or amphibole occurred, or (2) partial melting of lower crustal rocks by mantle-derived magmas, with garnet in the residue. Although there are several issues associated with quantitative Ti-in-zircon thermometry (e.g. Chamberlain et al. 2014), Ti concentration can be used as a general tracer, with Ti decreasing as Hf increases, reflecting in part decreasing temperatures during melt evolution (e.g. Claiborne et al. 2006; Ferry and Watson 2007; Barth and Wooden 2010). Our data thus suggest that magmatic temperatures were higher and/or Ti activities lower for the younger KSCVG units than the older volcanic units (Figs. 9, 14), including the Shing Mun and Lantau ignimbrites and RBVG units. Similar inferences apply to the Ti-richer bright CL rims of the Che Kwu Shan and Pan Long Wan zircons, plus grains from the undifferentiated Kau Sai Chau ignimbrite from Lantau caldera complex.

Temporal relationships of volcanic and plutonic units

Repulse Bay Volcanic Group (RBVG) – Cheung Chau Suite. Overall, the SIMS ages match the field stratigraphic relationships of the volcanic units (Sewell et al. 2012a; Tang 2016). In cases where the ages of units overlap within error, field relationships have been decisive in interpreting the stratigraphy and age data. SIMS ages of the RBVG units overlap at 95% confidence, although field evidence shows that the Mount Davis Formation is overlain by the Long Harbour, Ap Lei Chau and Che Kwu Shan ignimbrites (Sewell et al. 2012a; Tang 2016). The RBVG and Cheung Chau Suite rocks were previously interpreted as coeval at ~143 Ma (Sewell et al. 2000, 2012b; Campbell et al. 2007). The SIMS age data (Table 3), however, imply that the RBVG represents eruptions spaced over ~143 to 141 Ma, rather than representing a single ~143 Ma pulse of volcanism. The Cheung Chau Suite was previously linked to the RBVG based on comparable ages from ID-TIMS determinations and whole rock geochemistry (e.g. Sewell et al. 2000, 2012a, b). However, SIMS ages of Shui Chuen O and Chi Ma Wan granites presented here are 141.9±0.8 Ma and 140.0±1.0 Ma, respectively, (Table 3). Our age data preclude any links between these two intrusions and the RBVG and suggest that their inclusion in the Cheung Chau Suite be reconsidered.

Kau Sai Chau Volcanic Group – Lion Rock Suite. Our SIMS data confirm that the KSCVG was erupted from ~141-140 Ma. The post-High Island lava is dated at 139.6±0.5 Ma (Table 3), consistent with it overlying the 140.9±0.4 Ma High Island Tuff. The Sok Kwu Wan Granite and D’Aguilar Quartz Monzonite are closely geographically related to the High Island caldera perimeter (Fig. 1) and yield indistinguishable SIMS ages of 140.7±1.2 Ma and 140.8±1.4 Ma, respectively (Table 3). The Kowloon and Mount Butler granites crystallized at 138.9±1.5 Ma and 137.8±0.8 Ma, respectively, 2-3 Myr after the eruption of the KSCVG, but consistent with their relative ages from field relationships (Strange and Shaw 1986; Sewell et al. 2000; Tang 2016). The previously proposed temporal linkage of these two plutons with the KSCVG is thus considered incorrect. Even though emplaced within the High Island caldera, the two plutons are inferred to represent separate, independent magmatic pulses emplaced at shallow levels in the crust.

Comparisons between volcanic and plutonic records from the High Island caldera complex

It is widely supposed that volcanic rocks represent short-lived snapshots of their magmatic systems whereas plutonic rocks record much longer evolutionary histories, including near- and sub-solidus processes (e.g. Glazner et al. 2004; Hildreth 2004; Bachmann et al. 2007; Lipman 2007; Miller et al. 2007; Barth et al. 2012; Davis et al. 2012; Lundstrom and Glazner 2016). Here zircon trace element patterns from the volcanic and plutonic units of the High Island caldera complex are compared and contrasted.

Volcanic records. Within the RBVG, zircons in the younger Ap Lei Chau and Che Kwu Shan ignimbrites grade in their rims towards lower Hf, U and Th, but higher Ti concentrations than the older Mount Davis and Long Harbour ignimbrites (Fig. 15). In the Eu/Eu* versus Hf plot, data from the younger two ignimbrites diverge into two groups: one (50-60% of analyses) trends in common with the older two ignimbrites and the other (50-40% of analyses) with the younger Pan Long Wan trachydacite (Figs. 9, 15). The Ap Lei Chau and Che Kwu Shan ignimbrites contain zircons with notable numbers of CL-bright rims, suggestive of later-stage magmatic reactivation by hotter, less evolved melts. All the KSCVG units, except the Pan Long Wan lava, have similar zircon trace element patterns that are largely distinct from those of the underlying RBVG sequence. The KSCVG zircons have generally lower Hf, U, Th and REE concentrations than those of the RBVG (Table 4), and show smaller ranges and lower values of Th/U and Yb/Gd ratios (Table 4; Fig. 15). The RBVG and KSCVG are thus inferred to represent two spatially-overlapping and temporally closely successive magmatic systems (Table 3), with a transition shown by melts that gave rise to the CL-brighter rims on the younger two RBVG ignimbrites and the Pan Long Wan lava (Fig. 15). Plots of the Eu-anomaly against Hf concentrations (Fig. 15) illustrate two aspects of the KSCVG magmatic system: (1) Eu/Eu* values around 1.0 or greater from some analyses, implying possibly melting of feldspar in the source and (2) steep gradients in Eu/Eu* versus Hf, implying strong feldspar fractionation during melt evolution.

Plutonic records. As in the volcanic units, trace elements from the plutonic zircons (Fig. 16) fall on two trends, corresponding to those of the RBVG and KSCVG individually, and defining two groups: 1, Shui Chuen O, Kowloon and Mount Butler granites and 2, Sok Kwu Wan Granite and D'Aguilar Quartz Monzonite. Overall, zircons from group 1 units yield wider ranges in Hf, Y, total 3+, Th and U concentrations than group 2 units. In particular, Hf variations from group 1 (~5,000-23,000 ppm) are notably greater than in group 2 (~6,000-13,000 ppm: Table 4) implying that the former saw higher degrees of melt fractionation during development. Consistent with this interpretation, larger inter-grain variations Th/U, Yb/Gd and U/Yb ratios (e.g. Barth and Wooden 2010) are also evident in group 1 units (Fig. 16). Maximum Ti concentrations are in general higher in group 2 zircons than in group 1 (Table 4), inferred to reflect hotter, and/or less-evolved, and/or more TiO_2-rich melts in the former. In a Eu/Eu* versus Hf plot (Fig. 16), data from group 2 units form an array with a steeper gradient than those from Group 1 units, interpreted to reflect stronger feldspar fractionation during melt evolution.

In their zircon trace element patterns the group 1 plutonic units are most similar to those of the RBVG units (Fig. 16, left panels), despite their age differences (Table 3). Their trace element data always plot in the same fields, although the Kowloon and Mount Butler granites contain some grains with Hf up to ~21,000 ppm. These high-Hf grains are interpreted to reflect extensive fractionation as a result of zircon crystallization in the latest-stage melts when the temperature approached the solidus (Barth and Wooden 2010), with accompanying low Ti (1-2 ppm). The two compositional groups seen in the volcanic units are also seen in the separated arrays from the granites. Data from the Shui Chuen O Granite plot in similar fashion to the part of the Ap Lei Chau and Che Kwu Shan ignimbrites that is out of the main trend of the RBVG (cf. Fig. 15), whereas the Kowloon and Mount Butler granites overlap with the Long Harbour and Mount Davis ignimbrites. Zircons from group 2 units (Sok Kwu Wan Granite, D'Aguilar Quartz Monzonite), share similar trace element characteristics to the KSCVG units (excluding the Pan Long Wan trachydacite) (Fig. 16), matched by the similarity in age data.

"Cold-" and "hot-" granites in the Hong Kong record. Zircon inheritance characteristics of granites were discussed by Miller et al. (2003) in terms of zircon saturation temperature (T_{zr}), calculated from whole rock compositions using the Watson and Harrison (1983) thermometry. Here, we use the whole rock data (Sewell and Campbell 2001) to determine the T_{zr} for the granitic units studied here using the Watson and Harrison (1983) thermometry (Table 5) for comparison with the Miller et al. (2003) results. The applicability of zircon saturation thermometry to determine magmatic conditions, in particular for the Hong Kong samples which lack fresh minerals for other geothermometers, is questionable because the composition of the fully crystallized rock may differ greatly from that of the melt at the time of zircon crystallization. Nonetheless, the estimated temperatures provide broad indicators of magmatic conditions under which zircons behave in silicic melts (cf. Charlier et al. 2005; Reid et al. 2011; Barker et al. 2014).

Two groups of intrusive units are identified based on their averaged T_{zr} (Table 5), and their age patterns are presented in Table 3. The Lantau, Chi Ma Wan, Shui Chuen O, Kowloon and Mount Butler granites have averaged T_{zr} values from ~740-770 °C; whereas the Sok Kwu Wan Granite, and D'Aguilar and Tong Fuk quartz monzonites have averaged T_{zr} values from ~820-860 °C (Table 5). These two groups would be labelled as "cold" and "hot" granites, respectively, by Miller et al. (2003). This "cold/hot" subdivision matches the grouping of granitic plutons based on zircon trace element patterns here as well as whole rock geochemical patterns (Sewell and Campbell 2001). The "cold" granites are scattered at the highly fractionated end of the data sets, whereas the "hot" granites show clear fractionation trends comparable to those of the KSCVG units. The "hot" granites are thus inferred to be genetically related to those magma chambers that fed the KSCVG (Fig. 16). In contrast, the "cold" Kowloon and Mount Butler granites are here inferred to be not co-magmatic with the KSCVG units (cf. Sewell et al. 2012a).

Values of T_{zr} are also compared with apparent magma temperatures of the plutonic and volcanic units determined using Ti-in-zircon thermometry of Ferry and Watson (2007) with assumed $a\mathrm{SiO_2}$ and $a\mathrm{TiO_2} = 1$ (Table 5). For "hot" granites, our trace element data yielded Ti-in-zircon temperatures that are slightly lower or equal to T_{zr} of the units. For "cold" granites and the RBVG and KSCVG volcanic units, some of the analyses have yielded Ti-in-zircon temperatures > T_{zr}. However, zircon crystallization occurs only when the melt temperature falls below its T_{zr}. Therefore, either the apparent melt temperatures determined from Ti-in-zircon thermometry are overestimated (i.e. higher than the actual melt temperature), or the T_{zr} values based on Watson and Harrison (1983) are underestimated for these units. This discrepancy, among other concerns (see e.g. Fu et al. 2008; Chamberlain et al. 2014), illustrates the limitation of Ti-in-zircon thermometry for inferring melt temperature during zircon crystallization. In addition, the recently revised T_{zr} calibration by Boehnke et al. (2013) yields T_{zr} values in low Zr rocks that are significantly lower than the temperature estimates modeled from other geothermometers (e.g. Fe-Ti oxides, amphiboles, etc.; Barker et al. 2014).

Two groups of volcanic-plutonic products from the High Island caldera complex. Data presented here highlight two groups of volcanic-plutonic products in the magmatic system encompassed by the High Island caldera complex: the RBVG and "cold" granites, and the KSCVG and "hot" granites. Controls on the magmatic system(s) below the High Island caldera, however, cannot be fully established here, because the units available represent widely spaced snapshots of the ~3 Myr evolutionary history of the magmatic system. Two end-member scenarios are considered here for its development. First, the system operated as a single domain that varied in temperature, controlled by varying interaction of hotter melts. In this scenario, the two groups of volcanic-plutonic products record a series of random snapshots of the fluctuating magmatic system. The second scenario consists of two interacting crustal domains of contrasting temperature and broad compositional characteristics. The lower temperature domain dominated at first (e.g. Mount Davis and Long Harbour ignimbrites), but was gradually superseded by the higher-temperature domain that culminated in the high-silica rhyolites of the KSCVG.

Hong Kong perspectives on large silicic magmatic systems

Two contrasting end-member views exist on the volcanic-plutonic connections of large silicic systems (Lundstrom and Glazner 2016, for overviews). One considers volcanic rocks and sub-volcanic plutons to be genetically related and share a common magmatic origin (Bachmann and Bergantz 2004; Hildreth 2004; Hildreth and Wilson 2007). In this view, plutons represent either the non-erupted crystal mush or the remnant, crystal-dominated part of the system after withdrawal of rhyolitic melts (e.g. Smith 1979; Hildreth 1981; Shaw 1985; Bachmann et al. 2002; Bachmann and Bergantz 2004). The other model considers that voluminous ignimbrites are fed from transient magma chambers that are assembled very rapidly at shallow crustal levels during periods of intense heat influx and evacuate completely, thereby leaving very little plutonic record (Coleman et al. 2004; Glazner et al. 2004; Lipman 2007; Miller 2008). These views are discussed here from the Hong Kong perspective.

Volcanic-plutonic connections. Here, revised linkages of volcanic and plutonic units in the High Island caldera complex have been established. The generation of volcanic rocks ranging from crystal-rich dacitic to rhyolitic ignimbrites (of the RBVG) to trachytic to high-silica rhyolite (of the KSCVG) is inferred to represent the evacuation of different parts (in space) or developmental stages (in time) of the magma chambers (the mush zones or rhyolitic melts extracted therefrom). The divergence in volcanic compositions also points to separate modes of volcanic-plutonic connections in large silicic systems in Hong Kong, which can co-exist and spatially overlap.

The magma bodies for two earlier units of the RBVG (Long Harbour and Mount Davis ignimbrites, crystal-rich and with relatively high proportions of inherited zircons) are inferred to have been sourced from partial melting of older Yanshanian granites and basement rocks, and a crystal-dominated, long-lived magma chamber is inferred to have been present. Subsequent eruptions (Ap Lei Chau, Che Kwu Shan and Pan Long Wan) show evidence for input from less evolved, hotter sources but are linked, through their abundance of inherited zircon cores, with the earlier "cold" granites. The volcanic-plutonic links are considered to have been indirect, through recycling in younger volcanic units of older, contrasting zircons from the larger scale magmatic reservoir beneath the erupted magma bodies. The Shui Chuen O, Kowloon and Mount Butler granites (linked through their geochemical characteristics) are inferred to represent part of the recycled crustal materials that solidified without any significant eruptive equivalents.

The Hong Kong situation supports the idea that an influx of hotter magma to shallow crustal levels is important in the development of voluminous high-silica rhyolite melts (e.g. Bachmann et al. 2007; Lipman 2007; de Silva and Gregg 2014). The zircon trace element signatures of the Pan Long trachydacite suggest the arrival of hotter, less-evolved melts prior to the building up of the high-silica rhyolitic melts of the KSCVG units. Eruption of the voluminous High Island Tuff then probably evacuated the crystal-poor melt-dominant magma chamber almost completely, leaving behind only small amounts of melt. The KSCVG units and the Sok Kwu Wan and D'Aguilar plutons are considered to be genetically linked on the basis of their bulk compositions (Sewell and Campbell 1997, 2001) and indistinguishable zircon age spectra. These "hot" granites probably represent the residual magmas subsequently emplaced along major conduits (the caldera bounding structures). Volumes of these intrusions, estimated from their exposure areas, are relatively small, however, when compared with their eruptive counterpart, the High Island Tuff.

Lifespan of silicic magmatic systems. Studies of Mesozoic to Tertiary granitic batholiths in the western USA (particularly the Sierra Nevada) have led to proposals that they are composite bodies, assembled over several million years or more (e.g. Coleman et al. 2004; Glazner et al.

2004; Matzel et al. 2006; Walker et al. 2007; Gaschnig et al. 2010, 2017; Lipman and Bachmann 2015; Coleman et al. 2016). In Hong Kong, >20 mappable granitic plutons, stocks and dyke swarms were emplaced over a period of ~26 Myr (Davis et al. 1997; Sewell et al. 2000, 2012b; this paper). These granitic rocks are spatially juxtaposed within a limited geographic area, but are not necessarily genetically related. Several of the plutons (e.g. Kowloon and Mount Butler granites: ~68 and 25 km^2, respectively: Sewell et al. 2000) yield inherited zircons that are several to >20 Myr older than their final solidification ages (Table 3). Instead of interpreting those time spans simply as the duration of pluton growth, the age data are considered to be the overall result of repeated recycling of zircons from earlier, independent magmatic episodes that happen to spatially overlap. This interpretation highlights issues of the definition of zircon xenocrysts and antecrysts, and how to distinguish them in understanding the evolutionary history of a magmatic system, within the constraints imposed by the precision of dating techniques.

In addition, the estimated long-term emplacement rate of composite plutons, as inferred from geochronological data and thermal modelling, is asserted to be too low ((O)10^{-3} km^3/yr) to sustain the development of any large magma chambers (Coleman et al. 2004, 2016; Glazner et al. 2004; Annen 2009). The geochronological data presented here show that the modal peaks in ages from the units yielding either multiple age or unimodal age components generally match the ages of the previously identified major volcanic-magmatic episodes (Davis et al. 1997; Sewell et al. 2012b). These coincidences of age peaks suggest that there were periods of increased zircon crystallisation, reflecting the pulsating nature of the emplacement and cooling of intrusions as demonstrated elsewhere (e.g. Walker et al. 2007; Lackey et al. 2012). Therefore, it is inappropriate to use a long-term average emplacement rate for the growth of granitic bodies for the Hong Kong case, because such an average does not meaningfully reflect the specific timescales of any magmatic processes that operated. In particular, such averaged growth rates are inappropriate to decide whether or not a given pluton could have given rise to a substantial volume of volcanic products.

The age data also show that the lifespan of large silicic magmatic systems within this constrained area of the broader Southeast China Magmatic Belt extended over several million years. The match in ages of, for example, the KSCVG and the Sok Kwu Wan Granite and D'Aguilar Quartz Monzonite implies that both eruptive and intrusive units reflect confluent processes during sporadic periods of relatively intensive magmatism. This interpretation contrasts with that of Lipman (2007) who proposed that large volcanic eruptions occur during magmatic "flare-ups", i.e. higher magmatic influx, whereas plutonic rocks are emplaced in waning stages. In short, the emplacement of most granitic plutons in Hong Kong occurred during pulsed, more intense magmatic influxes related also to the creation of magma chambers that fed major eruptions.

IMPLICATIONS

We have presented SIMS U-Pb age and trace element data, coupled with CL imagery, from zircons extracted from 21 late Mesozoic volcanic and plutonic rock samples. We have used these data to investigate magmatic systems in Hong Kong, particularly those related to the early Cretaceous High Island caldera complex. Both volcanic and plutonic samples fall into two groups, one with a unimodal age population, the other with multiple age components. The unimodal age group shows contrasting cores under CL imagery in some grains, but age data cannot resolve any time gap and weighted means from the SIMS data are within error the same as those from published ID-TIMS data. The group with multiple age components, linked to textural observations, contains common antecrystic and/or xenocrystic cores recycled from earlier Yanshanian magmatic episodes or much older basement rocks. Fifteen samples yield SIMS weighted-mean ages younger than the ID-TIMS values. Although the values in most cases overlap with 95% confidence, the close matches of SIMS and ID-TIMS ages from samples with unimodal age distributions suggests that any differences are real. Such differences might arise through (1) air/chemical abrasion before ID-TIMS analysis removing some geochronological information, (2) ID-TIMS ages reflecting the average, not youngest age within the grains, or (3) U-rich zircons measured by SIMS being affected by Pb-loss.

Our new data show that magmatism shallow enough to now be exposed lasted until 137.8±0.8 Ma (Mount Butler Granite) and was unrelated to any surface volcanism. Thermochronological data further imply that subsurface magmatism continued until 100-80 Ma (Tang et al. 2014). We infer that volcanism for the Repulse Bay Volcanic Group (RBVG) and Kau Sai Chau Volcanic Group (KSCVG) associated with the High Island caldera complex represent continuous (within analytical uncertainties) magmatic activity over ~5 Myr, instead of distinct phases at ~143 and ~141-140 Ma, respectively (Davis et al. 1997; Sewell et al. 2000, 2012b). Some direct volcanic-plutonic linkages previously proposed (e.g. High Island Tuff and Kowloon Granite: Sewell et al. 2012a) are not supported by our age data, whereas other linkages (e.g. High Island Tuff and D'Aguilar Quartz Monzonite) are reinforced.

Zircon CL textures show wide ranges in growth patterns in both volcanic and plutonic zircons, indicative of widely variable crystallisation conditions and/or inheritance histories during development of the magmatic systems. Significant inter- and intra-grain variations occur in zircon trace element concentrations, both between cores and rims and between CL-bright (side) versus CL-dark (tip) sectors of grains, which cause complexities in interpretations (e.g.

Ti-in-zircon thermometry: cf. Reid et al. 2011; Chamberlain et al. 2014). Overall, trace element data from volcanic and plutonic samples indicate the presence of two groups of products at the High Island caldera complex: (1) the RBVG and "cold" granites, and (2) the KSCVG and "hot" granites (sensu Miller et al. 2003). Zircons from the former yield wider ranges in Hf, Y, Th, U and total trivalent element concentrations , and Th/U, Yb/Gd and U/Yb ratios than the latter. Larger ranges in Hf concentrations and a gentler gradient in a plot of Eu/Eu* versus Hf imply that the RBVG and "cold" granites spanned larger degrees of melt fractionation during their magmatic histories.

A widely perceived contrast between the volcanic and plutonic records (e.g. Glazner et al. 2004; Lundstrom and Glazner 2016) is bridged in the Hong Kong record. Plutons like the Kowloon and Mount Butler granites are unrelated to and younger than any volcanic outburst and represent separate, independent magmatic pulses. Other intrusions, like the Sok Kwu Wan Granite and D'Aguilar Quartz Monzonite, are in contrast closely linked to voluminous volcanism (the High Island Tuff in this case). The exposed "Hong Kong Pluton" thus represents a long-lived (26 Myr) composite of multiple magmatic systems, with frequent volcanic tappings, but also independently generated, shallowly emplaced plutonic components. In general, any dichotomy between the volcanic and plutonic records reflects a number of factors, not least of which is that the precision for age dating of rocks used to represent the plutonic record in nearly all examples is too coarse to capture the volcanic processes that can be inferred to operate in modern volcanic systems (and their plutonic roots) (e.g. Barker et al. 2014, 2015). Composite plutons, like those which occur beneath Hong Kong and elsewhere in the Southeast China Magmatic Belt, grow by increments. Their overall averaged growth rates are a misleading representation of complex, episodic and dynamic growth histories.

Acknowledgements

DLKT acknowledges support from a Victoria University Doctoral Scholarship. CJNW acknowledges support from the Royal Society of New Zealand (Cook Fellowship, Marsden Fund grant VUW0813) and Victoria University (University Research Fund). LSC acknowledges support from the research funding of the Department of Earth Sciences, HKU. We thank Matt Coble, Peter Holden and Brad Ito for their support in the ion probe laboratory work. DLKT and RJS publish with the permission from Head of Geotechnical Engineering Office and Director of Civil Engineering and Development Department. We thank Rich Gaschnig and Calvin Miller for their constructive comments, and Fang-zhen Teng for editorial handling.

References

Allan, A.S.R., Barker, S.J., Millet, M.-A., Morgan, D.J., Rooyakkers, S.J., Schipper, C.I., and Wilson, C.J.N. (2017). A cascade of magmatic events during the assembly and eruption of a super-sized magma body. Contributions to Mineralogy and Petrology, 172, 49.

Annen, C. (2009) From plutons to magma chambers: thermal constraints on the accumulation of eruptible silicic magma in the upper crust. Earth and Planetary Science Letters, 284, 409-416.

Bachmann, O., and Bergantz, G.W. (2004) On the origin of crystal-poor rhyolites: extracted from batholithic crystal mushes. Journal of Petrology, 45, 1565-1582.

Bachmann, O., and Bergantz, G.W. (2008) Rhyolites and their source mushes across tectonic settings. Journal of Petrology, 49, 2277-2285.

Bachmann, O., and Huber, C. (2016) Silicic magma reservoirs in the Earth's crust. American Mineralogist, 101, 2377-2404.

Bachmann, O., Dungan, M.A., and Lipman, P.W. (2002) The Fish Canyon magma body, San Juan volcanic field, Colorado: rejuvenation and eruption of an upper-crustal batholith. Journal of Petrology, 43, 1469-1503.

Bachmann, O., Miller, C.F., and de Silva, S.L. (2007) The volcanic-plutonic connection as a stage for understanding crustal magmatism. Journal of Volcanology and Geothermal Research, 167, 1-23.

Bacon, C.R., and Lowenstern, J.B. (2005) Late Pleistocene granodiorite source for recycled zircon and phenocrysts in rhyodacite lava at Crater Lake, Oregon. Earth and Planetary Science Letters, 233, 277-293.

Barker, S.J., Wilson, C.J.N., Smith, E.G.C., Charlier, B.L.A., Wooden, J.L., Hiess, J., and Ireland, T.R. (2014) Post-supereruption magmatic reconstruction of Taupo volcano (New Zealand), as reflected in zircon ages and trace elements. Journal of Petrology, 55, 1511-1533.

Barker, S.J., Wilson, C.J.N., Allan, A.S.R., and Schipper, C.I. (2015) Fine-scale temporal recovery, reconstruction and evolution of a post-supereruption magmatic system. Contributions to Mineralogy and Petrology, 170, 5.

Barker, S.J., Wilson, C.J.N., Morgan, D.J., and Rowland, J.V. (2016) Rapid priming, accumulation and recharge of magma driving recent eruptions at a hyperactive caldera volcano. Geology, 44, 323-326.

Barth, A.P., and Wooden, J.L. (2010) Coupled elemental and isotopic analyses of polygenetic zircons from granitic rocks by ion microprobe, with implications for melt evolution and the sources of granitic magmas. Chemical Geology, 277, 149-159.

Barth, A.P., Feilen, A.D.G., Yager, S.L., Douglas, S.R., Wooden, J.L., Riggs, N.R., and Walker, J.D. (2012) Petrogenetic connections between ash-flow tuffs and a granodioritic to granitic intrusive suite in the Sierra Nevada arc, California. Geosphere, 8, 250-264.

Barth, A.P., Wooden, J.L., Jacobson, C.E., and Economos, R.C. (2013) Detrital zircon as a proxy for tracking the magmatic arc system: the California arc example. Geology, 41, 223-226.

Black, L.P., Kamo, S.L., Allen, C.M., Davis, D.W., Aleinikoff, J.N., Valley, J.W., Mundil, R., Campbell, I.H., Korsch, R.J., Williams, I.S., and Foudoulis, C. (2004) Improved ^{206}Pb/^{238}U microprobe geochronology by the monitoring of a trace-element-related matrix effect; SHRIMP, ID–TIMS, ELA–ICP–MS and oxygen isotope documentation for a series of zircon standards. Chemical Geology, 205, 115–140.

Boehnke, P., Watson, E.B., Trail, D., Harrison, T.M., and Schmitt, A.K. (2013) Zircon saturation re-revisited. Chemical Geology, 351, 324-334.

Brophy, J.G. (1991) Compositional gaps, critical crystallinity, and fractional crystallization in orogenic (calc-alkaline) magmatic systems. Contributions to Mineralogy and Petrology, 109, 173-182.

Cameron, M., Bagby, W.C., and Cameron, K.L. (1980) Petrogenesis of voluminous mid-Tertiary ignimbrites of the Sierra Madre Occidental, Chihuahua, Mexico. Contributions to Mineralogy and Petrology, 74, 271-284.

Campbell, S.D.G., and Sewell, R.J. (1997) Structural control and tectonic setting of Mesozoic volcanism in Hong Kong. Journal of the Geological Society, London, 154, 1039-1052.

Campbell, S.D.G., Sewell, R.J., Davis, D.W., and So, A.C.T. (2007) New U-Pb age and geochemical constraints on the stratigraphy and distribution of the Lantau Volcanic Group, Hong Kong. Journal of Asian Earth Sciences, 31, 139-152.

Chamberlain, K.J., Wilson, C.J.N., Wooden, J.L., Charlier, B.L.A., and Ireland, T.R. (2014) New perspectives on the Bishop Tuff from zircon textures, ages and trace elements. Journal of Petrology, 55, 395-426.

Charlier, B.L.A., and Wilson, C.J.N. (2010) Chronology and evolution of caldera-forming and post-caldera magma systems at Okataina volcano, New Zealand from zircon U-Th model-age spectra. Journal of Petrology, 51, 1121-1141.

Charlier, B.L.A., Wilson, C.J.N., Lowenstern, J.B., Blake, S., Van Calsteren, P.W., and Davidson, J.P. (2005) Magma generation at a large, hyperactive silicic volcano (Taupo, New Zealand) revealed by U-Th and U-Pb systematics in zircons. Journal of Petrology, 46, 3-32.

Charlier, B.L.A., Wilson, C.J.N., and Mortimer, N. (2010) Evidence from zircon U-Pb age spectra for crustal structure and felsic magma genesis at Taupo volcano, New Zealand. Geology, 38, 915-918.

Claiborne, L.L., Miller, C.F., Walker, B.A., Wooden, J.L., Mazdab, F.K., and Bea, F. (2006) Tracking magmatic processes through Zr/Hf ratios in rocks and Hf and Ti zoning in zircons: an example from the Spirit Mountain batholith, Nevada. Mineralogical Magazine, 70, 517-543.

Claiborne, L.L., Miller, C.F., and Wooden, J.L. (2010) Trace element composition of igneous zircon: a thermal and compositional record of the accumulation and evolution of a large silicic batholith, Spirit Mountain, Nevada. Contributions to Mineralogy and Petrology, 160, 511-531.

Coleman, D.S., Gray, W., and Glazner, A.F. (2004) Rethinking the emplacement and evolution of zoned plutons: geochronologic evidence for incremental assembly of the Tuolumne Intrusive Suite, California. Geology, 32, 433-436.

Coleman, D.S., Mills, R.D., and Zimmerer, M.J. (2016) The pace of plutonism. Elements, 12, 97-102.

Cooper, G.F., Wilson, C.J.N., Wooden, J.L., Charlier, B.L.A., and Ireland, T.R. (2014) Temporal evolution and compositional signatures of supervolcanic systems recorded in zircons from Mangakino volcanic centre, New Zealand. Contributions to Mineralogy and Petrology, 167, 1018.

Corfu, F., Hanchar, J.M., Hoskin, P.W.O., and Kinny, P. (2003) Atlas of zircon textures. Reviews in Mineralogy and Geochemistry, 53, 469-500.

Crowley, J.K., Schoene, B., and Bowring, S.A. (2007) U-Pb dating of zircon in the Bishop Tuff at the millennial scale. Geology, 35, 1123-1126.

Darbyshire, D.P.F., and Sewell, R.J. (1997) Nd and Sr isotope geochemistry of plutonic rocks from Hong Kong: implications for granite petrogenesis, regional structure and crustal evolution. Chemical Geology, 143, 81-93.

Davis, D.W., Sewell, R.J., and Campbell, S.D.G. (1997) U-Pb dating of Mesozoic igneous rocks from Hong Kong. Journal of the Geological Society, London, 154, 1067-1076.

Davis, J.W., Coleman, D.S., Gracely, J.T., Gaschnig, R., and Stearns, M. (2012) Magma accumulation rates and thermal histories of plutons of the Sierra Nevada batholith, CA. Contributions to Mineralogy and Petrology, 163, 449-465.

de Silva, S.L., and Gregg, P.M. (2014) Thermomechanical feedbacks in magmatic systems: implications for growth, longevity, and evolution of large caldera-forming magma reservoirs and their supereruptions. Journal of Volcanology and Geothermal Research, 282, 77-91.

Ferry, J.M., and Watson, E.B. (2007) New thermodynamic models and revised calibrations for the Ti-in-zircon and Zr-in-rutile thermometers. Contributions to Mineralogy and Petrology, 134, 429-437.

Finch, R.J., Hanchar, J.M., Hoskin, P.W., and Burns, P.C. (2001) Rare-earth elements in synthetic zircon: Part 2. A single-crystal X-ray study of xenotime substitution. American Mineralogist, 86, 681-689.

Fletcher, C.J.N., Campbell, S.D.G., Carruthers, R.M., Busby, J.P., and Lai, K.W. (1997) Regional tectonic setting of Hong Kong: implications of new gravity models. Journal of the Geological Society, London, 154, 1021-1030.

Frazer, R.E., Coleman, D.S., and Mills, R.D. (2015) Zircon U-Pb geochronology of the Mount Givens Granodiorite: implications for the genesis of large volumes of eruptible magma. Journal of Geophysical Research: Solid Earth, 119, 2907-2924.

Fu, B., Page, F.Z., Cavosie, A.J., Fournelle, J. Kita, N.T., Lackey, J.S., Wilde, S.A., and Valley, J.W. (2008) Ti-in-zircon thermometry: applications and limitations. Contributions to Mineralogy and Petrology, 156, 197-215.

Gaschnig, R.L., Vervoort, J.D., Lewis, R.S., and McClelland, W.C. (2010) Migrating magmatism in the northern US Cordillera: in situ U-Pb geochronology of the Idaho batholith. Contributions to Mineralogy and Petrology, 159, 863-883.

Gaschnig, R.L., Vervoort, J.D., Tikoff, B., and Lewis, R.S. (2017) Construction and preservation of batholiths in the northern U.S. Cordillera. Lithosphere, 9, 315-324.

Glazner, A.F., Bartley, J.M., Coleman, D.S., Gray, W., and Taylor, R.Z. (2004). Are plutons assembled over millions of years by amalgamation from small magma chambers? GSA Today, 14 (4/5), 4-11.

Grimes, C.B., Wooden, J.L., Cheadle, M.J., and John, B.E. (2015) "Fingerprinting" tectono-magmatic provenance using trace elements in igneous zircon. Contributions to Mineralogy and Petrology, 170, 46.

Hanchar, J.M., and Miller, C.F. (1993) Zircon zonation patterns as revealed by cathodoluminescence and backscattered electron images - Implications for interpretation of complex crustal histories. Chemical Geology, 110, 1-13.

Hildreth, W. (1981) Gradients in silicic magma chambers: implications for lithospheric magmatism. Journal of Geophysical Research, 86, 10153-10192.

Hildreth, W. (2004) Volcanological perspectives on Long Valley, Mammoth Mountain, and Mono Craters: several contiguous but discrete systems. Journal of Volcanology and Geothermal Research, 136, 169-198.

Hildreth, W., and Wilson, C.J.N. (2007) Compositional zoning of the Bishop Tuff. Journal of Petrology, 48, 951-999.

Hoskin, P.W.O., and Schaltegger, U. (2003) The composition of zircon and igneous and metamorphic petrogenesis. Reviews in Mineralogy and Geochemistry, 53, 27-62.

Huber, C., Bachmann, O., and Dufek, J. (2011) Thermo-mechanical reactivation of locked crystal mushes: melting-induced internal fracturing and assimilation processes in magmas. Earth and Planetary Science Letters, 304, 443-454.

Huber, C., Bachmann, O., and Dufek, J. (2012) Crystal-poor versus crystal-rich ignimbrites: a competition between stirring and reactivation. Geology, 40, 115-118.

Krogh, T.E. (1982) Improved accuracy of U-Pb zircon ages by the creation of more concordant systems using an air abrasion technique. Geochimica et Cosmochimica Acta, 46, 637-649.

Lackey, J.S., Cecil, M.R., Windham, C.J., Frazer, R.E., Bindeman, I.N., and Gehrels, G.E. (2012) The Fine Gold Intrusive Suite: the roles of basement terranes and magma source development in the Early Cretaceous Sierra Nevada batholith. Geosphere, 8, 292-313.

Langford, R.L., James, J.W.C., Shaw, R., Campbell, S.D.G., Kirk, P.A., and Sewell, R.J. (1995) Geology of Lantau District. Hong Kong Geological Survey Memoir No. 6, Hong Kong, Geotechnical Engineering Office, Hong Kong Government.

Li, Z.X., and Li, X.H. (2007) Formation of the 1300-km-wide intracontinental orogen and postorogenic magmatic province in Mesozoic South China: a flat-slab subduction model. Geology, 35, 179-182.

Li, X.C., Sewell, R.J., and Fletcher, C.J.N. (2000) The dykes of northeastern Lantau Island. Geological Report, Geotechnical Engineering Office, Hong Kong SAR Government.

Lipman, P.W. (1984) The roots of ash flow calderas in western North-America: windows into the tops of granitic batholiths. Journal of Geophysical Research, 89, 8801-8841.

Lipman, P.W. (2007) Incremental assembly and prolonged consolidation of Cordilleran magma chambers: Evidence from the Southern Rocky Mountain volcanic field. Geosphere, 3, 42-70.

Lipman, P.W., and Bachmann, O. (2015) Ignimbrites to batholiths: integrating perspectives from geological, geophysical, and geochronological data. Geosphere, 11, 705-743.

Lipman, P.W., and McIntosh, W.C. (2008) Eruptive and noneruptive calderas, northeastern San Juan Mountains, Colorado: where did the ignimbrites come from? Geological Society of America Bulletin, 120, 771-795.

Ludwig, K.R. (2008) Isoplot/Ex version 3.70, A Geochronological Toolkit for Microsoft Excel. Berkeley Geochronology Center Special Publication 4.

Ludwig, K.R. (2009) User's Manual for Isoplot 3.75., A Geochronological Toolkit for Microsoft Excel. Berkeley Geochronology Center Special Publication 5.

Lundstrom, C.C., and Glazner, A.F. (Editors) (2016) Enigmatic relationship between silicic volcanic and plutonic rocks: silicic magmatism and the volcanic–plutonic connection. Elements, 12, 91-127.

Macdonald, R., and Smith, R.L. (1988) Relationships between silicic plutonism and volcanism: geochemical evidence. Transactions of the Royal Society of Edinburgh: Earth and Environmental Science, 79, 257-263.

Mahood, G.A. (1990) Second reply to comment of R.S.J. Sparks, H.E. Huppert, and C.J.N. Wilson on: 'Evidence for long residence times of rhyolitic magma in the Long Valley magmatic system: the isotopic record in the precaldera lavas of Glass Mountain'. Earth and Planetary Science Letters, 99, 395-399.

Mattinson, J.M. (2005) Zircon U-Pb chemical abrasion ("CA-TIMS") method: combined annealing and multi-step partial dissolution analysis for improved precision and accuracy of zircon ages. Chemical Geology, 220, 47-66.

Matzel, J.E.P., Bowring, S.A., and Miller, R.B. (2006) Time scales of pluton construction at differing crustal levels: Examples from the Mount Stuart and Tenpeak intrusions, North Cascades, Washington. Geological Society of America Bulletin, 118, 1412-1430.

Mazdab, F.K., and Wooden, J.L. (2006) Trace element analysis in zircon by ion microprobe (SHRIMP-RG): Technique and applications. Geochimica et Cosmochimica Acta, 70 (18, supplement), p. A405.

Miller, C.F., McDowell, S.M., and Mapes, R.W. (2003) Hot and cold granites? Implications of zircon saturation temperatures and preservation of inheritance. Geology, 31, 529-532.

Miller, J.S. (2008) Assembling a pluton...one increment at a time. Geology, 36, 511-512.

Miller, J.S., Matzel, J.E.P., Miller, C.F., Burgess, S.D., and Miller, R.B. (2007) Zircon growth and recycling during the assembly of large, composite arc plutons. Journal of Volcanology and Geothermal Research, 167, 282-299.

Paterson, B.A., and Stephens, W.E. (1992) Kinetically induced compositional zoning in titanite: implications for accessory-phase melt partitioning of trace-elements. Contributions to Mineralogy and Petrology, 109, 373-385.

Poller, U., Huth, J., Hoppe, P., and Williams, I.S. (2001) REE, U, Th, and Hf distribution in zircon from western Carpathian Variscan granitoids: a combined cathodoluminescence and ion microprobe study. American Journal of Science, 301, 858-876.

Quick, J.E., Sinigoi, S., Peressini, G., Demarchi, G., Wooden, J.L., and Sbisa, A. (2009) Magmatic plumbing of a large Permian caldera exposed to a depth of 25 km. Geology, 37, 603-606.

Reid, M.R., Vazquez, J.A., and Schmitt, A.K. (2011) Zircon-scale insights into the history of a supervolcano, Bishop Tuff, Long Valley, California, with implications for the Ti-in-zircon geothermometer. Contributions to Mineralogy and Petrology, 161, 293-311.

Rubin, A., Cooper, K.M., Leever, M., Wimpenny, J., Deering, C., Rooney, T., Gravley, D., and Yin, Q.-Z. (2016) Changes in magma storage conditions following caldera collapse at Okataina Volcanic Center, New Zealand. Contributions to Mineralogy and Petrology, 171, 4.

Sambridge, M.S., and Compston, W. (1994) Mixture modeling of multicomponent data sets with application to ion-probe zircon ages. Earth and Planetary Science Letters, 128, 373-390.

Schermer, E.R., and Busby, C. (1994) Jurassic magmatism in the central Mojave Desert: Implications for arc paleogeography and preservation of continental volcanic sequences. Geological Society of America Bulletin, 106, 767-790.

Sewell, R.J., and Campbell, S.D.G. (1997) Geochemistry of coeval Mesozoic plutonic and volcanic suites in Hong Kong. Journal of the Geological Society, London, 154, 1053-1066.

Sewell, R.J., and Campbell, S.D.G. (2001) Geochemical Data for Hong Kong Rocks. Hong Kong Geological Survey, Geotechnical Engineering Office.

Sewell, R.J., Darbyshire, D.P.F., Langford, R.L., and Strange, P.J. (1992) Geochemistry and Rb-Sr geochronology of Mesozoic granites from Hong Kong. Transactions of the Royal Society of Edinburgh: Earth Sciences, 83, 269-280.

Sewell, R.J., Campbell, S.D.G., Fletcher, C.J.N., Lai, K.W., and Kirk, P.A. (2000) The pre-Quaternary geology of Hong Kong. Civil Engineering Department, Hong Kong SAR Government, Hong Kong.

Sewell, R.J., Tang, D.L.K., and Campbell, S.D.G. (2012a) Volcanic-plutonic connections in a tilted nested caldera complex in Hong Kong. Geochemistry, Geophysics, Geosystems, 13, Q01006.

Sewell, R.J., Davis, D.W., and Campbell, S.D.G. (2012b) High precision U-Pb zircon ages for Mesozoic igneous rocks from Hong Kong. Journal of Asian Earth Sciences, 43, 164-175.

Shaw, H.R. (1985) Links between magma-tectonic rate balances, plutonism, and volcanism. Journal of Geophysical Research, 90, 11275-11288.

Sides, J.R., Bickford, M.E., Shuster, R.D., and Nusbaum, R.L. (1981) Calderas in the Precambrian terrane of the St. Francois Mountains, southeastern Missouri. Journal of Geophysical Research, 86, 10349–10364.

Smith, R.L. (1979) Ash-flow magmatism. Geological Society of America Special Paper, 180, 5-27.

So, A.C.T. (1999) Petrology and Geochemistry of Volcanic Rocks of the Lantau Peak Area, Lantau Island, Hong Kong. MPhil thesis, The University of Hong Kong.

Speer, J.A. (1980) Zircon. Reviews in Mineralogy and Geochemistry, 5, 67-112.

Stacey, J.S., and Kramers, J.D. (1975) Approximation of terrestrial lead isotope evolution by a two-stage model. Earth and Planetary Science Letters, 26, 207-221.

Storm, S., Shane, P., Schmitt, A.K., and Lindsay, J.M. (2012) Decoupled crystallization and eruption histories of the rhyolite magmatic system at Tarawera volcano revealed by zircon ages and growth rates. Contributions to Mineralogy and Petrology, 163, 505-519.

Strange, P.J., and Shaw, R. (1986) Geology of Hong Kong Island and Kowloon. Hong Kong Geological Survey Memoir No. 2. Hong Kong, Geotechnical Control Office.

Strange, P.J., Shaw, R., and Addison, R. (1990) Geology of Sai Kung and Clear Water Bay. Hong Kong Geological Survey Memoir No. 4. Hong Kong, Geotechnical Control Office.

Tang, D.L.K. (2016) Aspects of the tectono-magmatic evolution of late Mesozoic silicic magmatic systems in Hong Kong. PhD thesis, Victoria University, Wellington, New Zealand.

Tang, D.L.K., Seward, D., Wilson, C.J.N., Sewell, R.J., Carter, A., and Paul, B.T. (2014) Thermo-tectonic history of SE China since the late Mesozoic: insights from detailed thermochronological studies of Hong Kong. Journal of the Geological Society, London, 171, 591-604.

Trail, D., Watson, E.B., and Tailby, N.D. (2012) Ce and Eu anomalies in zircon as proxies for the oxidation state of magmas. Geochimica et Cosmochimica Acta, 97, 70-87.

Vavra, G., Gebauer, D., Schmid, R., and Compston, W. (1996) Multiple zircon growth and recrystallization during polyphase Late Carboniferous to Triassic metamorphism in granulites of the Ivrea Zone (Southern Alps): an ion microprobe (SHRIMP) study. Contributions to Mineralogy and Petrology, 122, 337-358.

Walker, B.A., Miller, C.F., Claiborne, L.L., Wooden, J.L., and Miller, J.S. (2007) Geology and geochronology of the Spirit Mountain batholith, southern Nevada: implications for timescales and physical processes of batholith construction. Journal of Volcanology and Geothermal Research, 167, 239-262.

Wang, Q., Zhu, D.-C., Zhao, Z.-D., Guan, Q., Zhang, X.-Q., Sui, Q.-L., Hu, Z.-C., and Mo, X.-X. (2012) Magmatic zircons from I-, S- and A-type granitoids in Tibet: trace element characteristics and their application to detrital zircon provenance study. Journal of Asian Earth Sciences, 53, 59-66.

Watson, E.B., and Harrison, T.M. (1983) Zircon saturation revisited: temperature and composition effects in a variety of crustal magma types. Earth and Planetary Science Letters, 64, 295-304.

Watson, E.B., and Liang, Y. (1995) A simple model for sector zoning in slowly grown crystals: implications for growth rate and lattice diffusion, with emphasis on accessory minerals in crustal rocks. American Mineralogist, 80, 1179-1187.

White, L.T., and Ireland, T.R. (2013) High-uranium matrix effect in zircon and its implications for SHRIMP U-Pb age determinations. Chemical Geology, 306-307, 78-91.

Wilson, C.J.N., and Charlier, B.L.A. (2009) Rapid rates of magma generation at contemporaneous magma systems, Taupo volcano, New Zealand: insights from U-Th model-age spectra in zircons. Journal of Petrology, 50, 875-907.

Zeh, A., Ovtcharova, M., Wilson, A.H., and Schaltegger, U. (2015) The Bushveld Complex was emplaced and cooled in less than one million years – results of zirconology, and geotectonic implications. Earth and Planetary Science Letters, 418, 103-114.

Zhou, X.M., Sun, T., Shen, W.Z., Shu, L.S., and Niu, Y.L. (2006) Petrogenesis of Mesozoic granitoids and volcanic rocks in South China: a response to tectonic evolution. Episodes, 29, 26-33.

Zimmerer, M.J., and McIntosh, W.C. (2012) The geochronology of volcanic and plutonic rocks at the Questa caldera: constraints on the origin of caldera-related silicic magmas. Geological Society of America Bulletin, 124, 1394-1408.

Figure Captions

Fig. 1. Igneous geology of southern Hong Kong (modified after Sewell et al. 2000), showing sites of sample locations (HK numbers). Ages marked in the key are those established in previous studies using ID-TIMS zircon chronology (Davies et al. 1997; Campbell et al. 2007; Sewell et al. 2012b); these ages are modified later in this paper.

Fig. 2. Illustration of systematic classification of zircon textures in CL imagery. See text for details.

Fig. 3. Stacked age histograms and relative probability curves (left panels) and $^{206}Pb/^{238}U$ ages versus U concentrations (right panels) for volcanic rock samples from the Lantau caldera complex. A: Shing Mun tuff (ignimbrite: HK12025); B: Lantau tuff (HK11052); and C: undifferentiated Kau Sai Chau tuff (ignimbrite: HK12070). Left panels: darker-grey histograms and blue relative probability curves are data from cores; lighter-grey histograms and red relative probability curves are data from rims. Ages given are the weighted mean age of all (cores and rims) data. Right panels: open squares represent data from cores and closed squares represent data from rims. Error bars represent 1 s.d..

Fig. 4. Stacked age histograms and relative probability curves (left panels) and $^{206}Pb/^{238}U$ ages versus U concentrations (right panels) for intrusive rock samples from the Lantau caldera complex. A: Lantau Granite (HK11822); B: East Lantau porphyry (HK11832); C: Chi Ma Wan Granite (HK8353); and D: Tong Fuk Quartz Monzonite (HK8758). Left panels: darker-grey histograms and blue relative probability curves are data from cores; lighter-grey histograms and red relative probability curves are data from rims. Ages given are the weighted mean age of all (cores and rims) data. Right panels: open

squares represent data from cores and closed squares represent data from rims. Error bars represent 1 s.d.

Fig. 5. Stacked age histograms and relative probability curves (left panels) and $^{206}Pb/^{238}U$ ages versus U concentrations (right panels) for ignimbrite samples from the RBVG. A: Mount Davis ignimbrite (HK13275); B: Long Harbour ignimbrite (HK11835); C: Ap Lei Chau ignimbrite (HK11840); D: Che Kwu Shan ignimbrite (HK11836). Left panels: darker-grey histograms and blue relative probability curves are data from cores; whereas lighter-grey histograms and red relative probability curves are data from rims. Ages given are the weighted mean age of all (cores and rims) data. Right panels: open squares represent data from cores; closed squares represent data from rims. Error bars represent 1 s.d.

Fig. 6. Stacked age histograms and relative probability curves (left panels) and $^{206}Pb/^{238}U$ ages versus U concentrations (right panels) for samples from the KSCVG. A: Pan Long Wan trachydacite lava (HK13277); B: Clear Water Bay tuff (ignimbrite: HK11834); C: Clear Water Bay rhyolite lava (HK12073); D: High Island Tuff (ignimbrite: HK12001); and E: post-High Island rhyolite lava (HK13343). Left panels: darker-grey histograms and blue relative probability curves are data from cores; whereas lighter-grey histograms and red relative probability curves are data from rims. Ages given are the weighted mean age of all (cores and rims) data. Right panels: open squares represent data from cores and closed squares represent data from rims. Error bars represent 1 s.d.

Fig. 7. Stacked age histograms and relative probability curves (left panels) and $^{206}Pb/^{238}U$ ages versus U concentrations (right panels) for intrusive rock samples from the High Island caldera complex. A: Shui Chuen O Granite (HK12072); B: D'Aguilar Quartz

Monzonite (HK12022); and C: Sok Kwu Wan Granite (HK12023). Left panels: darker-grey histograms and blue relative probability curves are data from cores; whereas lighter-grey histograms and red relative probability curves are data from rims. Ages given are the weighted mean age of all (cores and rims) data. Right panels: open squares represent data from cores and closed squares represent data from rims. Error bars represent 1 s.d.

Fig. 8. Stacked age histograms and relative probability curves (left panels) and $^{206}Pb/^{238}U$ ages versus U concentrations (right panels) for intrusive rock samples associated by Sewell et al. (2012a) with the High Island caldera complex. A: Kowloon Granite (HK11042); and B: Mount Butler Granite (HK13407). Left panels: dark-grey histograms and blue relative probability curves are data from cores; whereas light-grey histograms and red relative probability curves are data from rims. Ages given are the weighted mean age of all (cores and rims) data. Right panels: open squares represent data from cores and closed squares represent data from rims. Error bars represent 1 s.d.

Fig. 9. Plots of selected trace elements and trace element ratios showing all data collected for this study from volcanic and plutonic rock samples from Hong Kong.

Fig. 10. Plots of selected zircon trace elements to illustrate the intra-grain core-rim variations from the Pan Long Wan trachydacite lava (HK13277), and to compare them with those of the Ap Lei Chau and Che Kwu Shan ignimbrites (HK11840, HK11836). Outlined area encloses data from the zircon cores that show common CL textural characteristics and trace element signatures in the three samples. Closed symbols are core (C) data; open symbols are rim (R) data.

Fig. 11. Plots of selected zircon trace elements to illustrate the intra-grain variations from the Kowloon Granite (HK11042). Outlined area encloses data from the evolved intermediate zones in this sample. See text for discussion.

Fig. 12. Plots of selected zircon trace elements to illustrate the influence of sector zoning in volcanic and granitic units, using samples (A) HK11835 (Mount Davis ignimbrite) and (B) HK13407 (Mount Butler Granite) as examples. Only data from zircon rims are plotted. Tie-lines connect the data points from the light-dark sectors of the same growth zones in the sample rims. Open symbols represent data from lighter sectors and closed symbols represent data from darker sectors.

Fig. 13. Plots of selected zircon trace elements of (A) Shing Mun ignimbrite (HK12025, left panels) and (B) undifferentiated Kau Sai Chau ignimbrite (HK12070, right panels), highlighting the characteristics of some dated xenocrystic cores that plot outside the main trends. Closed and open symbols represent zircon cores and rims, respectively. In-situ SIMS ages of selected cores were obtained from the same analytical spots as the trace element analyses. See text for detailed discussion.

Fig. 14. Plots of averaged values of trace element concentrations and ratios for zircon rims from the volcanic samples, plotted in chronological order. Blue strips highlight the volcanic units from the Lantau Caldera; white strips highlight the volcanic units from the High Island Caldera; purple and grey strips highlight the Pan Long Wan trachydacite and post-High Island rhyolite lavas, respectively, both of which were extruded along the boundary of the High Island caldera.

Fig. 15. Selected zircon trace element plots of the RBVG units (HK11835: Long Harbour; HK13275: Mount Davis; HK11840: Ap Lei Chau; HK11836: Che Kwu Shan) and Pan

Long Wan trachydacite (HK13277). Trace element data from all the KSCVG are plotted as grey circles for comparison. Zircon trace element data from the two crystal-rich ignimbrites (Long Harbour and Mount Davis) are generally plotted outside the field in which the KSCVG data plot; while data from the Ap Lei Chau and Che Kwu Shan ignimbrites plot in the zone partly overlapping with the KSCVG data.

Fig. 16. Selected zircon trace element plots of intrusive units from the High Island caldera complex. Left panel: HK12072: Shui Chuen O Granite; HK11042: Kowloon Granite; HK13407: Mount Butler Granite. Grey diamonds are data from the RBVG units for comparison. Right panel: HK12023 Sok Kwu Wan Granite; HK12022: D'Aguilar Quartz Monzonite. Grey circles are data from the KSCVG units for comparison.

This is a preprint, the final version is subject to change, of the American Mineralogist (MSA)
Cite as Authors (Year) Title. American Mineralogist, in press.
(DOI will not work until issue is live.) DOI: http://dx.doi.org/10.2138/am-2017-6071

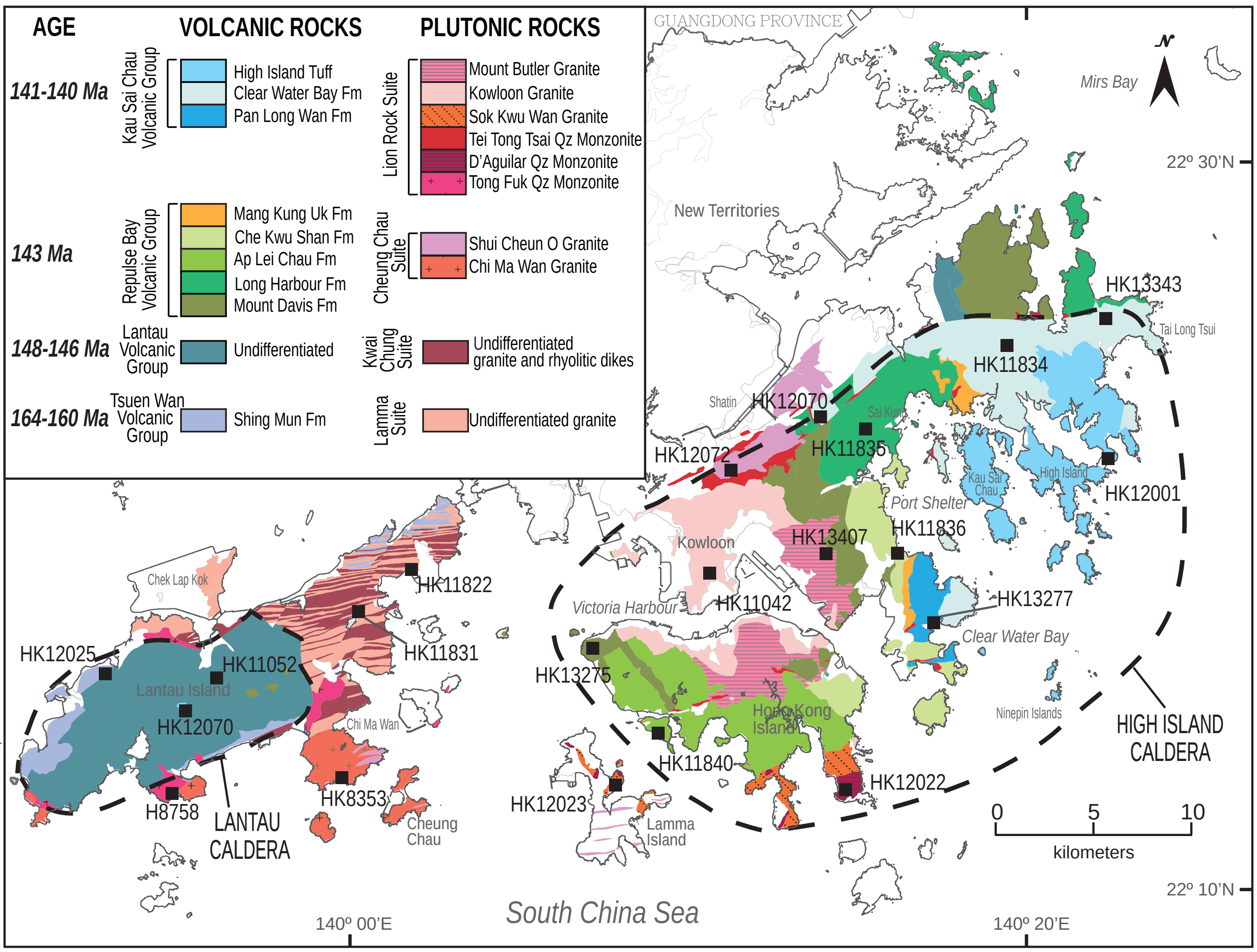

Tang et al. Figure 1

This is a preprint, the final version is subject to change, of the American Mineralogist (MSA)
Cite as Authors (Year) Title. American Mineralogist, in press.
(DOI will not work until issue is live.) DOI: http://dx.doi.org/10.2138/am-2017-6071

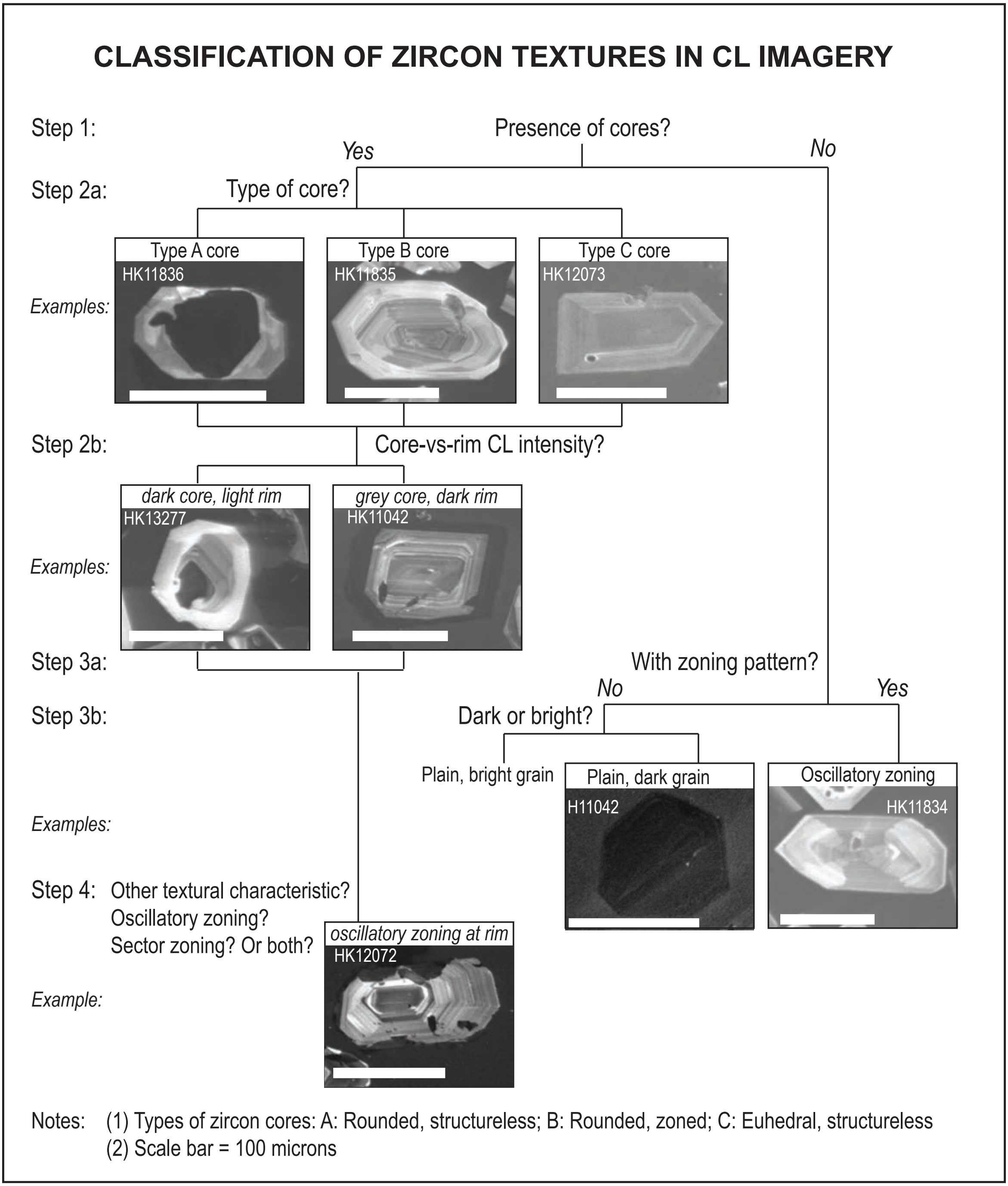

Tang et al. Figure 2

This is a preprint, the final version is subject to change, of the American Mineralogist (MSA)
Cite as Authors (Year) Title. American Mineralogist, in press.
(DOI will not work until issue is live.) DOI: http://dx.doi.org/10.2138/am-2017-6071

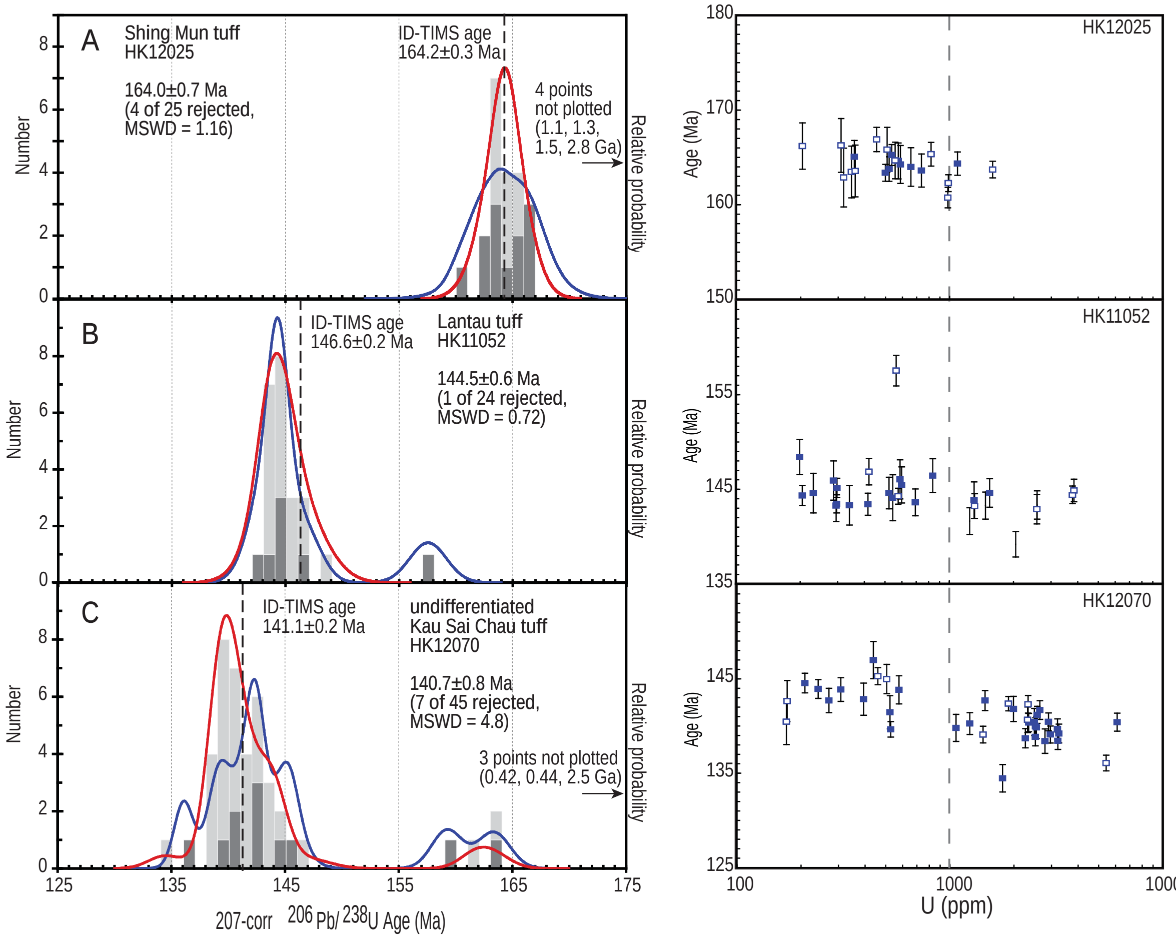

Tang et al. Figure 3

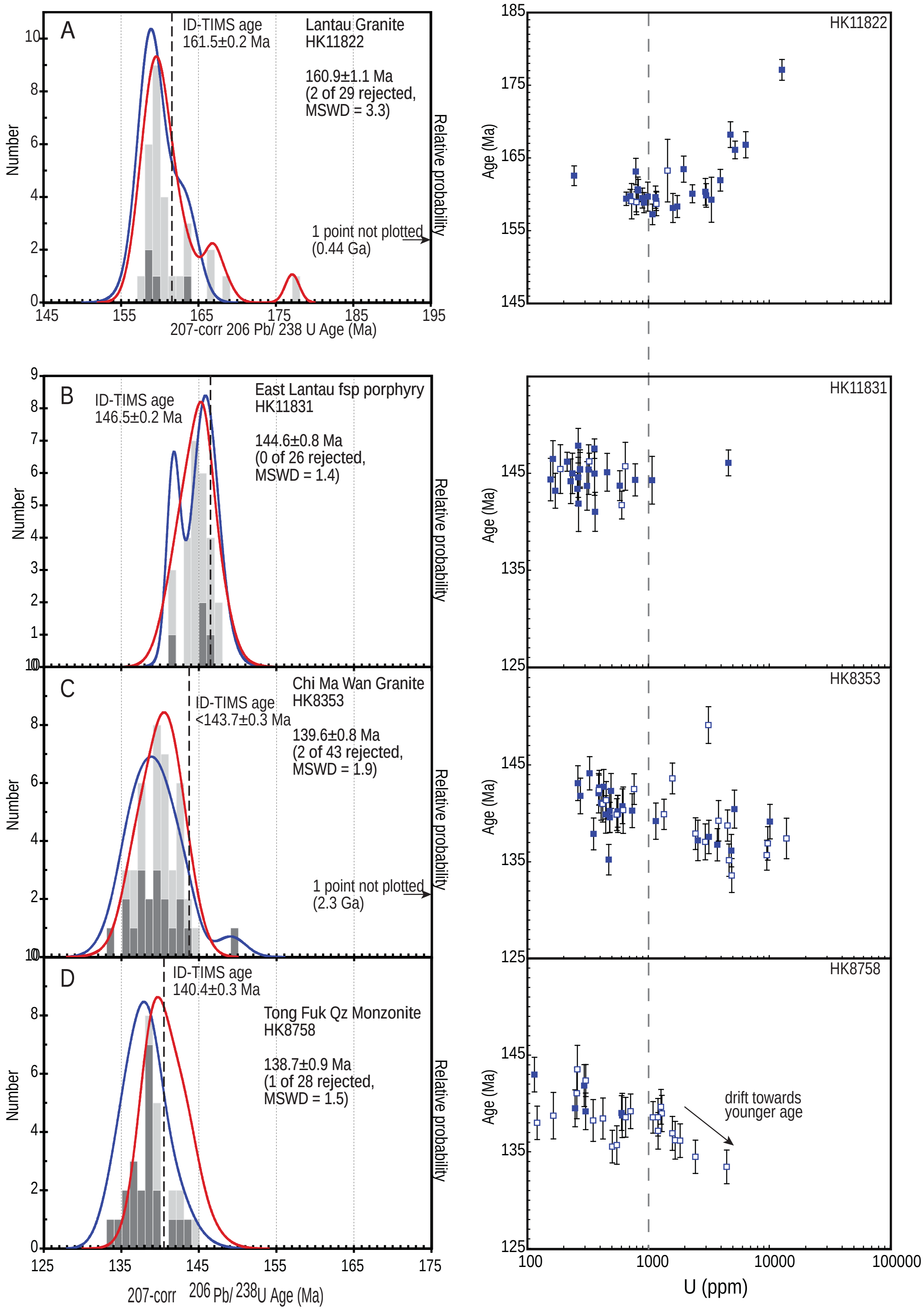

Tang et al. Figure 4

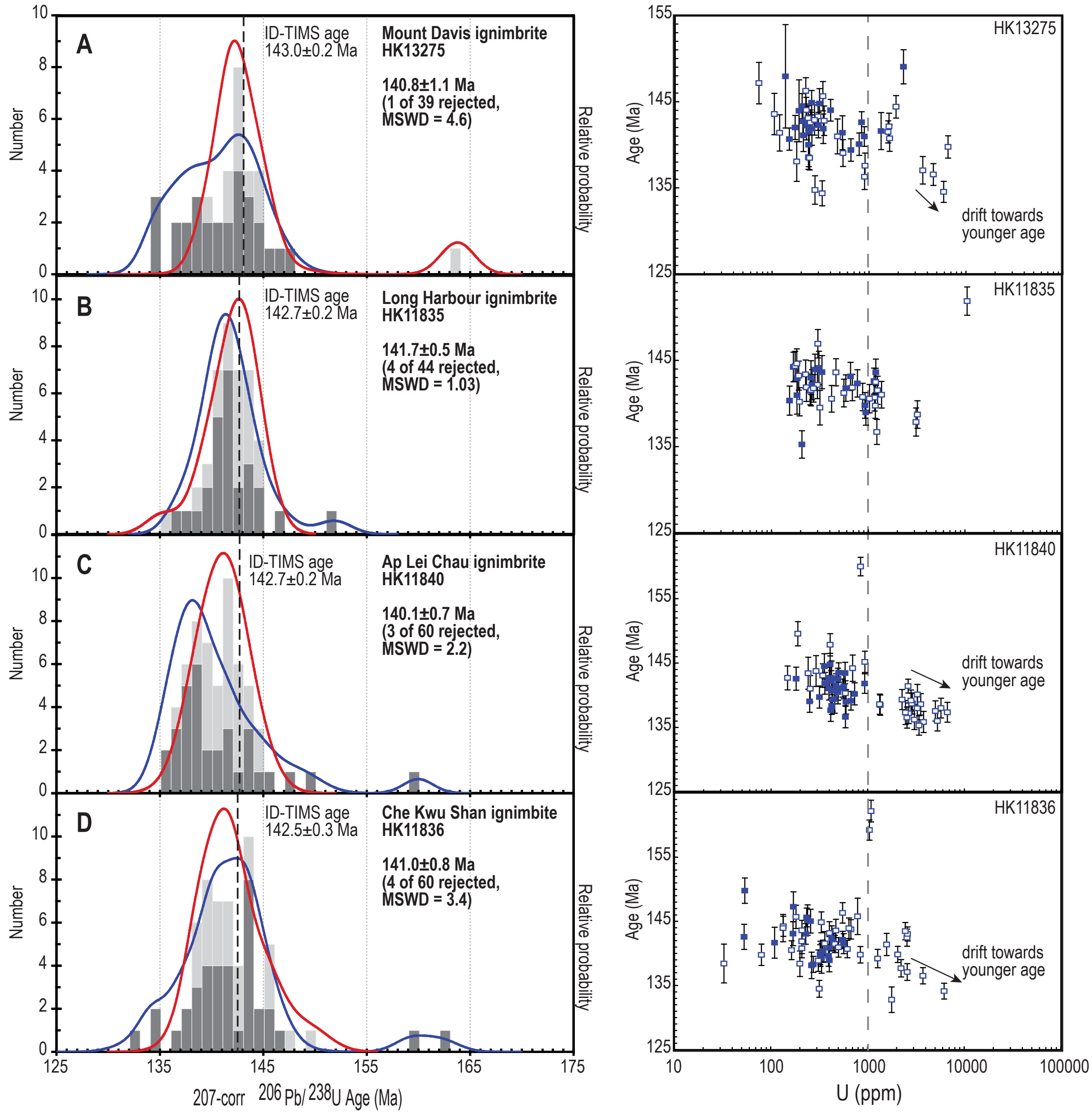

Tang et al. Figure 5

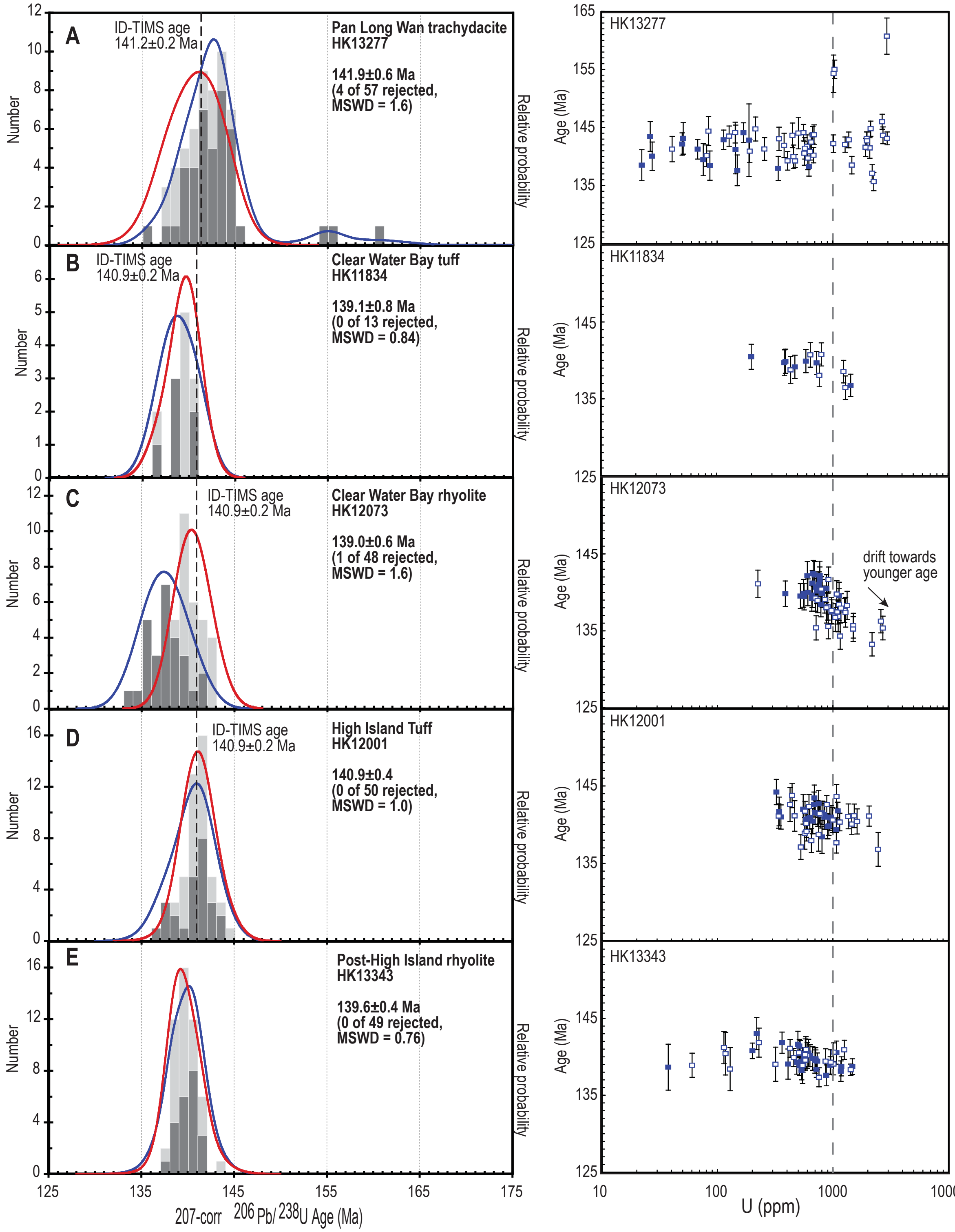

Tang et al. Figure 6

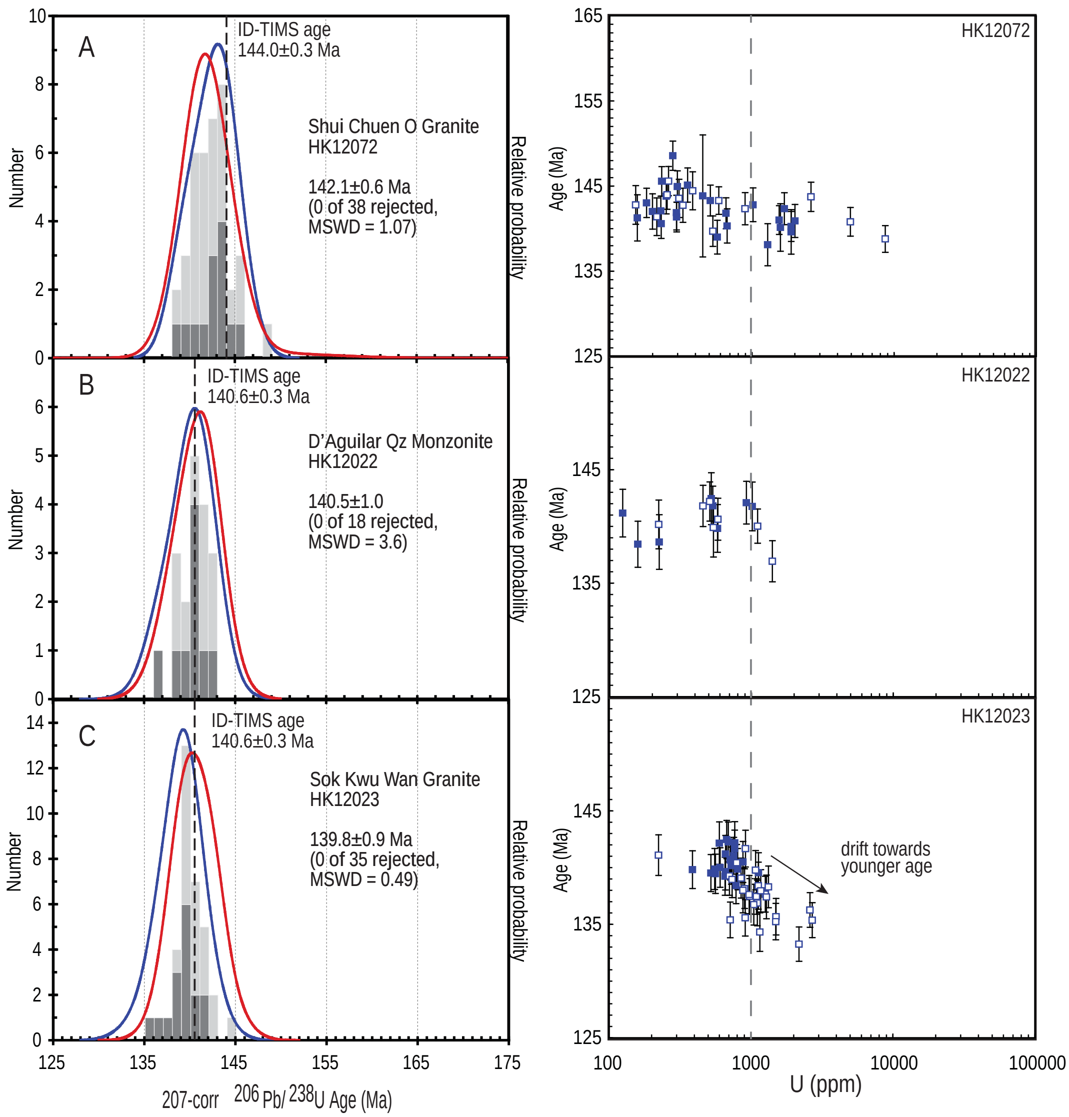

Tang et al. Figure 7

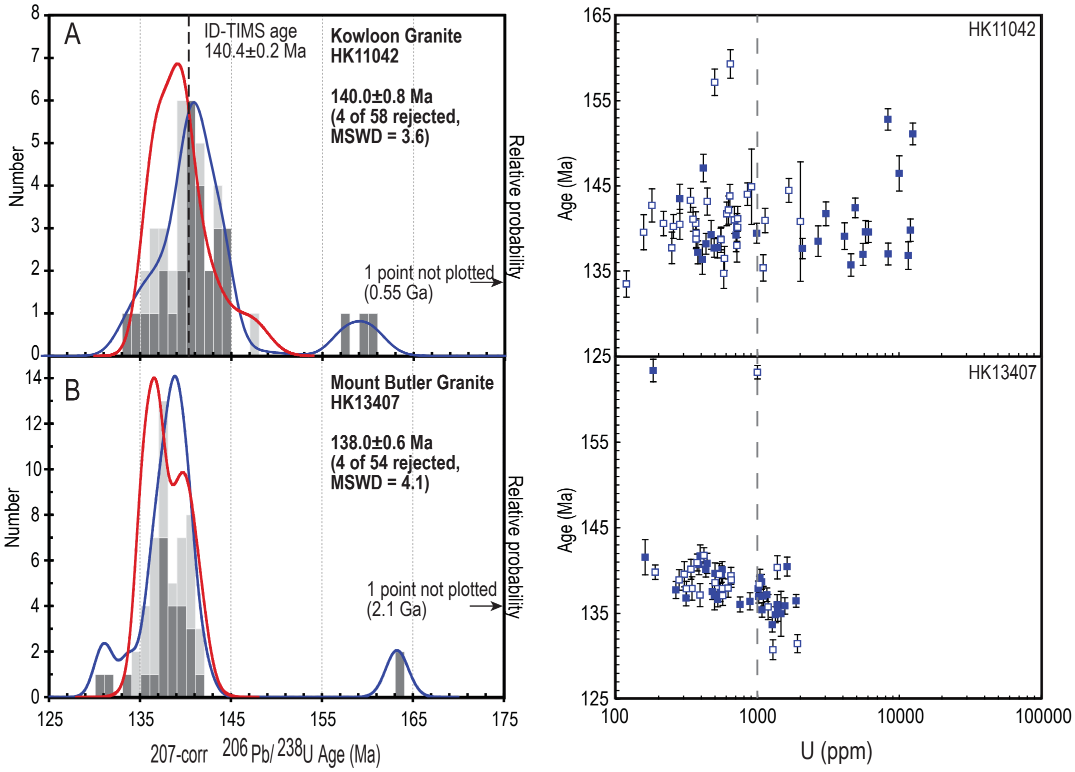

Tang et al. Figure 8

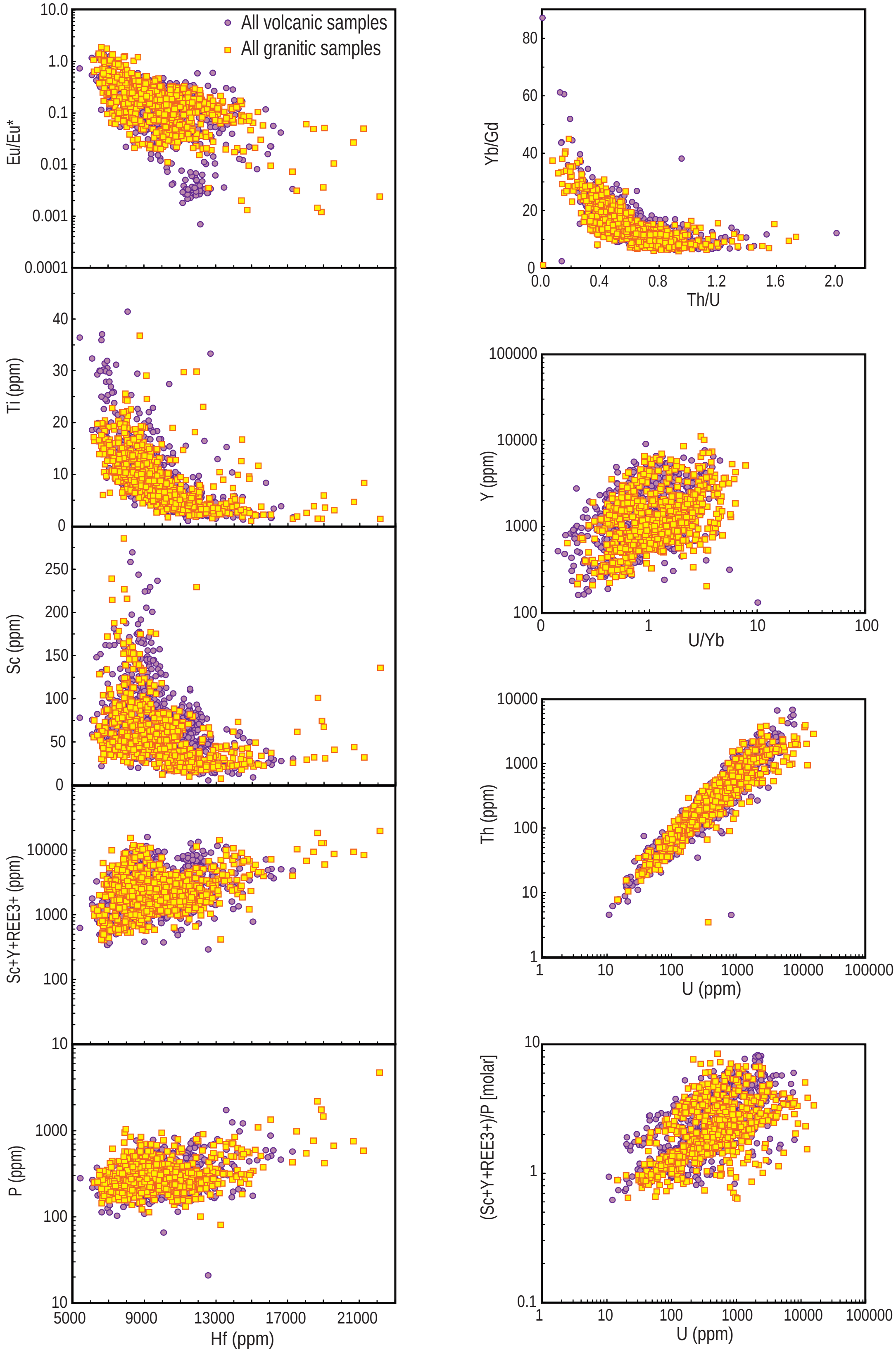

Tang et al. Figure 9

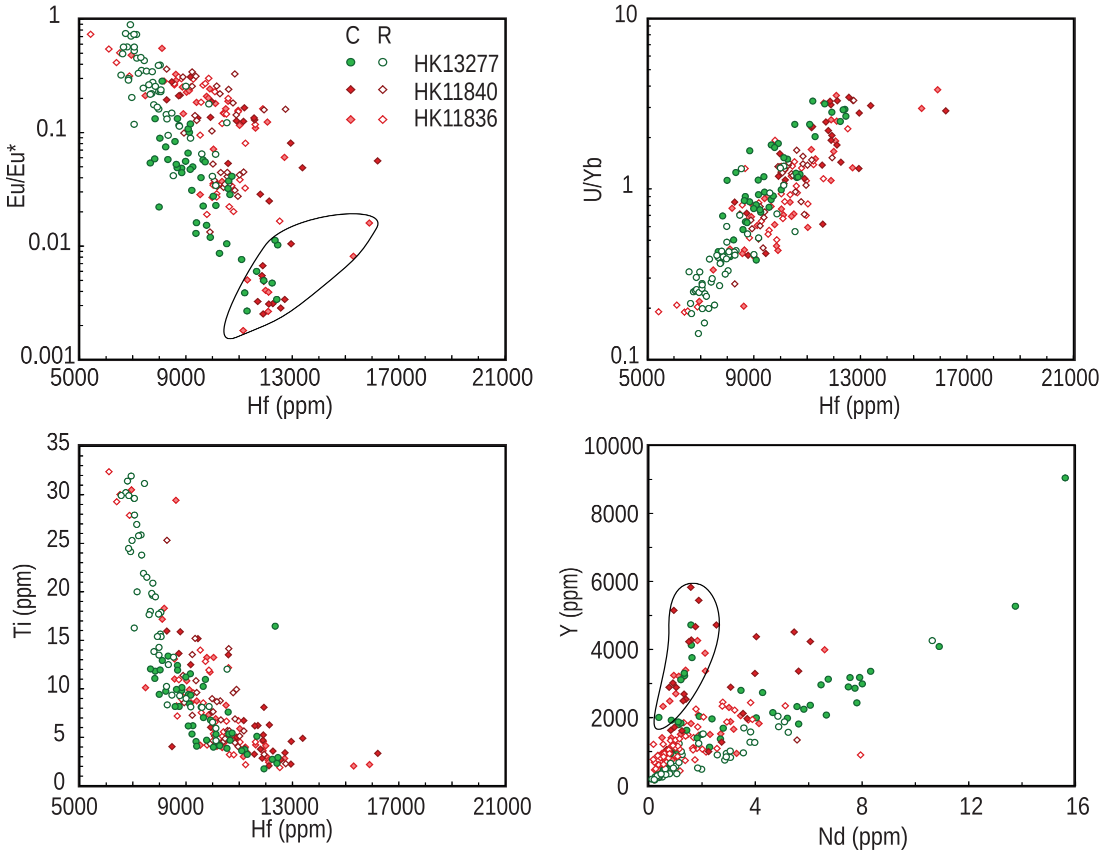

Tang et al. Figure 10

This is a preprint, the final version is subject to change, of the American Mineralogist (MSA)
Cite as Authors (Year) Title. American Mineralogist, in press.
(DOI will not work until issue is live.) DOI: http://dx.doi.org/10.2138/am-2017-6071

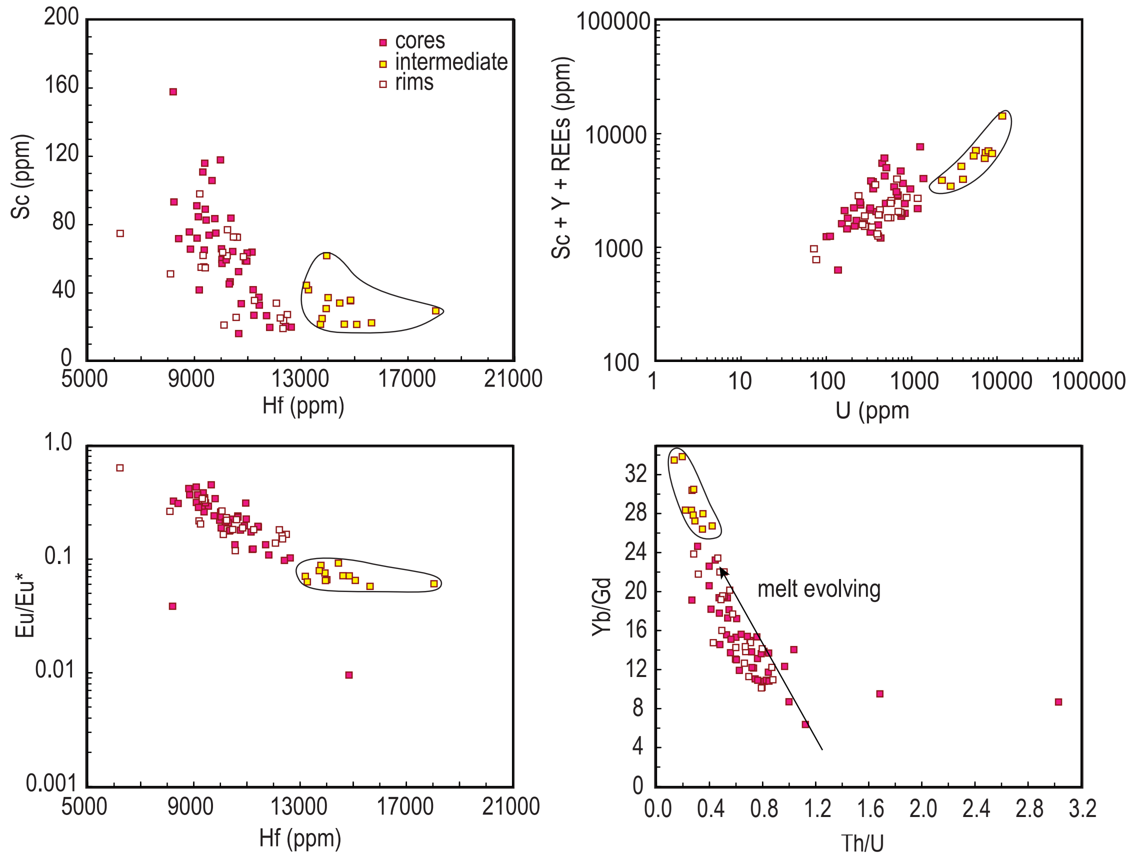

Tang et al. Figure 11

(A) Mount Davis ignimbrite HK11835

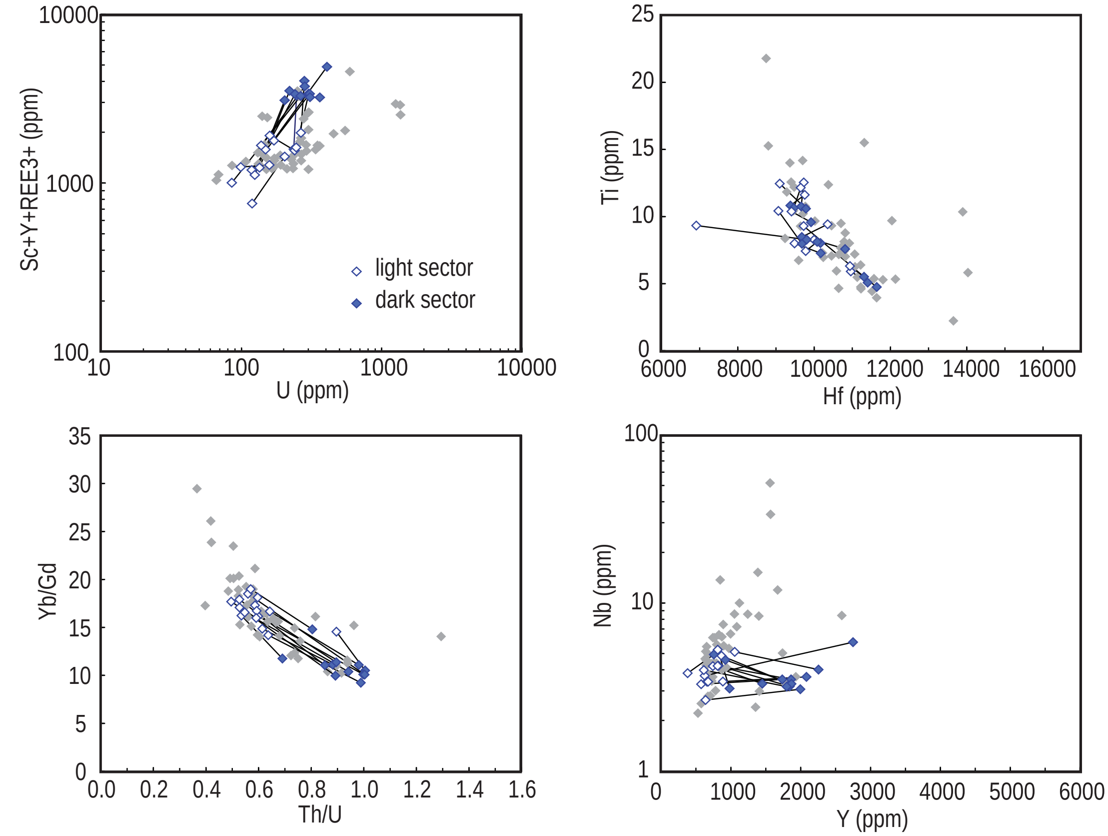

(B) Mount Butler Granite HK13407

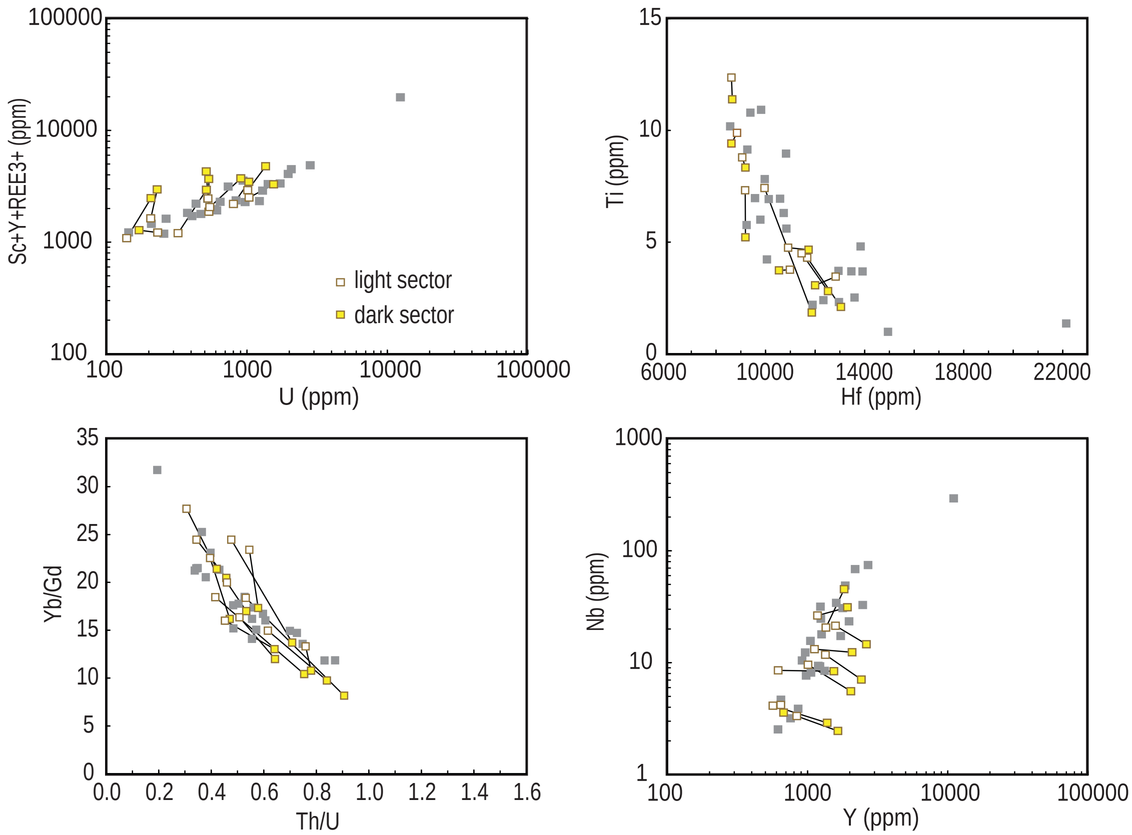

Tang et al. Figure 12

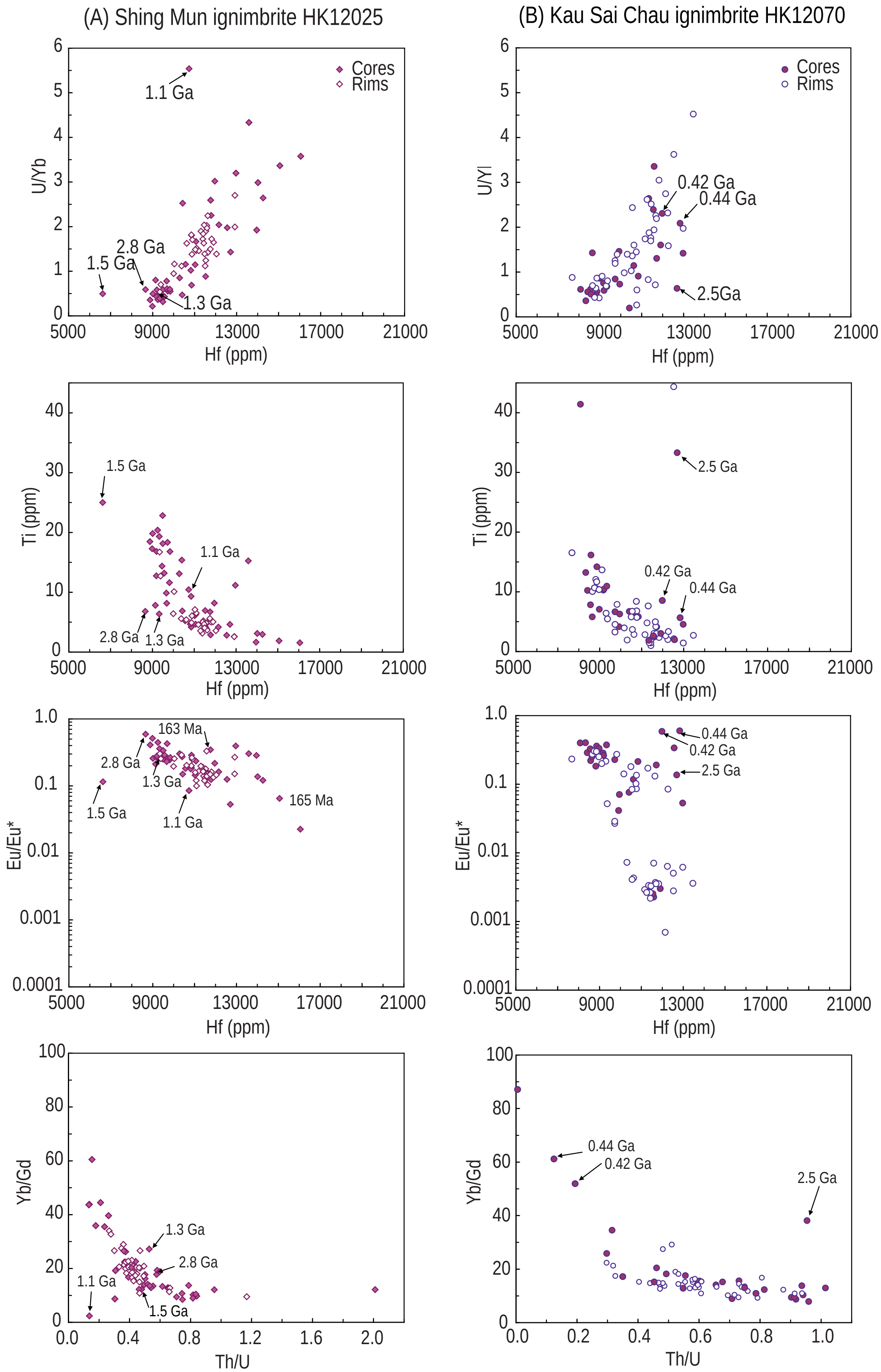

Tang et al. Figure 13 parts A and B

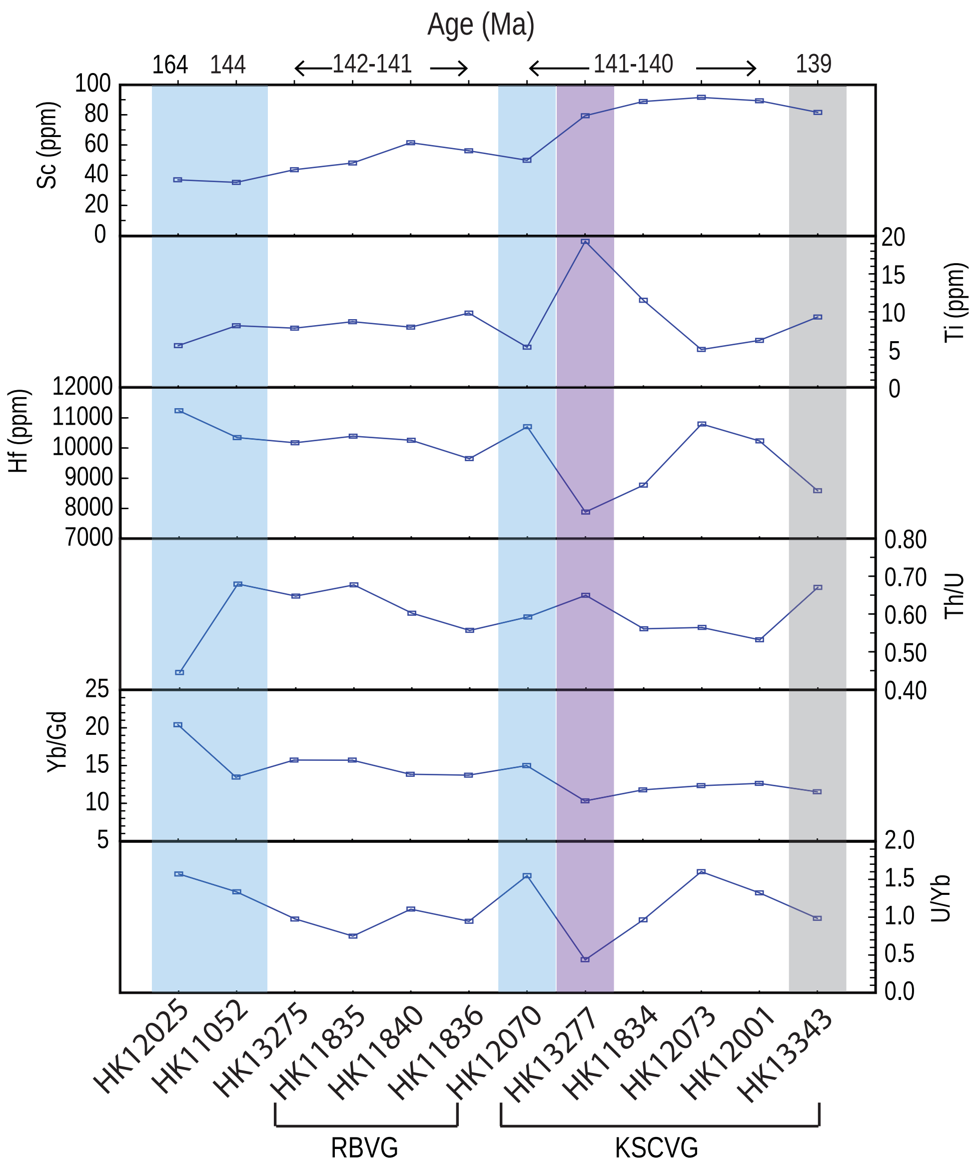

Tang et al. Figure 14

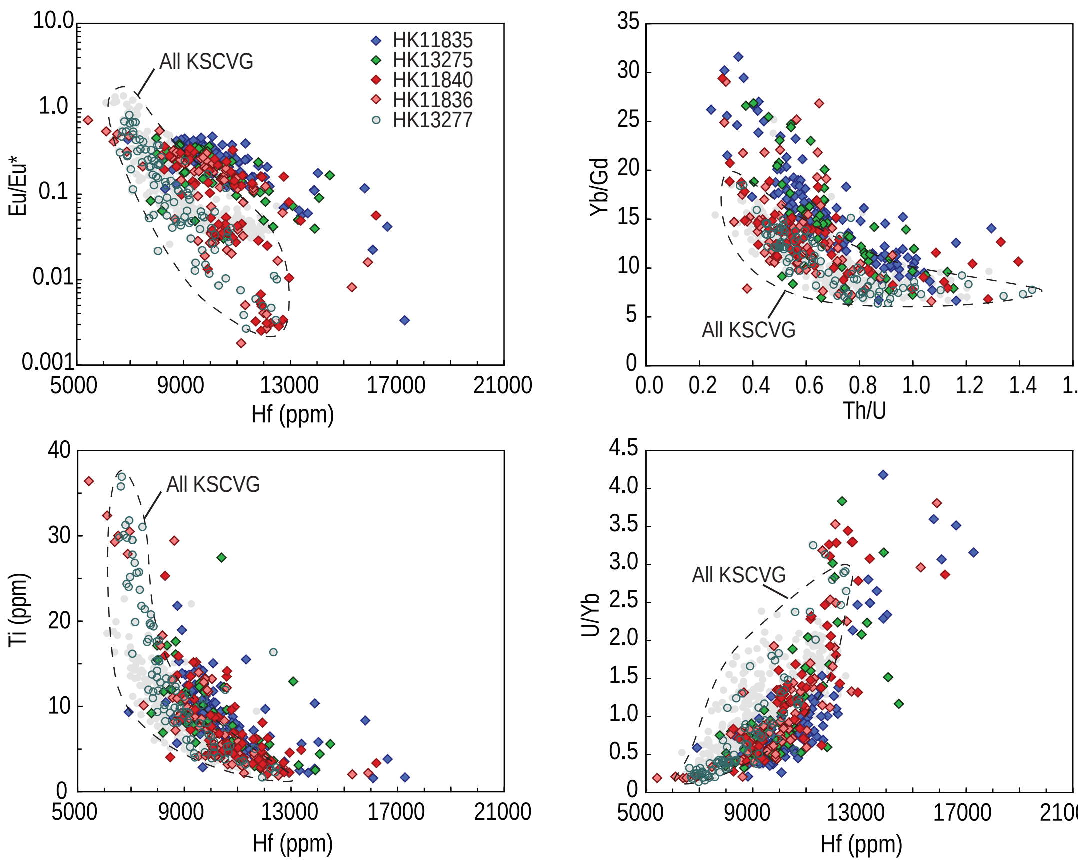

Tang et al. Figure 15

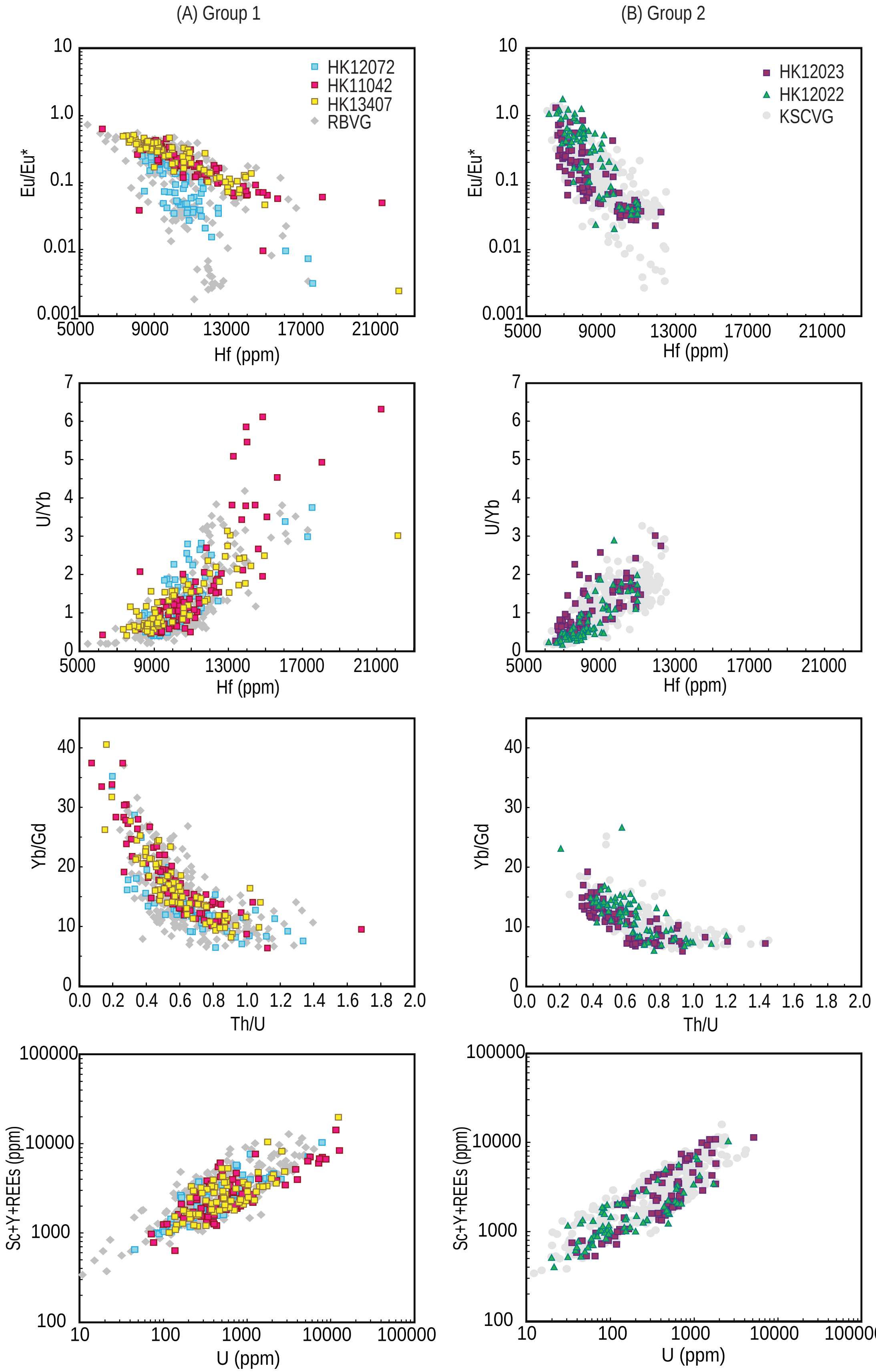

Tang et al. Figure 16

TABLE 1. Summary of the groups and formations forming late Mesozoic volcanic-plutonic assemblages in Hong Kong

Age	Volcanic Rocks		Granitic Rocks	
	Volcanic Groups/Formations	sample no.	Plutonic Suites/Units	sample no.
141-140 Ma	*Kau Sai Chau Volcanic Group (KSCVG)*		*Lion Rock (LR) Suite*	
	Post-High Island lava	(HK13343)	Mount Butler Granite	(HK13407)
	High Island Tuff	(HK12001)	Kowloon Granite	(HK11042)
	Clear Water Bay tuff	(HK11834)	Fan Lau Granite	
	Clear Water Bay lava	(HK12073)	Sok Kwu Wan Granite	(HK12023)
	Pan Long Wan lava	(HK13277)	Tei Tong Tsui Quartz Monzonite	(HK8758)
	undifferentiated Kau Sai Chau tuff	(HK12070)	Tong Fuk Qz Monzonite	(HK12022)
			D'Aguilar Qz Monzonite	
143 Ma	*Repulse Bay Volcanic Group (RBVG)*		*Cheung Chau (CC) Suite*	
	Mount Davis	(HK13275)	Luk Keng Qz Monzonite	
	Long Harbour	(HK11835)	Chi Ma Wan Granite	(HK8353)
	Mang Kung Uk		Shui Chuen O Granite	(HK12072)
	Che Kwu Shan	(HK11836)		
	Ap Lei Chau	(HK11840)		
	Ngo Mei Chau			
148-146 Ma	*Lantau Volcanic Group (LVG)*		*Kwai Chung (KC) Suite*	
	Lai Chi Chong		Shatin Granite	
	undifferentiated tuff	(HK11052)	East Lantau Dyke Swarm	(HK11831)
			Needle Hill Granite	
			Sham Chung Rhyolite	
			Po Toi Granite	
			Shan Tei Tong Rhyodacite	
			South Lamma Granite	
164-160 Ma	*Tsuen Wan Volcanic Group*		*Lamma (LA) Suite*	
	Sai Lau Kong		Tai Lam Granite	
	Tai Mo Shan		Tsing Shan Granite	
	Shing Mun	(HK12025)	Chek Lap Kok Granite	
	Yim Tin Tsai		Chek Mun Rhyolite	
			Lantau Granite	(HK11822)
			Tai Po Granodiorite	

Notes: Names of units are from Sewell et al. (2012a). HK numbers are given for samples analyzed for this paper. Age ranges are the existing values based on published ID-TIMS studies (after Sewell et al. 2012b), and are modified in this paper.

TABLE 2. Characterisation of zircon textures under CL imagery.

Sample No.	No. of grains	With core? (Y/N) Step 1*	Core type Step 2a*	Textural characteristics Steps 2b, 3a & 3b*	Oscillatory zoning Step 4*	Sector zoning Step 4*
Volcanic Rocks						
HK12025 Shing Mun ignimbrite	299	76% (Y)	74% (B) 2% (C)	26%: Dark core, light rim 21%: Light core, dark rim 29%: Dark core, dark rim	91%	22%
		24% (N)		23%: Grain with OZ pattern 1%: Dark or intermediate grain		
HK11052 undifferentiated Lantau tuff	295	59% (Y)	24% (A) 35% (B)	37%: Dark core, light rim 18%: Light core, dark rim 4%: Dark core, dark rim	46%	15%
		41% (N)		20%: Dark grain 2%: Light or intermediate grain 19%: Grain with OZ pattern		
HK11835 Long Harbour crystal-rich ignimbrite	364	57% (Y)	7% (A) 50% (B)	39%: Dark core, dark rim 13%: Light core, dark rim 5%: Dark core, bright rim	91%	36%
		43% (N)		42%: Grain with OZ pattern 1%: Dark or intermediate grain		
HK13275 Mount Davis crystal-rich ignimbrite	184	85%	19% (A) 62% (B) 4% (C)	64%: Dark core, light rim 19%: Light core, dark rim 2%: Dark core, dark rim	48%	23%
		15%		4%: Dark grain 1%: Light grain 10%: Grain with OZ pattern		
HK11836 Che Kwu Shan ignimbrite	323	73% (Y)	27% (A) 40% (B) 6% (C)	66%: Dark core, light rim 6%: Light core, dark rim 1%: Dark core, dark rim	41%	20%
		27% (N)		14%: Grain with OZ pattern 6%: Dark grain 7%: Light grain		
HK11840 Ap Lei Chau ignimbrite	570	72% (Y)	31% (A) 39% (B) 2% (C)	69%: Dark core, light rim 3%: Light core, dark rim	23%	9%
		28% (N)		14%: Dark grain 7%: Light grain 7%: Grain with OZ pattern		
HK12070 Undifferentiated Kau Sai Chau tuff	364	37% (Y)	31% (B) 6% (C)	28%: Dark core, light rim 7%: Light core, dark rim 2%: Dark core, dark rim	42%	11%
		63% (N)		31%: Grain with OZ pattern 30%: Dark grain 2%: Bright grain		
HK13277 Pan Long Wan trachydacite lava	522	62% (Y)	48% (A) 14% (B)	62%: Dark core, bright rim	15%	9%
		38% (N)		5%: Dark grain 29%:Bright grain 4%: Grain with OZ pattern		

TABLE 2. (Continued)

Sample No.	No. of grains	With core? (Y/N) Step 1*	Core Type Step 2a*	Textural characteristics Steps 2b, 3a & 3b*	Oscillatory Zoning Step 4*	Sector Zoning Step 4*
Volcanic Rocks						
HK11834 Clear Water Bay rhyolite ignimbrite	778	50% (Y)	11% (A) 21% (B) 18% (C)	45%: Dark core, light rim 4%: Dark core, dark rim 1%: Light core, dark rim	41%	20%
		50% (N)		19%: Dark grain 31% Grain with OZ pattern		
HK12073 Clear Water Bay rhyolite lava	256	75% (Y)	32% (A) 10% (B) 33% (C)	65%: Dark core, light rim 6%: Light core, dark rim 4%: Dark core, dark rim	66%	13%
		25% (N)		7%: Dark grain 18%: Grain with OZ pattern		
HK12001 High Island Tuff	842	62% (Y)	32% (B) 30% (C)	58%: Dark core, dark rim 3%: Light core, dark rim 1%: Dark core, light rim	54%	2%
		38% (N)		23%: Dark grain 1%: Light grain 14% Grain with OZ pattern		
HK13343 Post-High Island rhyolite lava	254	52% (Y)	18% (A) 11% (B) 23% (C)	30%: Dark core, light rim 17%: Dark core, dark rim 5%: Light core, dark rim	61%	17%
		48% (N)		15%: Dark grain 4%: Light grain 29%: Grain with OZ pattern		
Plutonic Rocks						
HK11822 Lantau Granite	252	80% (Y)	27% (A) 49% (B) 4% (C)	60%: Light core, dark rim 15%: Dark core, dark rim 5%: Dark core, light rim	26%	8%
		20% (N)		3%: Dark grain 4% Light grain 13%: Grain with OZ pattern		
HK11831 East Lantau porphyry	300	73% (Y)	29% (A) 41% (B) 3% (C)	67%: Dark core, light rim 5%: Light core, dark rim 1%: Dark core, dark rim	65%	24%
		27% (N)		25%: Grain with OZ pattern 2%: Dark or intermediate grain		
HK12072 Shui Chen O Granite	157	60% (Y)	5% (A) 42% (B) 13% (C)	49%: Dark core, light rim 7%: Light core, dark rim 4%: Dark core, dark rim	69%	47%
		40% (N)		16%: Dark or intermediate grain 24%: Grain with OZ pattern		
HK8353 Chi Ma Wan Granite	336	70% (Y)	28% (A) 40% (B) 2% (C)	29%: Dark core, light rim 25%: Light core, dark rim 16%: Dark core, dark rim	38%	7%
		30% (N)		17%: Dark grain 3%: Light to intermediate grain 10%: Grain with OZ pattern		

(DOI will not work until issue is live.) DOI: http://dx.doi.org/10.2138/am-2017-6071

TABLE 2. (Continued)

Sample No.	No. of grains	With core? (Y/N) Step 1*	Core Type Step 2a*	Textural characteristics Steps 2b, 3a & 3b*	Oscillatory Zoning Step 4*	Sector Zoning Step 4*
Intrusive Rocks						
HK12023 Sok Kwu Wan Granite	301	58% (Y)	39% (B) 19% (C)	53%: Dark core, light rim 3%: Light core, dark rim 2%: Dark core, dark rim	52%	14%
		42% (N)		27%: Grain with OZ pattern 13%: Dark to intermediate grain 2%: Light grain		
HK12022 D'Aquilar Quartz Monzonite	262	79% (Y)	55% (A) 24% (B)	76%: Dark core, light rim 2%: Light core, dark rim 1%: Dark core, dark rim	32%	38%
		21% (N)		4%: Dark grain 6%: Light grain 11%: Grain with OZ pattern		
HK8758 Tong Fuk Quartz Monzonite	313	62% (Y)	36% (A) 18% (B) 8% (C)	60%: Dark core, bright rim 2%: Light core, dark rim	36%	17%
		38% (N)		12%: Dark grain 6%: Bright or intermediate grain 20%: Grain with OZ pattern		
HK11042 Kowloon Granite	674	87% (Y)	82% (B) 5% (C)	76%: Light core, dark rim 6%: Dark core, dark rim 5%: Dark core, light rim	8%	2%
		13% (N)		10%: Dark grain 3%: Grain with OZ pattern		
HK13407 Mount Butler Granite	297	63% (Y)	33% (A) 29% (B) 1% (C)	50%: Light core, dark rim 4%: Dark core, dark rim 9%: Dark core, light rim	56%	12%
		37% (N)		18%: Dark grain 19%: Grain with OZ pattern		

Note: See Fig. 2 and associated text for the system used to classify the zircon grains and descriptions of each step (*) listed.

This is a preprint, the final version is subject to change, of the American Mineralogist (MSA)
Cite as Authors (Year) Title. American Mineralogist, in press.
(DOI will not work until issue is live.) DOI: http://dx.doi.org/10.2138/am-2017-6071

TABLE 3. Weighted mean ages and age components of volcanic and plutonic rocks from in-situ SHRIMP U-Pb age determinations.

Sample	No. of analyses and spot location[a]	Weighted mean age of all data[b] (Ma)	Weighted mean age of data from rims only (Ma)	Multiple age components[c] (Ma)	ID-TIMS ages[d] (Ma)	Inheritance identified in previous ID-TIMS work
Volcanic Rocks						
HK12025 Shing Mun ignimbrite	C 8 R 17	164.0 ± 0.7 (4 of 25 rejected, MSWD = 1.16)* (4 analyses returned ages >1 Ga)	164.7 ± 0.8 (0 of 17 rejected, MSWD = 0.41)	(single population*)	164.2 ± 0.3[f]	>1.8 Ga[f]
HK11052 undifferentiated LVG tuff	C 7 R 17	144.5 ± 0.6 (1 of 24 rejected, MSWD = 0.72)	144.5 ± 0.7 (0 of 17 rejected, MSWD = 0.67)	144.5 ± 0.57 (96 ± 40%) 157.5 ± 3.2 (4 %)	146.6 ± 0.2[e]	Nil[e]
HK13275 Mount Davis crystal-rich ignimbrite	C 28 R 9	140.8 ± 1.1 (1 of 39 rejected, MSWD = 4.6)	142.3 ± 1.2 (1 of 11 rejected, MSWD = 1.2)	137.1 ± 1.1 (31 ± 20%) 142.8 ± 0.8 (66 ± 27%) 163.8 ± 3.3 (3 %)	143.0 ± 0.2[g]	Nil[g]
HK11835 Long Harbour crystal-rich ignimbrite	C 26 R 18	141.7 ± 0.5 (4 of 44 rejected, MSWD = 1.03)	141.4 ± 1.0 (0 of 18 rejected, MSWD = 1.18)	137.1 ± 2.8 (8 ± 13%) 142.0 ± 0.6 (90 ± 30%) 151.7 ± 3.8 (2 %)	142.7 ± 0.2[e]	>3.0 Ga[e]
HK11840 Ap Lei Chau ignimbrite	C 29 R 31	140.1 ± 0.7 (3 of 60 rejected, MSWD = 2.2)	141.0 ± 0.7 (1 of 31 rejected, MSWD = 1.3)	138.5 ± 0.9 (57 ± 25%) 142.7 ± 1.0 (43 ± 23%) 160.3 ± 2.9 (2 %)	142.7 ± 0.2[e]	>2.4 Ga[e]
HK11836 Che Kwu Shan ignimbrite	C 35 R 25	141.0 ± 0.8 (4 of 60 rejected, MSWD = 3.4)	141.6 ± 1.0 (2 of 25 rejected, MSWD = 1.9)	141.0 ± 0.4 (97 ± 25%) 160.6 ± 2.3 (3 %)	142.5 ± 0.3[e]	~146 Ma[e]
HK12070 undifferentiated Kau Sai Chau tuff	C 16 R 29	140.7 ± 0.8 (7 of 45 rejected, MSWD = 4.8) (1 analysis returns age >2.5 Ga, 2 analyses return age >400 Ma)	140.7 ± 0.7 (2 of 29 rejected, MSWD = 2.7)	139.1 ± 1.0 (44 ± 38%) 141.7 ± 2.1 (30 ± 33%) 144.4 ± 1.3 (17 ± 19%) 161.8 ± 1.4 (10 %)	141.1 ± 0.2[f]	Nil[f]
HK13277 Pan Long Wan trachydacite lava	C 42 R 15	141.9 ± 0.6 (4 of 57 rejected, MSWD = 1.6)	141.0 ± 1.3 (0 of 15 rejected, MSWD = 1.16)	139.0 ± 1.5 (23 ± 23%) 142.7 ± 0.7 (72 ± 29%) 155.9 ± 2.6 (5 %)	141.2 ± 0.3[f]	Nil[f]
HK12073 Clear Water Bay rhyolite lava	C 27 R 21	139.0 ± 0.6 (1 of 48 rejected, MSWD = 1.6)	140.5 ± 0.7 (0 of 21 rejected, MSWD = 0.45)	(single population)	140.9 ± 0.2[g]	>1.8 Ga[g]
HK11834 Clear Water Bay ignimbrite	C 8 R 7	139.1 ± 0.8 (0 of 13 rejected, MSWD = 0.84)	139.3 ± 1.1 (0 of 7 rejected, MSWD = 0.68)	(single population)	140.7 ± 0.2[e]	Nil[e]
HK12001 High Island Tuff	C 28 R 22	140.9 ± 0.4 (0 of 50 rejected, MSWD = 1.0)	141.3 ± 0.7 (0 of 22 rejected, MSWD = 0.57)	(single population)	140.9 ± 0.2[e]	Nil[e]
HK13343 undifferentiated post-High Island rhyolite lava	C 22 R 27	139.6 ± 0.4 (0 of 49 rejected, MSWD = 0.76)	139.6 ± 0.5 (0 of 27 rejected, MSWD = 0.85)	(single population)	No ID-TIMS age	(This study only)

TABLE 3. (Continued)

Sample	No. of analyses and spot location[a]	Weighted mean age of all data[b] (Ma)	Weighted mean age of data from rims only (Ma)	Multiple age component[c] (Ma)	ID-TIMS ages[d] (Ma)	Inheritance identified in previous ID-TIMS work
Plutonic Rocks						
HK11822 Lantau Granite	C 4 R 25	160.9 ± 1.1 (2 of 29 rejected, MSWD = 3.3) (1 analysis returns age >440 Ma)	161.4 ± 1.4 (1 of 25 rejected, MSWD = 4.8)	159.9 ± 0.7 (85 ± 35%) 166.9 ± 1.6 (12 ± 14%) 177.1 ± 1.8 (3 %)	161.5 ± 0.2[e]	~713 Ma[e]
HK11831 East Lantau feldspar porphyry	C 4 R 22	144.6 ± 0.8 (0 of 26 rejected, MSWD = 1.4)	144.9 ± 0.7 (0 of 22 rejected, MSWD = 0.96)	(single population)	146.5 ± 0.2[e]	~150 Ma[e]
HK8353 Chi Ma Wan Granite	C 19 R 24	139.6 ± 0.8 (2 of 43 rejected, MSWD = 1.9) (1 analysis returns age >2.3 Ga)	140.0 ± 1.0 (0 of 24 rejected, MSWD = 1.7)	137.1 ± 1.5 (35 ± 28%) 140.9 ± 1.0 (63 ± 33%) 149.1 ± 3.8 (2 %)	<143.7 ± 0.3[e]	>1.8 Ga[e]
HK12072 Shui Chen O Granite	C 13 R 25	142.1 ± 0.6 (0 of 38 rejected, MSWD = 1.07)	141.9 ± 0.8 (0 of 25 rejected, MSWD = 0.98)	(single population)	144.0 ± 0.3[g]	Nil[g]
HK8758 Tong Fuk Quartz Monzonite	C 21 R 7	138.7 ± 0.9 (1 of 28 rejected, MSWD = 1.5)	140.6 ± 1.5 (0 of 7 rejected, MSWD = 1.05)	(single population)	140.4 ± 0.3[e]	Nil[e]
HK12023 Sok Kwu Wan Granite	C 16 R 19	139.8 ± 0.9 (0 of 35 rejected, MSWD = 0.49)	140.7 ± 1.2 (0 of 19 rejected, MSWD = 0.36)	(single population)	140.6 ± 0.3[e]	Nil[e]
HK12022 D'Aguilar Quartz Monzonite	C 9 R 9	140.5 ± 1.0 (0 of 18 rejected, MSWD = 3.6)	140.8 ± 1.4 (0 of 9 rejected, MSWD = 0.50)	(single population)	140.6 ± 0.3[e]	Nil[e]
HK11042 Kowloon Granite	C 32 R 26	140.0 ± 0.8 (4 of 58 rejected, MSWD = 3.6) (1 analysis >550 Ma)	139.1 ± 1.0 (3 of 26 rejected, MSWD = 2.7)	138.7 ± 0.7 (69 ± 25%) 143.3 ± 1.3 (24 ± 18%) 154.2 ± 1.4 (7 %)	140.4 ± 0.2[e]	Nil[e]
HK13407 Mount Butler Granite	C 26 R 28	138.0 ± 0.6 (4 of 54 rejected, MSWD = 4.1) (1 analysis returns age >2.1 Ga)	137.8 ± 0.8 (0 of 28 rejected, MSWD = 4.6)	132.0 ± 1.5 (5 ± 7%) 136.5 ± 0.6 (43 ± 21%) 139.7 ± 0.5 (48 ± 22%) 163.3 ± 1.8 (4 %)	No ID-TIMS age	(This study only)

Notes:
[a] Spot location: C = Core; R = Rim.
[b] Weighted mean ages calculated at 95% confidence level using Isoplot. MSWD = Mean square weighted deviation (see text for discussion). The 'reject?' option in Isoplot was used to determine the grains that are marked as rejected for the mean age groups.
[c] Deconvolution of multiple age components using the Gaussian distribution of the Sambridge and Compston (1994) "mixture modelling" method, as implemented in Isoplot (Ludwig, 2008). The corresponding fraction of each age component and the associated error is shown in brackets. Note that no error is given for the oldest age component, as its value is constrained to be 100% minus the total of the fractions of the other components.
[d] Published ID-TIMS ages from [e] Davis et al. (1997); [f] Campbell et al. (2007); [g] Sewell et al. (2012b).

TABLE 4. Summary of the zircon trace element data for volcanic and plutonic units.

Sample No	Spot location and number		Sc (ppm)	Y (ppm)	Total Sc+Y+REE (ppm)	Hf (ppm)	Th (ppm)	U (ppm)	Ti (ppm)	Eu/Eu*	Ce/Sm	Th/U	Yb/Gd	U/Yb	Total 3+ [molar]/P [molar]
Volcanic rocks															
HK12025	C	44	9-140 (56)	260-2,400 (880)	510-4,100 (1,660)	6,600-16,100 (10,420)	20-1,000 (120)	40-3,300 (240)	2-25 (9)	0.02-0.59 (0.25)	1.1-22.2 (6.6)	0.13-2.01 (0.51)	2.4-60.5 (14.0)	0.21-5.54 (0.83)	0.8-3.0 (1.7)
	R	32	15-100 (32)	240-4,100 (750)	480-7,300 (1,420)	9,300-12,900(11,420)	50-1,300 (180)	80-1,400 (420)	3-17 (5)	0.10-0.33 (0.16)	3.8-28.5 (12.6)	0.27-1.17 (0.42)	9.5-34.0 (20.4)	0.54-2.70 (1.6)	0.8-3.4 (1.6)
HK11052	C	39	20-120 (47)	340-7,600 (1,550)	690-13,400 (2,710)	8,000-14,900 (9,350)	30-6,800 (260)	50-7,900 (300)	1-23 (11)	0.01-0.27 (0.13)	1.6-11.0 (5.2)	0.26-1.53 (0.72)	7.3-24.2 (12.5)	0.40-3.91 (0.77)	0.8-4.2 (2.3)
	R	40	20-50 (35)	450-3,200 (830)	820-5,600 (1,510)	8,500-13,200 (10,470)	60-1,800 (190)	90-2,400 (310)	4-15 (7)	0.03-0.23 (0.11)	1.6-14.9 (8.3)	0.43-0.93 (0.66)	7.6-21.3 (13.1)	0.45-2.99 (1.2)	1.2-3.8 (1.8)
HK13275	C	30	20-100 (57)	730-7,900 (1,930)	1,400-12,800 (3,560)	7,800-14,100 (9,750)	80-4,200 (310)	130-6,300 (310)	3-27 (9)	0.03-0.45 (0.18)	1.4-10.0 (4.3)	0.37-1.15 (0.76)	6.6-26.6 (11.3)	0.32-3.82 (0.71)	1.4-7.6 (3.0)
	R	37	20-80 (46)	530-3,500 (920)	1,000-6,400 (1,710)	8,200-14,500 (9,960)	70-1,800 (160)	70-2,900 (260)	2-17 (8)	0.05-0.39 (0.23)	1.4-16.8 (10.4)	0.40-1.00 (0.64)	7.0-26.9 (15.0)	0.39-2.24 (0.81)	0.9-5.7 (1.7)
HK11835	C	52	10-180 (53)	190-5,600 (1,400)	370-10,100 (2,530)	8,300-17,300 (9,990)	7-1,500 (240)	20-4,900 (320)	2-19 (9)	<0.01-0.47 (0.25)	1.1-16.8 (7.4)	0.24-1.16 (0.70)	6.7-31.6 (14.2)	0.21-4.18 (0.67)	1.0-6.6 (2.6)
	R	75	20-110 (48)	380-2,800 (870)	760-4,900 (1,620)	6,900-14,000 (10,200)	40-700 (33)	70-1,400 (240)	2-22 (8)	0.06-0.46 (0.29)	2.8-19.6 (10.3)	0.37-1.29 (0.61)	9.2-29.5 (16.0)	0.35-2.65 (0.67)	0.9-4.8 (1.7)
HK11840	C	31	20-140 (48)	890-5,800 (2,886)	1,600-10,200 (5,126)	8,300-16,200 (11,640)	80-2,800 (1,200)	110-5,000 (1,958)	2-16 (5)	<0.01-0.31 (0.05)	2.2-158.6 (4.8)	0.31-1.40 (0.59)	8.0-20.8 (13.6)	0.41-3.44 (1.7)	1.0-8.2 (3.6)
	R	34	20-100 (63)	630-2,500 (1,105)	1,200-4,400 (2,025)	8,300-12,700 (10,310)	60-500 (240)	150-1,100 (426)	2-25 (7)	0.01-0.36 (0.10)	0.8-257.8 (7.5)	0.27-1.28 (0.55)	6.8-37.1 (12.7)	0.26-3.30 (1.2)	0.9-4.3 (2.2)
HK11836	C	37	10-120 (48)	160-4,300 (1,590)	340-7,300 (2,800)	7,000-15,900 (10,040)	5-2,400 (240)	10-3,700 (400)	2-31 (7)	<0.01-0.55 (0.15)	1.0-14.6 (5.6)	0.29-1.07 (0.59)	6.6-26.8 (12.2)	0.21-3. 81 (0.83)	0.9-8.1 (2.8)
	R	41	20-130 (54)	230-2,200 (1,060)	490-4,000 (2,000)	5,400-12,600 (10,030)	7-1,000 (180)	20-3,900 (360)	2-36 (7)	0.02-0.73 (0.15)	0.6-22.3 (7.6)	0.25-0.82 (0.51)	7.2-29.4 (13.9)	0.19-4.58 (0.93)	0.7-4.7 (2.0)
HK12070	C	28	5-90 (49)	130-7,200 (1,100)	290-12,600 (2,090)	8,100-13,000 (9,940)	4-5,300 (230)	70-7,000 (430)	2-41 (7)	<0.01-0.60 (0.22)	1.4-17.9 (8.4)	0.01-1.01 (0.67)	7.9-87.1 (14.9)	0.20-10.1 (0.85)	0.9-6.8 (2.2)
	R	41	10-120 (50)	600-5,800 (1,570)	1,100-10,200 (2,810)	7,700-13,500 (10,760)	39-5,600 (320)	120-7,700 (530)	1-17 (5)	<0.01-0.30 (0.03)	2.6-14.2 (8.1)	0.30-0.94 (0.58)	9.3-29.2 (14.5)	0.27-4.52 (1.4)	1.2-8.1 (3.0)
HK13277	C	48	30-190 (70)	460-9,000 (2,110)	940-15,900 (3,810)	7,700-12,500 (9,390)	70-2,900 (520)	120-4,100 (690)	2-16 (8)	<0.01-0.28 (0.04)	1.3-9.0 (4.7)	0.35-1.45 (0.68)	6.8-18.4 (10.7)	0.38-3.27 (1.1)	1.1-8.3 (3.5)
	R	51	30-150 (71)	160-4,300 (510)	340-7,600 (980)	6,600-10,500 (7,710)	6-900 (33)	10-800 (47)	5-37 (19)	0.03-0.89 (0.26)	0.7-12.5 (3.4)	0.37-1.18 (0.58)	6.3-18.5 (10.4)	0.14-1.36 (0.36)	0.6-4.5 (1.6)
HK12073	C	30	70-240 (110)	1,400-6,600 (3,810)	2,600-11,500 (6,730)	8,200-11,200 (9,340)	160-3,000 (850)	220-2,400 (1,040)	3-12 (6)	0.04-0.23 (0.06)	1.9-10.3 (3.0)	0.50-1.29 (0.81)	7.2-11.3 (8.4)	0.55-2.38 (1.1)	2.7-5.9 (5.2)
	R	46	60-200 (80)	800-5,400 (1,310)	1,600-9,800 (2,400)	8,800-12,200 (11,280)	140-1,900 (350)	320-1,900 (710)	3-10 (4)	0.03-0.10 (0.04)	2.5-9.6 (7.3)	0.38-1.10 (0.49)	7.9-16.7 (12.9)	0.79-2.34 (1.7)	1.0-5.6 (2.8)
HK11834	C	35	80-230 (120)	710-5,400 (2,100)	1,400-9,700 (3,880)	7,900-11,900 (8,870)	90-1,800 (480)	210-1,700 (780)	3-22 (9)	0.04-0.27 (0.09)	2.2-8.9 (5.7)	0.39-1.14 (0.76)	7.2-14.6 (10.0)	0.66-2.00 (1.4)	1.4-5.5 (3.1)
	R	37	50-220 (79)	390-5,500 (660)	760-9,800 (1,290)	7,700-11,700 (8,510)	40-1,700 (89)	90-1,800 (190)	4-18 (12)	0.04-0.54 (0.26)	1.5-9.7 (4.9)	0.36-0.96 (0.48)	7.5-16.9 (12.1)	0.49-2.06 (0.85)	0.9-4.9 (1.7)
HK12001	C	40	40-270 (100)	290-5,400 (1,820)	550-9,600 (3,340)	7,000-11,700 (8,740)	20-1,500 (330)	40-2,200 (620)	3-17 (8)	0.02-1.06 (0.17)	1.1-8.5 (3.3)	0.34-1.04 (0.68)	6.9-15.9 (10.3)	0.34-1.78 (0.88)	0.9-6.6 (3.1)
	R	52	50-260 (81)	380-5,200 (1,270)	740-9,300 (2,370)	7,100-12,500 (11,010)	30-2,700 (290)	40-2,200 (640)	3-20 (4)	0.03-1.26 (0.05)	1.0-8.3 (6.8)	0.32-1.20 (0.45)	7.0-18.5 (13.6)	0.23-2.18 (1.6)	1.7-5.9 (2.7)
HK13343	C	25	20-200 (86)	270-6,500 (1,230)	500-11,400 (2,300)	6,100-11,400 (7,730)	20-2,100 (180)	30-2,300 (270)	2-20 (11)	0.03-1.38 (0.21)	1.3-12.8 (3.6)	0.26-1.20 (0.70)	6.7-17.8 (8.9)	0.17-1.69 (0.67)	0.8-7.4 (2.6)
	R	51	20-180 (69)	290-3,600 (1,010)	590-6,500 (1,880)	6,400-11,100 (8,260)	20-700 (250)	30-900 (420)	3-23 (9)	0.03-1.41 (0.11)	1.2-13.9 (5.6)	0.33-1.08 (0.72)	6.7-25.2 (10.9)	0.20-2.09 (0.85)	0.9-6.0 (2.2)

TABLE 4. (Continued)

Sample number	Spot location and number	Sc (ppm)	Y (ppm)	Total Sc+Y+REE (ppm)	Hf (ppm)	Th (ppm)	U (ppm)	Ti (ppm)	Eu/Eu*	Ce/Sm	Th/U	Yb/Gd	U/Yb	Total 3+ [molar]/P [molar]
Plutonic rocks														
HK11822	C 47	7-140 (33)	200-4,800 (850)	420-8,900 (1,660)	7,800-15,500 (11,000)	40-2,900 (270)	40-3,800 (770)	2-19 (4)	0.03-0.43 (0.26)	0.6-32.3 (8.6)	0.11-1.36 (0.44)	7.5-45.0 (19.2)	0.35-4.42 (2.2)	0.9-4.8 (2.0)
	R 33	20-60 (26)	520-5,100 (1,280)	1,010-9,400 (2,370)	9,900-19,100 (12,840)	90-2,900 (670)	170-15,800 (1,900)	5-15 (3)	0.05-0.33 (0.15)	2.5-14.9 (10.8)	0.14-0.61 (0.33)	8.2-39.8 (24.9)	0.88-7.83 (4.1)	1.0-4.9 (2.4)
HK11831	C 26	20-70 (44)	320-5,700 (1,030)	590-10,000 (1,870)	8,100-14,100 (9,570)	40-1,600 (200)	70-4,000 (240)	4-19 (9)	0.02-0.22 (0.15)	1.5-15.8 (5.2)	0.38-1.73 (0.69)	7.1-18.1 (12.6)	0.43-2.92 (0.76)	0.9-4.3 (2.2)
	R 47	20-60 (34)	300-3,300 (760)	580-5,900 (1,390)	7,800-15,200 (9,820)	40-1,700 (150)	60-4,200 (220)	2-23 (10)	0.02-0.32 (0.14)	1.5-15.2 (7.1)	0.40-1.04 (0.68)	7.0-22.9 (11.8)	0.41-3.82 (1.0)	1.1-3.4 (1.6)
HK8353	C 36	10-150 (43)	50-10,100 (1,400)	100-18,400 (2,540)	6,700-19,000 (10,040)	3-3,900 (280)	120-11,800 (380)	1-37 (6)	<0.01-0.42 (0.12)	1.9-20.0 (9.0)	0.01-1.59 (0.62)	1.0-30.0 (13.3)	0.30-55.0 (1.3)	1.2-5.2 (2.1)
	R 40	20-100 (30)	510-5,000 (1,150)	970-9,400 (2090)	8,800-20,700 (10,800)	100-3,800 (330)	220-7,700 (600)	3-18 (4)	0.01-0.20 (0.06)	3.6-17.8 (11.1)	0.19-1.31 (0.53)	6.6-35.3 (17.5)	0.60-4.43 (1.8)	1.4-3.7 (2.3)
HK12072	C 33	30-90 (49)	330-5,500 (1,660)	620-10,300 (3,000)	8,400-17,500 (10,350)	30-2,600 (430)	50-7,900 (360)	1-14 (6)	0.01-1.21 (0.07)	2.0-11.3 (5.3)	0.35-1.55 (0.73)	6.5-16.0 (9.9)	0.33-3.07 (1.3)	0.9-6.8 (3.8)
	R 38	20-80 (47)	550-2,600 (1,060)	1,000-4,600 (1,950)	8,900-12,500 (10,230)	70-1,200 (250)	100-2,100 (390)	2-14 (6)	0.02-1.90 (0.26)	2.3-10.9(5.0)	0.36-1.07 (0.59)	6.7-23.0 (11.5)	0.22-2.88 (0.57)	0.7-6.7 (1.6)
HK8758	C 34	30-290 (87)	300-7,000 (1,880)	580-11,900 (3,350)	6,900-11,700 (8,440)	20-3,700 (430)	30-3,100 (710)	2-15 (9)	0.01-0.28 (0.07)	2.0-11.3 (5.5)	0.20-1.39 (0.67)	6.4-35.2 (13.1)	0.39-3.75 (1.0)	0.7-6.0 (2.0)
	R 47	30-130 (60)	210-5,800 (730)	410-10,200 (1,350)	6,400-12,700 (7,620)	8-2,200 (120)	20-2,500 (190)	3-22 (13)	0.02-0.29 (0.10)	2.3-10.9 (7.2)	0.29-1.25 (0.62)	7.0-24.9 (12.4)	0.40-2.82 (1.2)	0.9-3.9 (2.0)
HK12023	C 32	40-240 (110)	270-6,500 (2,440)	530-10,800 (4,300)	6,700-12,200 (8,110)	20-2,200 (550)	50-1,800 (750)	3-19 (9)	0.02-0.72 (0.08)	0.9-8.0 (3.1)	0.37-1.43 (0.75)	5.9-19.2 (7.7)	0.49-2.75 (0.92)	1.0-6.4 (4.0)
	R 52	30-220 (67)	280-4,300 (1,030)	530-7,600 (1,890)	6,600-11,100 (8,060)	20-1,200 (430)	40-1,600 (370)	2-20 (9)	0.03-1.31 (0.16)	0.9-10.6 (5.1)	0.33-0.91 (0.47)	7.2-17.0 (12.0)	0.26-1.90 (0.95)	0.8-7.1 (2.2)
HK12022	C 25	30-180 (67)	210-5,900 (1,500)	400-10,400 (2,750)	6,200-11,000 (7,950)	10-1,900 (220)	20-2,600 (370)	3-23 (11)	0.02-1.23 (0.17)	1.1-9.2 (2.8)	0.40-1.00 (0.68)	6.1-26.7 (9.4)	0.24-1.83 (0.63)	0.6-6.5 (3.1)
	R 48	30-130 (54)	260-1,900 (600)	510-3,500 (1,140)	6,600-11,000 (8,060)	20-1,200 (60)	20-1,700 (87)	3-26 (11)	0.02-1.77 (0.48)	1.4-13.8 (7.1)	0.21-1.20 (0.59)	6.8-23.2 (12.8)	0.17-2.90 (0.49)	0.8-3.4 (1.4)
HK11042	C 51	20-160 (64)	330-8,200 (1,140)	630-15,400 (2,230)	8,200-14,900 (10,040)	40-2,100 (280)	100-4,800 (420)	3-30 (9)	0.01-0.45 (0.23)	1.7-16.7 (7.7)	0.27-3.03 (0.69)	6.4-24.6 (13.9)	0.46-2.70 (1.0)	0.8-5.1 (2.0)
	R 36	20-100 (36)	400-7,400 (1,510)	780-14,200 (2,790)	6,200-21,200 (12,330)	30-3,900 (430)	70-13,300 (720)	2-17 (5)	0.05-0.63 (0.14)	2.9-20.7 (9.0)	0.07-0.88 (0.45)	3.1-37.4 (21.0)	0.42-6.32 (1.6)	1.2-7.0 (2.3)
HK13407	C 31	30-190 (67)	280-5,900 (1,480)	550-10,500 (2,820)	7,300-14,200 (8,740)	60-1,600 (270)	70-2,600 (400)	2-19 (10)	0.01-0.51 (0.35)	1.8-12.9 (5.0)	0.15-1.08 (0.61)	8.2-26.2 (14.0)	0.41-3.03 (0.72)	0.7-7.3 (2.8)
	R 49	20-140 (42)	570-11,000 (1,350)	1,100-19,800 (2,480)	8,600-22,100 (10,910)	80-2,000 (370)	140-12,400 (650)	1-12 (5)	<0.01-0.47 (0.19)	2.5-14.3 (8.9)	0.16-0.87 (0.48)	9.8-40.6 (17.6)	0.47-3.14 (1.5)	0.6-8.5 (1.7)

Notes: In the spot location column: C = Core; R = Rim. The ranges in values for the selected elements and ratios are given, with the mean values in brackets.

(DOI will not work until issue is live.) DOI: http://dx.doi.org/10.2138/am-2017-6071

TABLE 5. Zircon saturation temperatures of selected Hong Kong rock units.

Rock Unit	Mean T_{zr} (°C)	s.d. (°C)	*n*	T-in-Zir (°C)	Inheritance?
Lantau Granite	756	15	20	685-785	Yes
Chi Ma Wan Granite	764	28	15	644-804	Yes
Shui Chen O Granite	746	25	11	567-779	No
Kowloon Granite	768	26	16	614-798	Yes
Mount Butler Granite	741	18	25	567-763	Yes
Sok Kwu Wan Granite	865	1	2	614-815	No
Tei Tong Tsui Quartz Monzonite	854	30	11	-	-
Tong Fuk Quartz Monzonite	826	16	9	644-826	No
D'Aguilar Quartz Monzonite	850	4	7	644-844	No
Long Harbour ignimbrite	789	10	16	614-826	Yes
Mount Davis ignimbrite	793	20	27	614-798	Yes
Ap Lei Chau ignimbrite	798	15	23	614-826	Yes
Che Kwu Shan ignimbrite	821	24	25	614-882	Yes
Pan Long Wan lava	847	23	11	685-886	Yes
Clear Water Bay ignimbrite	815	28	20	667-826	No
High Island Tuff	796	12	15	644-815	No

Notes:

1. The zircon saturation temperatures were calculated using Watson and Harrison (1983) thermometry on whole-rock geochemical data from Sewell and Campbell (2001). Zircon saturation temperature was calculated using:

$$T_{zr} = 12{,}900 / [2.95 + 0.85\ M + \ln (Zr_{zircon} / Zr_{rock})],$$

where M = [(Na+K+2*Ca)/(Al*Si)] (all in cation fraction), Zr_{zircon} is the concentration of Zr in zircon (i.e. ~497,646 ppm), Zr_{rock} is the concentration of Zr in the sample, and T_{zr} is temperature (in Kelvins). The values given are averaged from multiple whole-rock geochemical analyses of the relevant unit (Sewell and Campbell, 2001).

2. The Ti-in-zircon temperatures were calculated using the calibration of Ferry and Watson (2007) on zircon trace element data obtained here, using:

$$\text{T-in-Zir} = -4{,}800 / [\log (\mathrm{Ti}) + \log (a\mathrm{SiO_2}) - \log (a\mathrm{TiO_2}) - 5.711],$$

where Ti is the Ti abundance in zircon (in ppm), $a\mathrm{SiO_2}$ and $a\mathrm{TiO_2}$ are activities of SiO_2 and TiO_2 (both assumed to be 1) and T-in-Zir is temperature (in Kevin). The range of Ti-in-zircon temperature of each unit is calculated based on the range of Ti abundance from rim analyses of the relevant unit.